3.2 First-Principles Calculation of Material Properties

Atomic Structures and Electronic Properties of Hard- and Soft-Nanomaterials

Atsushi Oshiyama
Department of Applied Physics, The University of Tokyo
Hongo, Tokyo 113-8656

Main purpose of this project is to develop the density-functional approach which enables us to perform more accurate and larger scale static and dynamical calculations on massively parallel architecture computers, to clarify underlying physics and chemistry in phenomena in nano-materials and structures, and to predict new phenomena in nano-world. The following is an example which we have achieved in 2015 fiscal year [J.-I. Iwata, C. Shinei and A. Oshiyama, Phys. Rev. B **93**, 125202 (2016)].

Magic Numers in Nano-size of Multivacancies in Silicon Carbide

Point defects inevitably exist in semiconductors and play important roles both in technology and science. Such point defects as lattice vacancies or interstitial atoms generally induce electron states localized around the defects, their energy levels being in the fundamental energy gap (deep levels). Those deep levels act as carrier traps. Hence structural identification of the deep levels is highly demanded from technology viewpoints. Scientifically, the deep localized state brings forth intriguing properties: It enhances electron-lattice interaction and then occasionally constitute Anderson negative U system with Jahn-Teller type local relaxation.

SiC is a promising material due to its attractive properties such as the high dielectric breakdown voltage and the high melting temperature. It is a tetrahedrally bonded covalent semiconductor and exists as many polytypes called 2H (wurtzite), 3C (zincblende), 4H, 6H and so forth. The most experimentally common polytype is 4H, which is corroborated by our density-functional calculations: The calculated cohesive energy with the generalized gradient approximation (GGA) by Perdew, Burke and Ernzerhof (PBE) in the density-functional theory (DFT) of the 4H polytype is the largest, followed by 6H, 3C, 2H with the cohesive-energy decrease of 0.1 meV, 1.0 meV and 8.0 meV per SiC unit, respectively.

Thermal treatment inevitably required in device fabrication causes diffusion of point defects and thus point defects are likely to segregate to be of complex forms. Some deep levels are indeed argued to be the divacancy or the trivacancy. However detailed investigation of energetics and electron states of such complex defects is lacking.

We have performed the density-functional calculations that clarify the atomic structures, the energetics and the electron states of the multivacancy V_n consisting of $n_{\rm Si}$ silicon vacant sites and $n_{\rm C}$ carbon vacant sites ($n = n_{\rm Si} + n_{\rm C}$) in the most stable silicon carbide polytype 4H-SiC. The calculations with the generalized gradient approximation (GGA) for the monovacancy, $V_{\rm Si}$ and $V_{\rm C}$, have clarified the significantly lower formation energy of the C vacancy accompanied with the efficient pairing relaxation of the surrounding Si dangling bonds. Based on this structural characteristics and the energetics for the monovacancy, we have proposed an extended dangling-bond counting (EDBC) model to discuss the stability of the multivacancy. The EDBC model predicts a new stable next-neighbor $V_{\rm C}V_{\rm C}$ divacancy (Fig.) which is lower in the formation energy than the usual nearest-neighbor divacancy $V_{\rm C}V_{\rm Si}$ discussed in the past. Our calculations with PBE functional and also with the hybrid functional (HSE06) have indeed clarified that the $V_{\rm C}V_{\rm C}$ is more stable than the $V_{\rm C}V_{\rm Si}$ under C-poor condition. Even under C-rich condition, the next-neighbor divacancy $V_{\rm C}V_{\rm C}$ is more stable than the nearest-neighbor $V_{\rm C}V_{\rm Si}$ when the Fermi level is located in the lower half of the energy gap. The next-neighbor divacancy is possible to be detected with its peculiar hyperfine coupling constants by

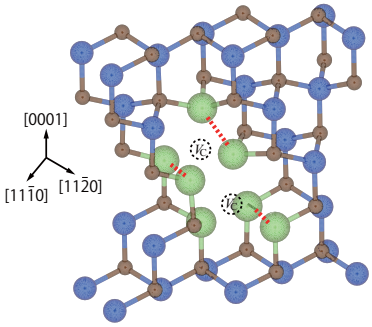

Figure 1: Geometry optimized structure of the divacancy $V_{\rm C}V_{\rm C}$ composed of a next-neighbor pair of two carbon vacancies. Blue (large) and brown (small) spheres depict Si and C atoms, respectively. The nearest neighbor Si atoms around $V_{\rm C}V_{\rm C}$ are marked by Green (large) spheres. The vacant sites are depicted by the dashed circles. The two of the nearest neighbor Si atoms connected by the red dashed line form the pairing relaxation.

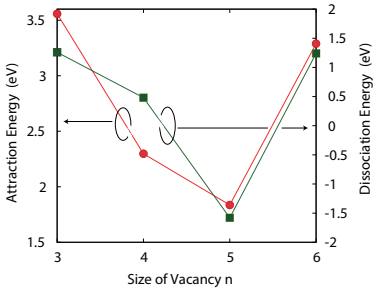

Figure 2: Dissociation energy ζ (squares) and the attraction energy η (circles) of the multivacancy V_n obtained from GGA calculations. Right and left axes represent ζ and η, respectively. Here the dissociation energy ζ_n is defined as $\zeta_n = E_{\rm f}(V_{\rm n+1}) + E_{\rm f}(V_{\rm n-1}) - 2E_{\rm f}(V_{\rm n})$ using the formation energies of each vacancy. The attraction energy is defined as $\eta_n = E_{\rm f}(V_{\rm n-1}) + E_{\rm f}(V_1) - E_{\rm f}(V_{\rm n})$.

the electron paramagnetic resonance (EPR) measurements.

The EDBC model has been also applied to larger multivacancy and revealed the energetically favorable pair ($n_{\rm Si}$, $n_{\rm C}$) and the topological network for the multivacancy V_n. As a result, V_n with $n = 6$, 9, 10, 14 has been shown to have relatively lower formation energies: the magic numbers of the stable multivacancy. We have also performed GGA calculations for the multivacancy V_n and clarified that V_3 and V_6 is energetically favorable (Fig.). The stable V_3 is a nearest neighbor complex of $V_{\rm C}$-$V_{\rm Si}$-$V_{\rm C}$, whereas the V_6 is the high symmetry V_5 (the central $V_{\rm Si}$ surrounded by 4 $V_{\rm C}$) plus symmetry breaking next-neighbor $V_{\rm C}$.

We have performed the GGA calculations for electronic structure of thus obtained stable V_3 and V_6 and discussed the possibility of detecting these multivacancies. We have clarified the existence of various charge states for V_3 and V_6, for which high-spin and low-spin states are possible depending on the charge states (Fig.). In particular, the EPR detected ANN1 center has been provisionally identified as the doubly positive trivacancy $V_{\rm C}$-$V_{\rm Si}$-$V_{\rm C}$. The present calculations provide a firm theoretical frame work to identify the multivacancies generated by heat treatments of SiC and discuss their physical properties.

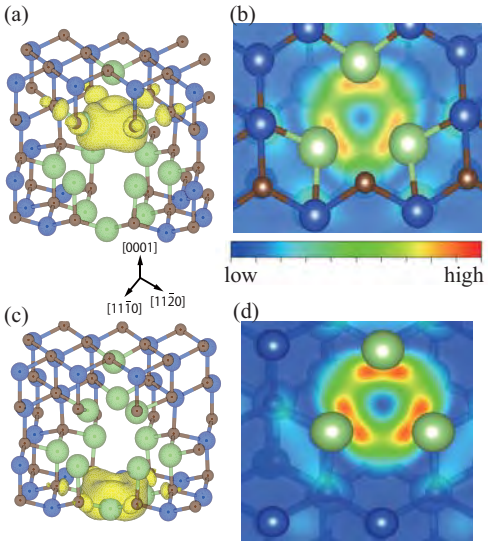

Figure 3: Spin densities for the doubly positive [(a) and (b)] and doubly negative [(c) and (d)] charge states of the hexavacancy. In (a) and (c), the iso-surfaces at the value of 20 % of the maximum value are shown, and (b) and (d) are the contour plots. The large (blue and green) spheres and the small (brown) spheres depict Si and C atoms, respectively. The green spheres depict the under-coordinated Si atoms.

First-principles statistical thermodynamics simulations on the structure and reactivity of heterogeneous catalysts

Fahdzi MUTTAQIEN, Shiro TORII, Yuji HAMAMOTO, Kouji INAGAKI,
Hidetoshi KIZAKI, and Yoshitada MORIKAWA
Department of Precision Science and Technology,
Osaka University, Yamada-oka, Suita, Osaka 565-0871

In our research project, we have investigated several systems including CO_2 adsorption and hydrogenation on Cu surfaces, Bathocuproine-metal interactions, naphthalene on graphite surfaces, ligand-free Suzuki-Miyaura cross coupling reactions in aqueous solutions, and stability of Pd atoms dissolved into $LaFeO_3$ perovskite oxides. In the present report, we explain some of our recent progresses.

Adsorption and decomposition of formic acid on Cu surfaces are attracting considerable attention because of their fundamental importance in catalysis and also applications experimentally reported that the formic acid decomposes to formate species upon adsorption on Cu(100)[1], and Cu(110)[2]. On the other hand, it was pointed out that formic acid does not dissociate at room temperature on the Cu(111) surface, At low temperature, the formic acid decomposition can be induced on Cu(111) from polymeric structures[3,4]. The hydrogen bonding network in polymeric structure is responsible to stabilize the formic acid and enhance its decomposition [4].

In the present works, we carried out self-consistent van der Waals density functional (vdW-DF) study of formic acid decomposition on the single crystal Cu(111) surface. We implemented vdW-DF based functionals (vdW-DF1 [5], rev-vdW-DF2 [6], and optB86b-vdW [7]) to describe the interaction between molecule-surface and molecule-molecule in the system more accurate [8]. To calculate self-consistent potential for vdW-DFs accurately

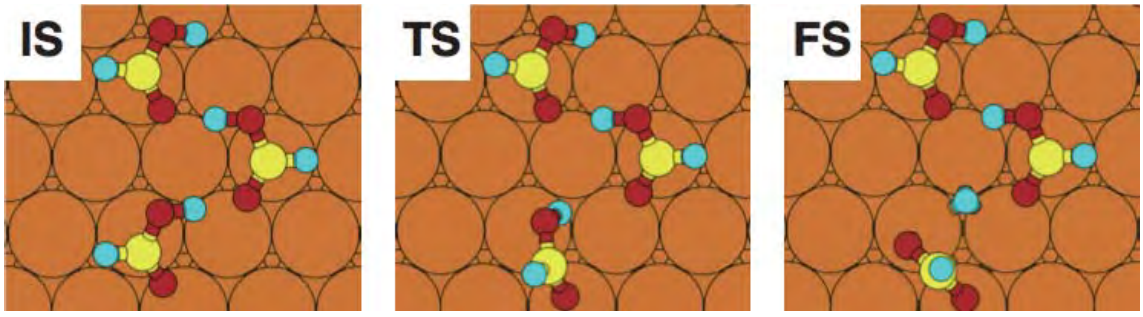

Fig. 1: Schematic of formic acid decomposition in the polymeric structure on the Cu(111) surface.

and efficiently, we employed separable form of vdW kernel proposed by Roman-Perez and Soler [9] with a modification by Wu and Gygi to suppress the divergence of the kernel [10]. Our results showed that isolated single formic acid is easily desorbed rather than decomposed on the Cu(111) surface. While, the polymeric structure of formic acid is more stable on the Cu(111) surface, and easily decomposed into formate species (Fig.1). We also noticed that the formate product tends to form bidentate formation on the surface. We clarified the mechanism for the enhancement of formic acid decomposition by the formation of polymeric formic acid.

References

[1]. B.E. Hayden, K. Prince, D.P. Woodruff, and A.M Bradshaw, *Surf. Sci*. **133**, 589 (1983).

[2] A. E. Baber, K. Mudiyanselage, S. D. Senanayake, A. Beatriz-Vidal, K. A. Luck, E. C. H. Sykes, P. Liu, J. A. Rodriguez, and D. J. Stacchiola, *Phys. Chem. Chem. Phys*. **15**, 12291 (2013).

[3] Y. Shiozawa, T. Koitaya, K. Mukai, S. Yoshimoto, J. Yoshinobu, *J. Chem. Phys*. **143**, 234707 (2015).

[4] F. Muttaqien, Y. Hamamoto, K. Inagaki, and Y. Morikawa, *J. Chem. Phys.* **141**, 034702 (2014).

[5] M. Dion, H. Rydberg, E. Schröder, D.C. Langreth, and B.I. Lundqvist, *Phys. Rev. Lett.*, **92**, 246401 (2004).

[6] I. Hamada, *Phys. Rev. B* **89**, 121103 (R) (2014).

[7] J. Klimeš, D.R. Bowler, and A. Michaelides, *Phys. Rev. B* **83**, 195131 (2011).

[8] Y. Hamamoto, I. Hamada, K. Inagaki, and Y. Morikawa, *Phys. Rev. B*, submitted.

[9] G. Román-Pérez and J.M. Soler, *Phys. Rev. Lett.*, **103**, 096102 (2009).

[10] J. Wu and F. Gygi, *J. Chem. Phys*. **136**, 224107 (2012).

First-principles calculation of interactions between extreme pulse light and matter

Kazuhiro YABANA

Center for Computational Sciences,

University of Tsukuba, Tsukuba, 351-8577

Interaction between intense and ultrashort laser pulse and solid is one of active subjects in current optical sciences. Employing a few-cycle femtosecond laser pulses, a number of intriguing phenomena reflecting extremely nonlinear light-matter interactions have been observed. We have been developing a first-principles computational method to describe electron dynamics in solids under irradiation of a pulsed electric field based on time-dependent density functional theory, solving time-dependent Kohn-Sham equation in real time for electron orbitals in a unit cell of crystalline solids.

For a quantitative description of light-matter interactions, it is important to employ a potential in the Kohn-Sham equation that describes the band gap of the material adequately. As is well known, a simple local density approximation underestimates the band gap systematically. Recently, a few potentials that describe band gaps reasonably have been proposed. We have investigated computational methods to use such potentials in our code and examined optical responses of dielectrics in both linear and nonlinear regimes [1].

We implemented two potentials in our code, a meta-GGA potential developed by Tran and Blaha and a hybrid functional of Heyd, Scuseria, and Ernzerhof. For the meta-GGA potential, we have found that a predictor-corrector step is essential for a stable time evolution. Since a computation of nonlocal exchange potential in the hybrid functional requires heavy computational costs, we have developed a code that efficiently utilizes GPU.

We applied the code to various optical phenomena. One of such applications is the nonlinear photogalvanic effect [2]. It was found that an extremely intense and ultrashort laser pulse produces a current in dielectrics of wide band gap. We have found that the induced current in such dielectrics shows complex behavior, changing its direction depending on the maximum intensity of the pulse.

References

[1] S.A. Sato et.al, J. Chem. Phys. **143**, 224116 (2015).

[2] G. Wachter et.al, New J. Phys. **17**, 123026 (2015).

Development of first-principles electronic-structure and transport calculation method based on real-space finite-difference approach

Tomoya Ono
Center for Computational Sciences, University of Tsukuba
Tennodai 1-1-1, Tsukuba, Ibaraki 305-8577

1 Introduction

SiC is attracted much attention due to its excellent physical properties, such as a high thermal conductivity, high breakdown strength, and large band gap. However, unlike Si metal-oxide-semiconductor (MOS) field-effect transistors (FETs), SiC MOSFETs suffer from unacceptably low carrier mobility. Large amount of defects at SiC/SiO_2 interface, which are generated in oxidation process, is expected to be one of the origins for the low carrier mobility. Therefore, understanding and precise control of the atomic structure of SiC/SiO_2 interface are vital to increase the carrier mobility of SiC MOSFETs. SiC has many different polytypes, determined based on their stacking along the [0001] direction. Si and C atoms can occupy one of three positions along the $[1\bar{1}00]$ direction, normally labelled ABC. Stacking ordered ABCAB... is called cubic whilst that ordered ABABA... is called hexagonal. The most commonly used polytype for electronic devices is 4H-SiC, which consists of four repeated SiC bilayers, ordered ABCBAB.... Within these four bilayers, there are two inequivalent lattice sites, usually known as h (hexagonal) and k (quasi-cubic) based on the site occupied by the Si atoms in the neighboring bilayers. h sites are equivalent to A or C stacking positions and k sites are equivalent to B stacking positions. The local structure around the SiC/SiO_2 interface will change depending on which of this stacking at the SiC surface. In this study, we have conducted density functional theory (DFT) calculations for the relation between the electronic structures at the interface and the local atomic structures which appear in the oxidation process.

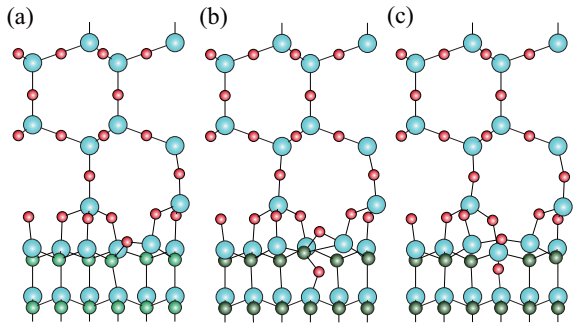

Figure 1: 4H-SiC(0001)/β-tridymite SiO_2 interface model. (a) O_{if}, (b) O_{if+sub}, and (c) V_CO_2. White, green (large dark gray), red (small dark gray), and blue (light gray) circles are H, C, O, and Si atoms, respectively.

2 Computational Methods

DFT calculations are performed using RSPACE code.[1] The lateral size of the supercell is the $(3 \times \sqrt{3})$ 4H-SiC(0001) surface and the substrate contains four Si-C bilayers. Dangling bonds at the bottommost Si-C bilayer as well as those at the topmost layers of SiO_2 are terminated by H atoms. The top bilayer of SiC shown in Fig. 1 is hexagonal

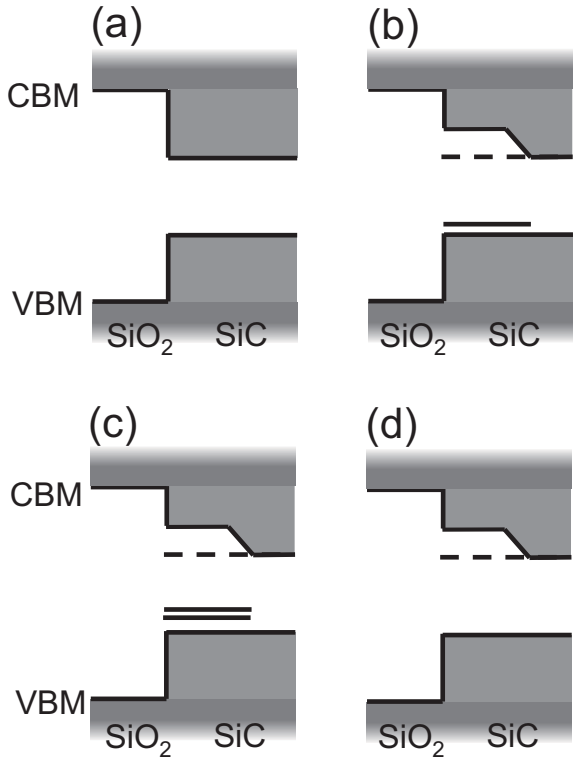

Figure 2: Band alignment of h type. (a) clean interface, (b) O_{if}, (c) O_{if+sub}, and (d) V_CO_2.

surface, in which the stacking sequence is ABCBA ... from the top bilayer. The details of the computational procedure are explained elesewhere.[2] The typical computational models for the oxidation are shown in Fig. 1(a), 1(b), and 1(c), which are obtained by our previous study.[3]

3 Results and Discussion

We examine the local density of states (LDOS) for the clean interface. Figure 2 shows the schematic image of LDOS at the interface. There are no significant changes at the valence band edge (VBE) between two types. On the other hand, the most interesting results are along the valence band edge (CBE), the location of which changes with interface type. The h type has CBE at the first bilayer of the interface, whereas one does not appear until the second bilayer for the k type. The states which contribute to the CBE are the previously noted floating states,[4] which only appear at the CBE in the cubic stacking regions (ABC or CBA) and are blocked by the hexagonal stacking regions.

We examine the LDOS for each structure, noting how it changes compared to the clean interfaces. We start with O_{if}. Notably, the CBE of the h type changes, while that of the k type does not. Next we examine O_{if+sub}. The same changes are observed at the CBE as before, with the CBE removed for h type. Finally, we consider the V_CO_2 structure, which looks similar to the clean interface. Although one CO molecule is removed from the vicinity of the Si-surrounded tetrahedron, there still remains two O atoms. Therefore, the CBE does not recover for the h type. For the k type, the CBE is not changed because the tetrahedron is located deep inside the substrate.

Since recent SiC-based MOSFETs mainly use the conduction band as a channel, the behavior of the CBE might play an important role in the performance of these devices. In the future we want to do more complete calculations for all of these structures, to get a fuller picture of how the scattering properties of the interface change with defect type using first-principles transport calculations.

References

[1] K. Hirose et al., First-Principles Calculations in Real-Space Formalism (Imperial College Press, London, 2005).

[2] T. Ono and S. Saito, Appl. Phys. Lett. **106**, 081601 (2015).

[3] C. Kirkham and T. Ono, J. Phys. Soc. Jpn. **85**, 024701 (2016).

[4] Y. Matsushita et al., Phys. Rev. Lett. **108**, 246404 (2012).

First-principles study of quantum transport in nanostructures

NOBUHIKO KOBAYASHI
Institute of Applied Physics, University of Tsukuba
1-1-1 tennodai Tsukuba Ibaraki 305-8573

1 Introduction

The aim of this project is to reveal charge and heat transport in materials using atomistic theory. Quantum nature is essential in nanoscale systems, and atomistic analysis based on detailed electronic states calculations are indispensable to discuss the transport property. In order to analyze transport properties, we have developed the nonequilibrium Green's function (NEGF) method, and the time dependent wave-packet diffusion (TD-WPD) method. Using these methods, we have investigated charge and heat transport properties of nanostrucures, organic molecules and so on.

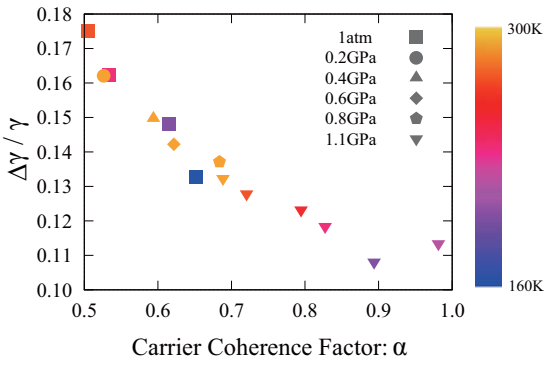

Figure 1: Correlation between carrier coherence factor α obtained from experimental data and calculated thermal fluctuation $\Delta\gamma/\gamma$. The data are taken at various temperatures and pressures.

2 Charge Transport

The recent progress in the fabrication technology of organic single-crystal semiconductors and thin-film field-effect transistors with very high carrier mobility up to 40 cm^2/Vs requires us to elucidate the mechanisms of carrier transport in organic semiconductors, which are assemblies of p-conjugate molecules weakly bonded by van der Waals interactions. Observations of the crossover from the hopping transport of localized carriers to bandlike transport with a diffusive nature are expected to provide us with clues allowing us to reveal the carrier transport mechanisms.

We show evidence of a strong correlation between the carrier coherence factor α and the thermally induced fluctuations of transfer energies with neighboring molecules. The thermal fluctuation effects of molecular motion have been discussed for transport properties of organic semiconductors. We present numerical data of transfer energy fluctuations of pentacene at various temperatures and pressures, and we compare them with experimental observations of α. As a result, we find a strong correlation between these two factors. We apply this method to other organic semiconductors and obtain consistent results with those of transport experiments. [1, 2]

3 Thermoelectricity

The thermoelectric properties of TiN/MgO superlattices have been analyzed using first-principles calculation techniques. The Seebeck coefficients, the electrical conductances, the thermal conductances, and the figure of merit are investigated employing electrical and thermal transport calculations based on density functional theory combined with the nonequilibrium Green !S function and nonequilibrium

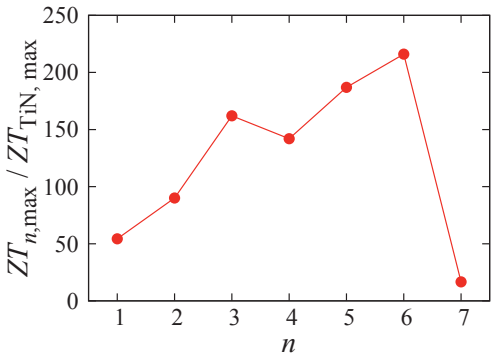

Figure 2: Maximum figure of merit ZT in the calculated configurations normalized by $ZT_{\mathrm{TiN,max}}$.

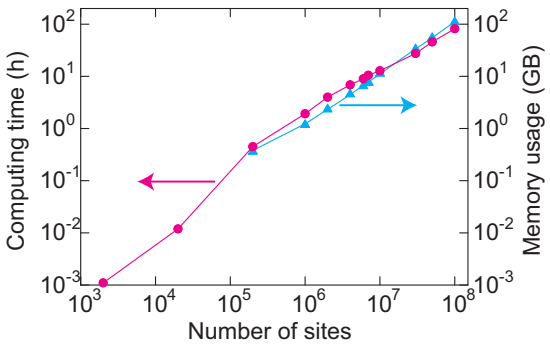

Figure 3: Computing time (red circles) and memory usage (blue triangles) per one initial wave packet as a function of site number of the lattice.

molecular dynamics simulation methods. The TiN/MgO superlattices with a small lattice mismatch at the interfaces are ideal systems to study the way for an enhancement of thermoelectric properties in artificial nanostructures. We find that the interfacial scattering between the two materials in the metal/insulator superlattices causes the electrical conductance to change rapidly, which enhances the Seebeck coefficient significantly. We show that the figure of merit for the artificial superlattice nanostructures has a much larger value compared with that of the bulk material and changes drastically with the superlattice configurations at the atomistic level. [3]

4 O(N) Method

We have also developed the O(N) TD-WPD method for the quantum transport calculation of huge systems of up to 100 million atoms.We calculated the conductance and the mobility of the system with micron-order lengths at room temperature based on the Kubo-Greenwood formula. Using this method we can study the transport properties from diffusive to ballistic regimes including the effect of realistic electron-phonon scattering, and determine the mean free path and relaxation time from an atomistic viewpoint. We performed DFT calculations of electronic structures and interactions between molecules of pentacene and rubrene single-crystal organic semiconductors including the effect of the van der Waals interaction, and applied the TD-WPD method to the analysis of transport properties of the organic semiconductors.

We have analyzed relationships between charge transport properties and disorder in rubrene single crystals. We take into account two different types of disorder, namely, intrinsic dynamical disorder due to intermolecular vibrations and extrinsic static disorder. Then we evaluate the transport properties using our wave-packet dynamical approach which gives us a unified theoretical description from hopping to band transport behavior. We show that the mobilities are completely changed from the intrinsic power-law temperature dependence to the thermally activated behavior by introduction of the extrinsic trap potentials. [4, 5]

References

[1] T. Fukami, H. Ishii, N. Kobayashi, T. Uemura, K. Sakai, Y. Okada, J. Takeya, and K. Hirose, Appl. Phys. Lett. 106 (2015) 143302.

[2] K. Sakai, Y. Okada, T. Uemura, J. Tsurumi, R. Hausermann, H. Matsui, T. Fukami, H. Ishii, N. Kobayashi, K. Hirose and J. Takeya, NPG Asia Materials, 8, e252 (2016).

[3] H. Takaki, K. Kobayashi, M. Shimono, N. Kobayashi, and K. Hirose,
J. Appl. Phys. 119 014302 (2016).

[4] H. Ishii, H. Tamura, M. Tsukada, N. Kobayashi, K. Hirose,
Phys. Rev. B 90 (2014) 155458 (1-5).

[5] H. Ishii, N. Kobayashi, K. Hirose, Mol. Cryst. Liq. Cryst. 620 (2015).

First-principles meta-dynamics analysis of Catalytic Referred Etching method (Analysis of atom removal process)

Kouji INAGAKI

Precision Science and Technology & Applied Physics, Graduate School of Engineering

Osaka University, Yamada-oka 2-1, Suita, Osaka 565-0871

We investigated reaction mechanisms of chemical etching processes in a surface smoothening technique named Catalyst Referred Etching (CARE)[1], in which etching is invoked by bringing the material surface (e.g. wide band-gap semiconductors) into contact with a catalyst (e.g. Pt) in an etching solution (e.g. aqueous HF solution for SiC etching or pure water for GaN etching). In SiC-HF system, we have already obtained findings in the previous study with respect to SiC back-bond cleavage and simultaneous dissociative adsorption of HF molecule as the first step of etching process. The reaction barrier is clarified to be strongly lowered by the existence of Pt catalyst [2]. In this project, we analyzed Pt position dependence particularly in distance between Pt and SiC [3]. It is clarified that the initial, medium metastable and final states in the reaction path are all destabilized by approaching Pt to SiC, but the initial state become relatively most unstable [3]. This means the dissociative adsorption is enhanced when Pt approaches to SiC surface. As for GaN, we firstly find that a spontaneous dissociative adsorption onto OH terminated kinked-GaN surface occurs in the presence of Pt catalyst (Fig. 1). This reaction strongly depends on the initial hydrogen-bond network configuration of the surface OH-termination groups. The accurate reaction barrier can be evaluated by thermal average molecular dynamics methods such as the blue moon ensemble or the meta-dynamics. To reduce the huge calculation costs in such kind of analysis, we proposed a new meta-dynamics method in which the shape of the penalty potential is controlled by the momentum along the corresponding reaction coordinate. The basic behavior of the method is confirmed and it will be applied to realistic models in the next project.

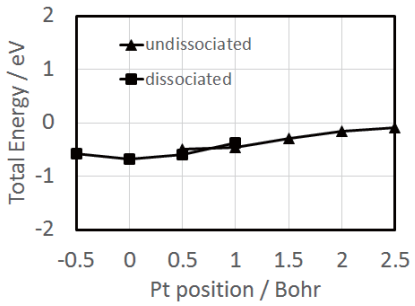

Fig. 1: Pt position dependence in GaN/H_2O/Pt initial state.

References

[1] H.Hara, et al., J.Electron.Mater. 35 (2006) L11.

[2] P. V. Bui, et al. Curr. Appl. Phys., 12 (2012) S42.

[3] P. V. Bui, et al. Appl. Phys. Lett. 107 (2015) 20160.

Quantum effects of hydrogen and oxygen reactions on solid surfaces, Investigations of hydrogen and oxygen reactions on oxide surfaces and interfaces

Hideaki Kasai

1) Department of Applied Physics, Osaka University, Suita, Osaka 565-0871, Japan

2) Center for International Affairs, Osaka University, Suita, Osaka 565-0871, Japan

3) National Institute of Technology, Akashi College, Japan, Akashi, Hyogo 674-8501, Japan

4) Institute of Industrial Science, The University of Tokyo, Meguro, Tokyo 153-8505, Japan

We have studied various surface reactions with a focus on hydrogen and oxygen reactions [1,2] using supercomputer system at ISSP.

Our original code “NANIWA” has allowed us to investigate various quantum states appeared in the reactions. In addition to electronic states, which can be calculated by conventional methods, NANIWA can simulate motions of nuclei based on quantum theory. Therefore, this method is applicable to analyze quantum effects like tunneling, and has been successful to reveal hydrogen reactions at low temperatures.

In this project, we clarified the quantum states of hydrogen atom on Pd(110) [1]. Based on the potential energy surface (PES), obtained from first principles calculations, we calculated the wavefunction of hydrogen atom on the surface. The ground quantum state shows localization of the wavefunction at the pseudo-threefold (P3F) site, which is the energetically most favorable adsorption site. However, the 1st excited state exhibits the localization at the short-bridge (SB) site, although the secondary favorable adsorption site is long-bridge (LB) site. This finding clearly indicates an importance of consideration of quantum behavior in the case of hydrogen reactions.

We also investigated effects of O-vacancies on O_2 adsorption on anatase TiO_2(001) [2]. Although the stoichiometric surface does not bind an oxygen molecule, the introduction of O-vacancies, that induces redistribution of excess electrons, results in strong promotion of O_2 binding. The view obtained in this study provide us a basic understanding of chemical reactivity of anatase TiO_2(001) and clues for designing novel materials.

References

[1] A.A.B. Padama, H. Nakanishi, H. Kasai: App. Surf. Sci. **359** (2015) 687-691.

[2] N.H. Linh, T.Q. Nguyen, W.A. Diño, H. Kasai: Surf. Sci., **633** (2015) 38-45.

Analyses on atomic structure, magnetism, and electronic structure in spintronics materials and molecular magnets

Tatsuki ODA[1,2], Daiki YOSHIKAWA[2], Hiroto NAKANO[2], Naohiro KITAGAWA[2], Yosuke FUNATO[2], Masao OBATA[2]

Institute of Science and Engineering, Kanazawa University, Kanazawa, Ishikawa 920-1192

Graduate School of Natural Science and Technology, Kanazawa University, Kanazawa, Ishikawa, 920-1192

We studied the several topics involved with this project; Rashba's effect of surface, magnetic anisotropy and its electric field effect in the thin film related with spintronic devices, and magnetic effects in molecular system. We also developed a method of van der Waals density functional (vdW-DF) approach for magnetic systems. These investigations have been done by employing the home-made density functional code, which has run efficiently in the architectures in Systems B and C in ISSP.

Rashba's effect of surface

The heavy-element-covered semiconductor surfaces show a giant Rashba-type spin splitting and many experiments have been reported for spintronics applications. In particular, the surface of Tl/Si(111) has been known to show out-of-plane spin textures in the surface bands. This is novel, compared with a normal Rashba spin texture, in which the spin lies within the surface plane. However, the vertical spin configuration may be useful, because of the suppressed spin scattering. The silicon based materials are still recommended as a new material in the next generation electronics (spintronics). In these contexts, it is important to clarify electronic structures in the surface.

Rashba's effects were investigated in the systems of both PbTl/Si(111) and Tl/Si(110). The calculation of the former revealed the electronic structure and spin.

We also revealed that the surface in Tl/Si(110) has vertical spin textures at around the parts of momentum space, which corresponds to the K-bar points in the 1st surface Brillouin zone. We calculated the distribution of the surface states given at constant energies. These results agreed well with the corresponding experimental result.

Magnetic anisotropy and electric field effect

Magnetic anisotropy energy (MAE) and its EF effect were investigated in the MgO/Fe/MgO and Fe/$SrTiO_3$(STO) systems. We also investigated under layer effects of Cr on the Fe/MgO.

The Fe/STO system was found to have a perpendicular magnetic anisotropy at zero EF and the MAE was estimated be 1.12 mJ/m^2. This is less than those of the interfaces of Fe/MgO (around 1.5 mJ/m^2). Such perpendicular magnetic anisotropy is commonly observed in the interface consisting of an two-dimensional alignment of Fe-O bonds.

In the STO system, we obtained an decrease of perpendicular MAE under the positive EF caused by electron depletion at the interface. This property on MAE is different from those of theoretical data and available experimental

data of the Fe/MgO interfaces and their family systems. Such difference may be devoted to a future research work for clarifying the origin on the response of EF. The interface Ti atom was found to play an important role in the electronic structure, where the orbital hybridization forms between 3d orbitals on Fe and Ti atoms. These effects never exist in the Fe/MgO systems. We discussed effects of in-plane lattice constant in both electronic structure and MAE, by comparing them with those of Fe/MgO.

The slope against for the external EF variation was estimated to be −7.28 fJ/Vm. Using the dielectric constant ε_r of STO, the MAE may be evaluated with the formula of $-7.28\ \varepsilon_r$ fJ/Vm for the present case. If one can keep a large ε_r in a real device under a large bias-voltage, the EF effect on MAE becomes very large and a candidate of materials for the EF driven magnetization. This is because the ε_r possiblely amounts to 30−300.

Charged six-coordinate Fe porphyrin complex

Properties on electronic structure in an Fe-porphyrin (FeP) complex with the proximal imidazole (Im) ligand, a model of active moiety of hemeprotein for analyzing bonding- and separating-processes of dioxygen molecule (O_2), were studied with the spin-polarized density functional theory. It was found that in the ionized model, the bonding stability of O_2 was reduced by one order in energy compared with that of the neutral model, implying existence of the state having a large fluctuation between bonded and separated configurations [1]. We proposed a microscopic scenario on O_2 dissociation phenomenon in terms of spin-crossover and allosteric mechanism.

Van der Waals density functional approach

The van der Waals density functional (vdW-DF) approach was developed for the spin polarized system. The development was tested in the oxygen systems of molecules and solids [2,3].

In the calculations of H-type oxygen molecular pair, the potential curve dependence of the functional parameters defined in a van der Waals density functional with spin-polarization-dependent gradient correction (vdW-DF-SPDGC) was investigated. These parameters were introduced to reduce the stability of antiferromagnetic interaction between oxygen molecules, so that using the set of optimal choices the resulting magnetic interaction was found to give more improved structural parameters in solid oxygen, compared with the functionals developed in the previous work. The finding in this work farely enabled to tune the magnetic interaction between ferromagnetic and antiferomagnetic interactions in density functional approach.We discussed general features of the functionals. The structural parameters of solid oxygen were improved in some choices of the potential parameters. It was also found that our treatment reduced both the binding and magnetic energies in the solid oxygen, indicating that the energy functional was improved for describing the energetics of spin-polarized vdW systems. Although the new approach developed in this work has parameters in the present stage, further investigation on the correlation energy functional may reveal applicability and limitation for an application range on real material.

[1] N. Kitagawa et al., Chem. Phys. Lett. **643** (2016) 119.
[2] M. Obata et al., JPS Conf. Proc, **5** (2015) 011011.
[3] M. Obata et al., Phys. Procedia. **75** (2015) 771.

DFT study on electron transfer and ionic transport at solid-liquid and solid-solid interfaces

Yoshitaka TATEYAMA

International Center for Materials Nanoarchitectonics (WPI-MANA), National Institute for Materials Science (NIMS), 1-1 Namiki, Tsukuba, Ibaraki 305-0044; Elements Strategy Initiative for Catalysts & Batteries (ESICB), Kyoto University, Goryo-Ohara, Nishikyo-ku 615-8245.

Transformation of energy management systems via success of efficient utilization of renewable energy and CO_2 zero emission is an urgent challenge in our society. To step toward its realization, development of larger batteries and next-generation solar cells has been extensively addressed. However, establishments of high-efficiency techniques as well as high reliability are not satisfactory yet for practical implementation. In the field of batteries such as lithium ion battery (LIB), safer electrolyte and high-performance film at the electrolyte-electrode interface to prevent the thermal runaway, in addition to the higher energy density, have been crucial issues. Perovskite solar cell (PSC) emerging quite recently still has problems such as the poor durability for its practical use. Due to the difficulty in experimental observations, these atomistic mechanisms are still open questions.

We addressed such issues with well-optimised first-principles calculations. In the studies on LIB, we demonstrated the reductive decomposition mechanism of electrolyte molecules and the subsequent processes of the decomposed products for solid electrolyte interphase (SEI) films formation, which overturns the conventional understandings. (Fig. 1a) [1]. Furthermore, we theoretically elucidated the electrochemical stability of highly-concentrated lithium salt electrolyte solution and the origin of its excellent transport characteristics[3)]. In the studies on PSC, the stability of surface and interface of the perovskite material and the probable cation diffusion in addition to the anion were theoretically demonstrated for the first time. Then, the possible degradation mechanism and how to control it was proposed as well (Fig. 1b) [2]. We are still keeping intensive collaborations with the experimentalists as well as the industries, and solving crucial issues for fundamental science and industrial application on the atomic scale. In the near future, our computational researches may play a decisive role in the transformation of energy management in our society.

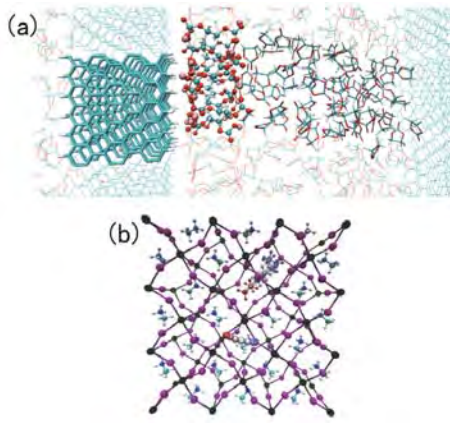

Fig. 1 (a) SEI film model in LIB. (b) Diffusion processes of anions & cations in PSC.

References

[1] K. Ushirogata, K. Sodeyama, Z. Futera, Y. Okuno, Y. Tateyama: J. Electrochem. Soc. **162** (2015) A2670-2678.

[2] J. Haruyama, K. Sodeyama, L. Han, Y. Tateyama: J. Am. Chem. Soc. **137** (2015) 10048-10051.

.

Materials design toward spin-valleytronics by using ferroelectric oxides

Kunihiko YAMAUCHI
ISIR-SANKEN, Osaka University, Ibaraki, Osaka 567-0047

When the bulk inversion symmetry us broken, spin-orbit coupling lifts the spin degeneracy of the electronic bandstructure, as leading to spin-splitting of bands known as Dresselhaus and Rashba effects. This phenomenon is typically realized at surface of interfaces where its structure breaks inversion symmetry. Alternatively, it has been recently proposed that bulk Rashba effect can be induced in ferroelectric structure, additionally providing a nonvolatile ferroelectric functionality. In this case, the spin polarization is strongly bound to spin polarization and, as such, allows for its full-electric control.

Recently, the spin-valley coupling has been studied in graphene and transition-metal chalcogenide such as MoS_2, where the valleys at the corner K points of the Brillouin zone is coupled with the spin degree of freedom. The coupling could be used in future valleytronic devices in which both the valley and spin polarized carriers have information. In order to propose new spin-valley-coupling system, we designed a new ferroelectric oxide heterostructure $BiAlO_3$/$BiIrO_3$ grown along the [111] direction. In this system, $BiIrO_3$ forms a bilayer, where Ir^{3+} ion is aligned in a corrugated graphene-like honeycomb lattice. Between a wide energy gap made by $BiAlO_3$, Ir-d^6 state is split into $P3$ crystal field states, as pushing up $3z^2 - r^2$ orbital level just below the Fermi energy. Since the orbital state is $m = 0$, it is further split into $j_z = \pm\frac{1}{2}$ states under spin-orbit coupling. This band is strongly spin-polarized at K point, because the three-fold rotation at K point allows the s_z state as the basis. Finally, we confirmed that the spin polarization is coupled with the structural ferroelectric distortion, which enables the control of the spin polarization by the external electric field. Interestingly, it is also found that the in-plane spin texture of Ir d state is transformed by flipping electric polarization. This is because the heterostructure has two different distortion, i.e. polar distortion and tilting of oxygen octahedra. The former is responsible for the out-of-plane spin polarization, whereas the latter modifies the in-plane spin polarization significantly.

We proposed a prototype of the ferroelectric spin-valley material by ab-initio materials design approach. We hope that the phenomenon will be confirmed by experiments and the spin-valley coupling property will be optimized by future works. The detail of the present work will be found in a reference[1].

References

[1] K. Yamauchi, P. Barone, T. Shishidou, T. Oguchi, and S. Picozzi: Phys. Rev. Lett. **115** (2015) 037601.

Theoretical Study on Electronic Structure of Bathocuproine: Renormalization of the Band Gap in the Crystalline State

Susumu Yanagisawa
Department of Physics and Earth Sciences, University of the Ryukyus
1 Senbaru, Nishihara, Okinawa, Japan 903-0213

Bathocuproine (BCP) is a well-known organic material of a hole blocking layer in organic light-emitting diodes and an electron buffer layer in organic photovoltaics (Fig. 1). The nature of the unoccupied electronic states is a key characteristic of the material, which play vital roles in the electron transport. In terms of the molecular orbital or the band structure, the roles played by the frontier energy levels such as the highest occupied molecular orbital (HOMO) and the lowest unoccupied molecular orbital (LUMO) levels are of importance, by which the carriers are transported in the solid or across the organic-organic or organic-inorganic interfaces.

To elucidate the electronic properties of the molecular or crystalline BCP, we use the *GW* approximation for calculation of the crystalline band gap[1]. We obtain the fundamental gaps of the gas and the crystalline phases with the one-shot self-energy correction denoted by G_0W_0 using the *GW* space-time method[2]. We use PBE eigenfunctions and eigenvalues as a zeroth-order starting point. For the band energies of the crystalline BCP, we use the plane wave cutoff energies of 60 Ry and 24 Ry for the static Hartree-Fock exchange ($\Sigma_{\rm x}$) and the dynamical *GW* correlation ($\Sigma_{\rm c}$), respectively. For the sum over unoccupied bands in the calculation of the Green's function required to calculate the *GW* correlation, we employ 4,852 unoccupied bands for the crystalline band energy (102 eV above the middle of the band gap). By the estimation of the convergence with respect to the number of the summed bands ($N_{\rm b}$) based on the fit to a linear polynomial of $1/N_{\rm b}$, we confirm that the calculated band gap is deviated from the extrapolated infinite $N_{\rm b}$ limit by 0.1–0.2 eV. We determine the GGA-PBE orbital energies of the gas phase relative to the vacuum level using the dipole correction, align the PBE band gap of the single crystal to the center of the PBE gas phase gap, and thus obtain the crystalline ionization potential (IP) and electron affinity (EA) within GGA-PBE. For the EA and the IP at the G_0W_0 level of theory, the fundamental gap is aligned to the center of the gap obtained with GGA-PBE. In other words, we assume that the self-energy corrections to the HOMO and LUMO levels with GGA-PBE are the same.

It is found that the band gap of the crystalline BCP is 4.39 eV. The result is in agreement with the experimental band gap of 4.58 eV, which is estimated using the experimental IP and EA measured with the photoemission yield spectroscopy (PYS) and low-energy inverse photoemission spectroscopy (LEIPS) techniques, respectively[3]. The theoretical gap for the single crystal, which is smaller by 0.2 eV than the experimental, is reasonable, given that the polarization energy in the single crystal may become larger than in thin film and noncrystalline phases fabricated in experiments, with their lower molecular packing den-

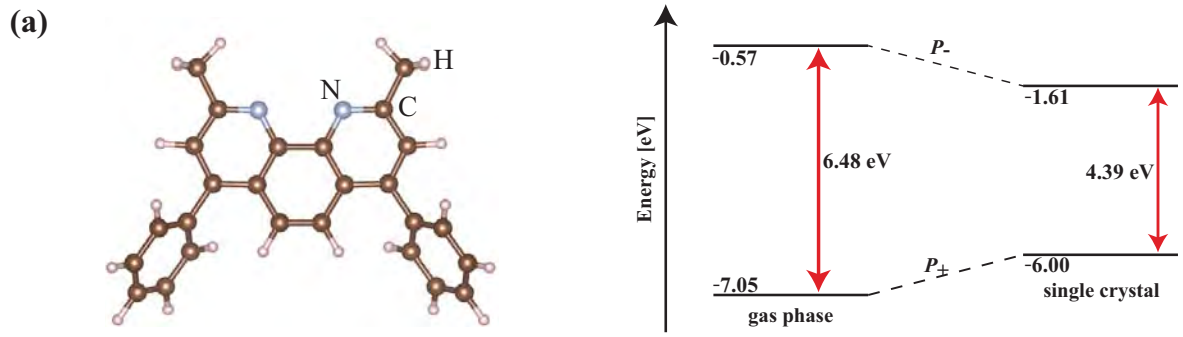

Figure 1: Schematics of (a) BCP molecule, and (b) the single crystal with the monoclinic c2/c symmetry

Figure 2: Frontier energy levels of the gas and the single crystal phases of BCP. Polarization energies on the HOMO and LUMO levels (P_+ and P_-, respectively) were assumed to be the same (1.05 eV).

sity than single crystals.

The polarization energy, obtained as the average of the polarization energies on HOMO and LUMO levels, is estimated to be 1.05 eV, demonstrating the large polarization effects induced by the electronic clouds surrounding the injected charge (Fig.2). The polarization energy of 1.05 eV is reasonable in organic solids, given a body of the polarization energies of the similar magnitude determined experimentally or theoretically, and that may be elucidated in terms of the organic crystal represented by a linear dielectric medium and the charged molecule by a hollow sphere, with a point charge put at its center[4].

The calculated IP (6.00 eV) and EA (1.61 eV) of the single crystal are in fair agreement with experimental IP (6.47 eV[3]) and EA (1.89±0.04 eV[3]). The theoretical IP is reasonably smaller than the experimental values, given that the calculation describes larger polarization in the single crystal than that in the thin-film or non-crystalline phases in the experiment. However, the calculated EA is not reasonable, in that it is smaller than the experimental value measured with the LEIPS technique[3]. We feel that the the IP and the EA should be calculated separately, rather than assume the polarization energies to be the same. Such a work is in progress.

References

[1] S. Yanagisawa, S. Hatada and Y. Morikawa: J. Chin. Chem. Soc. (Special Issue), *in press*.

[2] M. M. Rieger et al.: Comput. Phys. Commun. **117** (1999) 211; L. Steinbeck et al.: *ibid.* **125** (2000) 105; C. Freysoldt et al.: *ibid.* **176** (2007) 1.

[3] H. Yoshida and K. Yoshizaki: Org. Electron. **20** (2015) 24.

[4] N. Sato, K. Seki and H. Inokuchi: J. Chem. Soc., Faraday Trans. 2 **77** (1981) 1621.

DFT Investigations on the Electronic State Changes of Ferrocene-Terminated Self-Assembled Monolayers by Coadsorbed Species

Ken-ichi FUKUI

Department of Materials Engineering Science, Graduate School of Engineering Science, Osaka University, Machikaneyama, Toyonaka, Osaka 560-8531

Ferrocene(Fc)-terminated self-assembled monolayers (SAMs) have been widely studied in the last quarter century to reveal the electrochemical properties of chemically modified electrodes. It has been well known that the formal potential of the system strongly depends on the local environment of the Fc moiety [1]. Although electronic states of the Fc-terminated SAMs should directly affect the electrochemical properties, knowledge concerning electronic structures with respect to different local environment is very limited. In this study, we performed density functional theory calculations of Fc-terminated SAMs with different coadsorbed species to reveal the relationship between the electronic structures and the local environment of Fc moieties [2].

All calculations were carried out by using DFT as implemented in the STATE (simulation tool for atom technology) code. In a unit cell a Fc-terminated thiol molecule (C5Fc) was coadsorbed with three matrix thiols possessing different terminal functional groups (C4 and C4X: X= OH, CN, and -Br) on Au(111) consisting of 12 Au atoms at the surface as shown in the inset of Fig. 1.

After structure optimization for the mixed SAMs, the HOMO level localized on Fc moiety, work function (W) of the SAM, and electrostatic potential at the Fc moiety (V_{ES}(Fe)) were analyzed and the results are summarized in Fig. 1.

Whereas ΔW is positively correlated with $\Delta HOMO_{SAM}$, we found that only the C5Fc-substituted C4CN system increases the overall deviations from a dotted line. It is because the contribution of negative charge of the nitrogen atom to modulate the local electrostatic potential is compensated by the positive charge of the carbon atom. On the other hand, the fact that the average height of the nitrogen atom is higher than that of the carbon atom by 0.63 Å results in the large increase of the W value.

Instead, the $HOMO_{SAM}$ values have excellent correlation with V_{ES}(Fe). This analysis indicates that the energy shifts of the HOMO-related state are practically determined by V_{ES}(Fe) felt by the central iron atom in the Fc moiety.

While the structures of these systems are practically indistinguishable, HOMO-related states were found to largely shift due to the difference of the local electrostatic potential at the central iron atom in the Fc moiety.

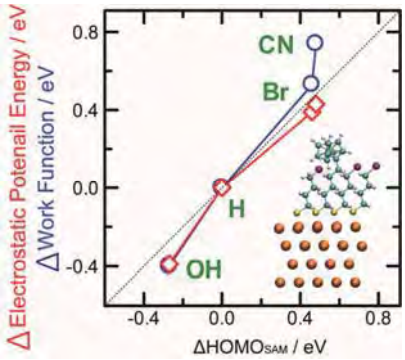

Fig. 1: Comparisons between electronic properties and $HOMO_{SAM}$ of C5Fc-substituted SAMs with various coadsorbed molecules.

References

[1] Y. Yokota, Y. Mino, Y. Kanai, T. Utsunomiya, A. Imanishi, M. Wolak, R. Schlaf , K. Fukui: J. Phys. Chem. C **118** (2014) 10936.

[2] Y. Yokota, S. Akiyama, Y. Kaneda, A. Imanishi, K. Inagaki, Y. Morikawa, K. Fukui: J. Phys. Chem. C, in press.

Spin-orbit coupling parameters at surfaces and interfaces of semiconductors: first-principles study

Fumiyuki ISHII
Faculty of Mathematics and Physics, Institute of Science and Engineering, Kanazawa University, Kanazawa, 920-1192, Japan

Spin-orbit coupling is key ingredient in the spintronics applications. The examples includes the Rashba-type spin-orbit coupling in the Datta-Das type spin field effect transistor (Spin-FET) where the spin direction of the electrons participating in the electric current could be controled by the gate voltage. The Rashba coefficient is an important parameter that determines the performance of the Spin-FET. In addtion, in recent years, the Rashba spin-orbit coupling is also quite important for the conversion between charge and spin currents.

In this study, by using OpenMX code[1], we have performed first-principles calculations on Zincblende structure III-V semiconductors and its heterostructures such as GaAlAs/GaAs and InAlAs/InAs with different orientations, (001) and (110).

Table I shows calculated Rashba parameters of valence band top for III-V semiconductors, its heterostructures and ZnO[2]. The calculated values are in the same order of magnitude compared to the experimental one, 90 meV·Å for InAs/GaSb, 40 meV ·Å for InGaAs/InAlAs and 72 meV ·Å for $In_{0.53}Ga_{0.47}As/In_{0.52}Al_{0.48}As$. The origin of Rashba parameters is the strength of atomic spin-orbit coupling constant ruled by atomic numbers.

We have also evaluated spin distribution in momentum space by using our developed post-processing code for OpenMX code, SOfield[3]. The origin of spin textures is built-in electric field, i.e., electric polarization. In order to analyze the electric polarization in the heterostructures and superlattice system, we have calculated the layer polarization evaluated by one-dimensional Wannier functions.

Table 1: Calculated Rashba paraemters α_R for III-V semiconductors, its (001) orientation heterostructures, and ZnO[2].

Materials	α_R(meVA)
AlP	–
AlAs	0.27
AlSb	1.22
GaP	14.66
GaAs	19.24
GaSb	9.42
InP	79.51
InAs	43.47
InSb	41.81
$(InP)_4/(GaAs)_4$	206.29
$(InP)_4/(InAs)_4$	795.57
ZnO	1.15

References

[1] T. Ozaki et al., http:// www.openmx-square.org/

[2] M.A.U. Adhib, H. Kotaka, F. Ishii and M.Saito, Appl. Phys. Express, **7**, 053002 (2014).

[3] H. Kotaka and F. Ishii, http://cphys.s.kanazawa-u.ac.jp/~lab-ishii/SOField/index.html

First-Principles Calculation of Spin-Orbit Field and Thermopower

Fumiyuki ISHII
Faculty of Mathematics and Physics, Institute of Science and Engineering, Kanazawa University, Kanazawa, 920-1192, Japan

We are interested in how to achieve much higher thermoelectric (TE) conversion efficiency by effectively manipulating electron-spin degree of freedom. As one possibility, we have been studying the contribution of the anomalous Hall conductivity (AHC) in TE power. Previously, we have shown quite large effect of AHC in a massive Dirac fermion model [1]. While seeking for novel systems that exhibit much larger AHC, hopefully leading to a favorable TE performance, we have noticed recent reports illustrating large AHC in some crystals of whirling spin textures, among which we taget the 2D skyrmion type case " *skyrmion crystal* " (SkX) here. We have performed first-priciples calculations of TE properties of some model SkXs, evaluated via an efficient method based on the interpolation of the ab-initio electronic band structure with Wannier functions (localised orbitals) realized by employing two open-source packages, namely, OpenMX[2] and Wannier90[3]. Our findings[4] include: (i)Larger size of unit skyrmion makes AHC larger [e.g. exceeding $12 \times e^2/h$ for 6×6 size, while limited up to $6 \times e^2/h$ for 4×4]. (ii) The larger AHC leads to larger transverse (anomalous Nernst) voltage in some filling (Fermi-level) range. As our future task, we hope to find good TE materials among skyrmion systems, by applying the above ab-initio method to realistic crystals.

We also studied thermoelectric properties of pyochlore iridate system as follwoing. Candidates for the ground state of pyrochlore iridates $A_2Ir_2O_7$ include various phases of metals, normal insulators, topological insulators and Weyl semimetals[5], accompanying diverse magnetic structures originating from the $4f$-electrons of A-ion and Ir $5d$-electrons. Regarding the transitions between some of these phases and transport properties there, discrepancies exist between the findings of different research groups. As a basic step in solving those problems and better understanding this series of compounds, we have investigated their electronic structures from first-principles using OpenMX package[2]. We have revealed, for the case of A=La, how its band-structure evolves as one of the structural parameters x (oxygen Wyckoff position) is varied. In addition, the behavior of its thermopower, a band-structure-sensitive quantity, is revealed. Since the variation of x and also the other one, i.e., lattice constant) can be viewed, for example, as corresponding to different A-ion species, our results give us information on how the A-ion affects each compound's band structure.

References

[1] Y.P. Mizuta and F. Ishii, JPS Conf. Proc. **5**, 011023 (2015).

[2] T. Ozaki et al., http:// www.openmx-square.org/

[3] A.A. Mostofi et al., Comput. Phys. Commun. **185**, 2309 (2014).

[4] Y.P. Mizuta and F. Ishii, arXiv:1601.03510.

[5] F. Ishii et al., J. Phys. Soc. Jpn. **84**, 073703 (2015).

Development and Application of First-Principles Simulation of Material Structure and Electronic Properties

Shinji TSUNEYUKI
Department of Physic, School of Science, The University of Tokyo
Hongo 7-3-1, Bunkyo-ku, Tokyo 113-0033
Institute for Solid State Physics, The University of Tokyo
Kashiwanoha 5-1-5, Kashiwa, Chiba 277-8581

First-principles electronic structure calculation based on the density functional theory (DFT) has been successfully used not only in the analysis of material structures and their electronic states but also for theoretical prediction of material properties, yet there are many problems remaining: (1) accuracy and reliability of the calculation, (2) calculable system size, (3) treatment of non-equilibrium dynamics, (4) exploration of complicated structure like amorphous or interfaces, etc. We have developed various simulation methods with or beyond DFT calculation to solve the parts the problems. Our achievements in FY2015 are summarized below.

Lattice thermal conductivity is a key parameter for thermoelectric materials, while its estimation needs accurate calculation of anharmonic force constants responsible for phonon-phonon scattering. Previously we developed a general method of calculating anharmonic force constants efficiently with first-principles molecular dynamics simulation, with which we calculated lattice thermal conductivity of various materials [1, 2]. We improved the method by the sparse modeling technique to obtain reliable results. Furthermore, we introduced the self-consistent-phonon approach to treat highly anharmonic lattice: the method is applicable even when the material has imaginary phonon modes with ordinary harmonic approximation. With the method, we succeeded in quantitative calculation of the temperature dependence of the soft phonon mode and the lattice thermal conductivity of $SrTiO_3$ in the high-temperature cubic phase (Fig.1) [3].

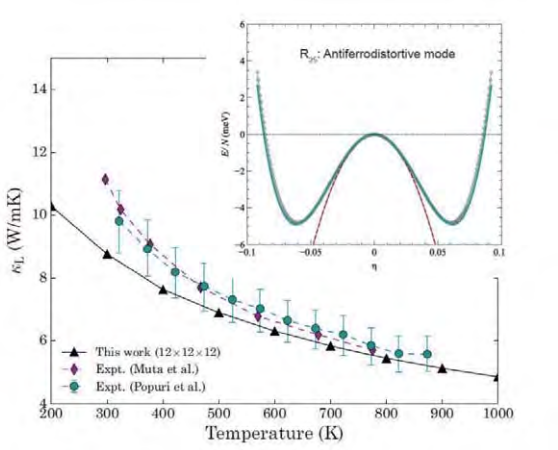

Figure 1: Temperature dependence of the lattice thermal conductivity of cubic $SrTiO_3$. The computational result is compared with experimental values reported by Muta et al.(J. Alloys Compd. 392, 306 (2005)) and Popuri et al. (RSC Adv. 4, 33720 (2014)). Lines are shown to guide the eye. (Inset) Potential energy surface for the deformation of the soft mode. The dotted line is the harmonic potential fitted at the symmetry center.

Development of the first-principles elec-

tronic structure theory for strongly correlated electrons is also one of our important activities, for which we have long investigated the first-principles transcorrelated (TC) method for periodic systems. We newly implemented an interative scheme for the solution of the TC self-consistent equation and succeeded in drastic speed-up of the calculation. With the new code, we examined the effect of atomic core states to the valence band structure by including the highly localized core orbitals [4].

Computational time of the DFT calculation usually scales as N^3 with N being the number of atoms in the system. So-called Order-N methods, in which the system is somehow divided into small fragments, enable us to calculate total energy and atomic force with the computational cost of order N, while the energy spectrum and wavefunctions of the whole system are not accessible directly. Borrowing an idea from the linear combination of the molecular orbitals (LCMO) scheme for the fragment orbital (FMO) method [5], based on the lean divide-and-conquer method [6], we developed an efficient method to derive one-electron Hamiltonian of the whole system from the orbital energies and orbital wavefunctions of each fragment of the system [7]. We implemented the method to xTAPP, a plane-wave DFT code, to find the energy spectrum of a large system with reasonable accuracy.

Finally, we developed a method to find activation barrier for the diffusion of an impurity in semiconductors considering the change in its charge state. The method is based on the nudged elastic band (NEB) method but potential energy hypersurfaces for different charge states are considered. With the method, we discussed the stability of hydrogen impurity (H^0, H^+, H^-) in SiO_2 [8].

References

[1] T. Tadano, Y. Gohda, and S. Tsuneyuki, J. Phys.: Condens. Matter **26**, 225402 (2014).

[2] T. Tadano, Y. Gohda, and S. Tsuneyuki, Phys. Rev. Lett. **114**, 095501 (2015).

[3] T. Tadano and S. Tsuneyuki, Phys. Rev. B **92**, 054301 (2015).

[4] M. Ochi, Y. Yamamoto, R. Arita, and S. Tsuneyuki, J. Chem. Phys. **144**, 104109 (2016).

[5] S. Tsuneyuki, T. Kobori, K. Akagi, K. Sodeyama, K.Terakura, and H. Fukuyama, Chem. Phys. Lett. **476**, 104 (2009).

[6] F. Shimojo, S. Hattori, R.K. Kalia, M. Kunaseth, W. Mou, A. Nakano, K. Nomura, S. Ohmura, P. Rajak, K. Shimamura and P. Vashishta, J. Chem. Phys. **140**, 18A529 (2014).

[7] Y. Yamada, R. Akashi and S. Tsuneyuki, in preparation.

[8] Y. Yamamoto, R. Akashi and S. Tsuneyuki, in preparation.

Atomic-Scale Structure and Local Chemistry of CoFeB-MgO Magnetic Tunnel Junctions

Mitsuhiro Saito[1,2], Keith P. McKenna[3], Yuichi Ikuhara[1,2]
[1]*Advanced Institute for Materials Research, Tohoku University, Sendai, Miyagi, 980-8577*
[2]*Institute of Engineering Innovation, The University of Tokyo, Yayoi, Tokyo, 113-8656*
[3]*Department of Physics, University of York, Heslington, York YO10 5DD, United Kingdom*

Magnetic tunnel junction(MTJ)s are the most important in random access memory and spintronics-based integrated circuits. The fundamental element of a MTJ consists of an atomically thin insulating tunnel barrier sandwiched in between two ferromagnetic electrodes. A giant tunneling magnetoresistance was identified in a (001)-oriented MgO MTJ with (001) CoFe electrodes due to coherent electron tunneling of the Δ_1 Bloch states. Clarifying how each species of atom diffuses and structure changes via annealing is critical in designing optimal stacks for the fabrication process.

We employed first-principles calculations conbined with advanced electron microscopy to unravel atomic-scale structure and local chemistry of confined stacking layers in the CoFeB-MgO based MTJ which could offer direct evidence of how B diffused in the MTJs via annealing. Such combined techniques allowed us to demonstrate that B diffused out of the crystalline CoFeB into Ta interstitial sites rather than into the MgO tunnel barrier after annealing, and CoFe atomically bonded to the textured MgO grains with an epitaxial orientation relationship by forming Fe(Co)-O bonds yet with no Co or Fe incorporation in MgO [1].

Calculations were performed with the Vienna ab initio simulation package within the framework of density function theory. The projector augmented wave method was employed and the generalized gradient approximation of Perdew-Burke-Ernzerhof was used to describe exchange and correlation. The $2s$ and $2p$ electrons of O and B, $2p$ and $3p$ electrons of Mg, and $3d$ and $4s$ electrons of Co and Fe were treated as valence electrons and expanded in a plane wave basis with a cutoff energy of 400 eV. A Monkhorst-Pack grid of $9\times9\times9$ k-points was adopted on primitive unit cells and equivalent k-point densities were used for supercells (up to 513 atoms). Interface models consisted of a 10-layer Fe_3Co (001) slab connected to a MgO (001) slab of six layers. A vacuum gap of 10Å was included in the supercell to avoid unwanted interactions between the slab and its periodic images. All atoms in the slabs were fully relaxed until the magnitude of the force on each atom fell below 0.05eV/Å. We also employed a first-principles thermodynamics method to assess the tendency for B, Co, and Fe to incorporate in MgO and Ta. The B incorporation in MgO turns thermodynamically favorable only for very high or very low Fermi energies. Such capability of direct spatial and chemical analysis of the buried polycrystalline stacking layers in MTJs will deepen our understanding of the physics of MTJs.

References

[1] Z.C. Wang, M. Saito, K.P. McKenna, S. Fukami, H. Sato, S. Ikeda, H. Ohno, and Y. Ikuhara: Nano Lett., **16** (2016) 1530.

First-Principles *GW*+Bethe-Saleter Calculation for a 160 Atom System

Yoshifumi NOGUCHI

Institute for Solid State Physics,

The University of Tokyo, Kashiwa-no-ha, Kashiwa, Chiba 277-8581

Green's function is a powerful method that is capable of determining the excited energy spectra of real materials from first-principles. However, the required computational cost is much higher than that of a conventional density functional theory (DFT)-based first-principles method. For example, a GW approximation (GWA), in which the one-electron self-energy operator (Σ) is expressed as the simple product of a one-particle Green's function (G) and a dynamically screened Coulomb interaction (W), requires a computational cost that scales as $O(n^4)$, and the Bethe-Salpeter method needs the computational cost that scales as $O(n^6)$ (note that the computational cost required when using DFT scalses as $O(n^3)$). Therefore, there is a strong limitation in treatable system size.

This year, we improved our original first-principles GW+Bethe-Salpeter program of hybrid parallel version to handle 288 Intel Xeon processors (=3456 CPU cores) on a new system B and to simulate systems of 100-200 atoms without the need to further reduce theoretical accuracy. By using our program, indeed, we succeeded in simulating the UV-Vis absorption spectra of [16]CPP ($C_{96}H_{64}$, see Fig. 1, the atomic geometry optimized for the ground state by B3LYP/cc-pVTZ). The simulated spectra were compared with the available experimental spectra. The agreement is fairly good, in particular, in terms of peak position and overall peak shape. Indeed, we newly introduced a method for exciton analysis that is based on a two-particle picture beyond the independent particle approximation and analyzed first dark (S_1) and bright (S_n, n >1) excitons. These results will be published soon [1].

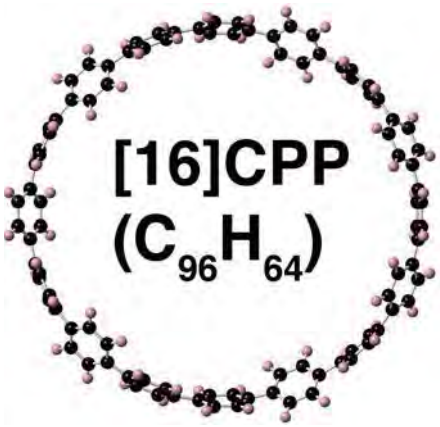

Fig. 1. Atomic geometry of [16]CPP optimized for ground state by using B3LYP/cc-pVTZ.

References

[1] Y. Noguchi and O. Sugino., in preparatio

First-principles calculation for device application of wide gap semiconductors

Mineo SAITO

Institute of Science and Technology, Kanazawa University

Kakuma, Kanazawa, 920-1192 Japan

GaN, which has a wide gap, has been attracting scientific and technological interests because of its device applications.

Hydrogen impurities have crucial effects on GaN. It is well known that hydrogen passivates acceptors. However, the understanding of mono-hydrogen impurities is still insufficient. A study based on a μSR experiment indicated that the neutral muonium in GaN induces a shallow donor level, suggesting that hydrogen should be a shallow donor [1]. On the other hand, first-principles study concludes that the mono-hydrogen has a negative-U property [2]. Theoretical analysis of the μSR experiment is necessary for clarifying the origin of the inconsistency,

The μSR spectroscopy exhibits strong anisotropy in the hyperfine structure and its origin is still unclear. In this study, we carry out first-principles calculations to clarify the origin of the anisotropy.

We find that the most stable site of hydrogen is in the trigonal channel. This stable site in the wurtzite structure is in sharp contrast with bonding and antibonding sites which were discussed in studies of diamond and zinc blend structures. We clarify that the spin density is large not only in the hydrogen site but also in the six near N sites. As a result, the spin density has a strongly anisotropic distribution in space, which is expected to be the origin of the observed anisotropic hyperfine constant.

Then, we carry out calculation of the hyperfine constant and find that the dipole-dipole interaction term induces strong anisotropy, i.e., this term is positive when the magnetic field is applied in the same direction as the c axis and is negative when the magnetic field is perpendicular to the c axis. These results are consistent with the experimental results [1].

References

[1] K. Shimomura et al., Phys. Rev. Lett., 92,135505 (2004).

[2] C. G. Van de Walle et al., Nature, 423, 626 (2003).

First Principles Study of Planar Pt Clusters Supported on Defective Graphene

Yuji HAMAMOTO
Department of Precision Science and Technology, Osaka University
Yamada-oka, Suita, Osaka 565-0871

Graphene, atomically thin two-dimensional material composed of a honeycomb lattice of carbon atoms, has drawn keen attention since its experimental realization, due to the peculiar electronic and structural properties. Nowadays, the applications of graphene to various industries have been explored extensively, among which one of the most promising candidates is the usage of graphene as a support material of metallic cluster catalysts. Experiments have demonstrated that Pt clusters deposited on graphene exhibit higher catalytic activity than on other carbon substrates such as carbon black and carbon nanotubes [1]. Similar phenomena have been observed for Pt clusters supported on highly-oriented pyrolytic graphite (HOPG) [2], in which the enhanced catalytic activity is attributed to planar cluster structures observed with scanning tunneling microscopy. Although the adsorption structures of Pt clusters on graphene has also been studied theoretically so far, such a planar cluster structure has never been reproduced on (undoped) graphene.

To explore possible planar cluster structures, we investigated Pt clusters on graphene with the Stone-Wales (SW) defects using the first principles calculation code STATE [6]. We first investigated adsorption of a Pt atom on the defective graphene with a SW defect. While the adsorption energy E_{ads} on a C–C bond of pristine graphene is -1.54 eV, we found that a C–C bond closer to the SW defect gives larger E_{ads} and we obtained $E_{\mathrm{ads}} = -2.85$ eV at the center of the SW defect. This suggests that, at finite temperature, Pt atoms diffusing on graphene are drawn into SW defects and form Pt clusters.

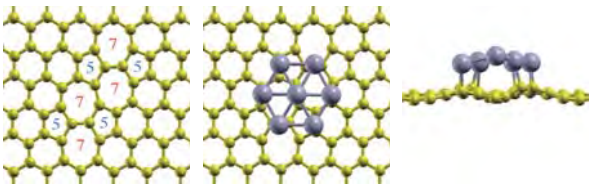

Figure 1: Planer Pt cluster structure obtained on a SW defect dimer in graphene.

To confirm whether this scenario leads to the planar cluster structure on graphene, we next examined the stability of a planar Pt_7 cluster adsorbed on SW defects. When the Pt_7 cluster was adsorbed on a single SW defect, it could not sustain the planar structure and was distorted after structure relaxation. On the other hand, the adsorption on a SW defect dimer shown in Fig. 1 was considered, it was found that the Pt_7 cluster remains planar in agreement with the experiments on HOPG [2]. Similar planar cluster structures were also obtained on a lattice completely consisting of five- and seven-membered rings, which indicates the importance of SW-type defects for the stabilization of planar cluster structures. However, these planar Pt clusters were found to be metastable and convert into spherical structures by using the finite-temperature molecular dynamics. Moreover, the dangling bonds of the planar cluster strongly bind CO molecules on the edges,

which could result in the reduction of catalytic activity of the Pt cluster. This strongly suggests that the support effect due to SW defects is not strong enough to stabilize the planar structure and enhance its catalytic activity.

References

[1] E. Yoo, T. Okata, T. Akita, M. Kohyama, J. Nakamura, and I. Honma, Nano Lett. **9**, 2255 (2009).

[2] T. Kondo, K. Izumi, K. Watahiki, Y. Iwasaki, T. Suzuki, and J. Nakamura, J. Phys. Chem. C, **112**, 15607 (2008).

[3] Y. Okamoto, Chem. Phys. Lett. **420**, 382 (2006).

[4] K. Okazaki-Maeda, Y. Morikawa, S. Tanaka and M. Kohyama, Surf. Sci. **604**, 144 (2010).

[5] T.-u. Park, Y. Tomita and T. Nakayama, Surf. Sci. **621**, 7 (2014).

[6] Y. Morikawa, K. Iwata, and K. Terakura, Appl. Surf. Sci. 169, 11 (2001).

Development and application of first-principles electron-transport simulator based on time-dependent density functional theory

Yoshiyuki EGAMI
Division of Applied Physics, Faculty of Engineering, Hokkaido University
Kita 13, Nishi 8, Kita-ku, Sapporo, Hokkaido 060-8628

Recently, numerical simulations have attracted much interest not only in fundamental science but also in industrial applications. For example, in the research and development of high-performance and high-integrated electronic devices, the electron-transport simulations of nanoscale materials play important roles. So far, many remarkable results have been reported using first-principles calculations. However, most of the calculations estimete the static characteristics of electrons in the steady state, and there remains a lot of uncertainty on the dynamic behavior of electrons flowing across the materials.

In order to examine the dynamic transport properties of the nanoscale materials, we developed the impulse response (IR) method [1] based on the real-space finite-difference approach [2] within the framework of the time-dependent density functional theory. The conventional IR method employs an algorithm for enabling efficient calculations on the assumption that the electrodes are imitated by the structureless jellium. In this subject, we attempted developing a new algorithm to treat the models sandwiched between semi-infinite crystalline electrodes. In the calculation, the time-evolution operation for an incident wave constructed by the propagating Bloch waves in the crystalline electrode is repeatedly performed. To reuse the algorithms in the conventional method, the Bloch waves are expanded by the plane wave basis set consisting of the Bloch waves in the jellium electrode.

To demonstrate the performance of the improved IR method, we carried out the time-dependent electron-transport simulations for the BN-dimer embedded graphene connected to semi-infinite graphene electrodes, where the calculations were performed with a few hundred cores on FUJITSU PREMEHPC FX10 in System C. As the results, we observed the time-dependent behavior of electrons flowing through the graphene and being scattered by the impurity potential of BN dimer. However, the flowing electrons exhibit unphysical behavior, where the time-evolved wave function is largely different from the scattering wave function in the steady state even if a sufficiently long time is passed. Challenges to resolve this problem are in progress.

References

[1] Y. Egami and K. Hirose: JPS Conf. Proc. **1**, 016012 (2014).

[2] K. Hirose *et al.*: *First-Principles Calculations in Real-Space Formalism*, (Imperial College Press, London, 2005).

Computational Design of SiC-Based Future Power Devices

Kenji SHIRAISHI

Institute of Materials and Systems for Sustainability,

Nagoya University, Furo-cho, Chikusa-ku, Nagoya, Aichi 464-8603

We clarify the intrinsic problems of SiC/SiO_2 interfaces by the first principles calculations.

We first discuss the oxidation induced C-C bond formation. O incorporation causes large bond rearrangement. Two Si-O bonds and one C-C bond are formed by breaking two Si-C bonds as shown in Fig. 1. A C-C bond causes local strain around it and it modifies the shape of internal space of NFE states. This results in the lowering of conduction band by about 100 meV, leading to the formation of interface states near conduction band bottoms.

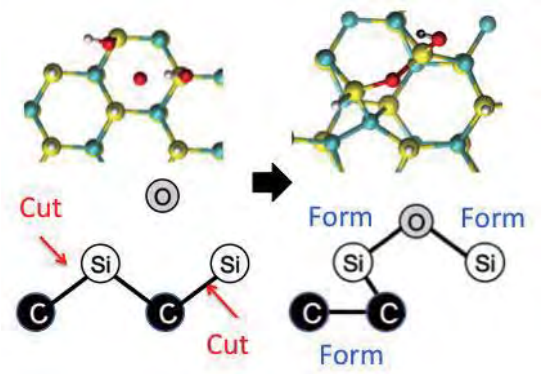

Fig.1: (a) Initial and (b) oxidized structure. O atom incorporation induces large bond rearrangement and forms C-C defects with large energy gain.

Next, we comment on the Vth instability of SiC-MOSFET caused by proton [1] It has been reported that C impurity in SiO_2 can form CO_3^- like ions [2] If proton forms complex with CO_3^- in SiO_2 as shown in Fig.2, hopping from one CO_3^- ion to another CO_3^- ion can cause Vth instability since proton act as positively charged mobile ions. This consideration coincides with recent experimental finding which indicate the existence of mobile ions in SiC-MOSFET [3].

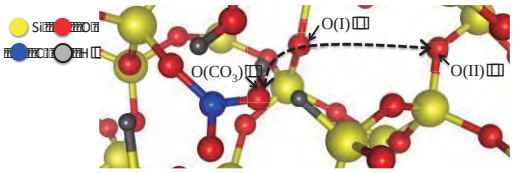

Fig.2:Atomistic structure of proton and CO_3^- ion complex and proton diffusion path.

References

[1] H. Shirakawa, M. Araidai, K. Kamiya, H. Watanabe, and K. Shiraishi, Appl. Phys. Exp. in press.

[2] Y. Ebihara, K. Chokawa, S. Kato, K. Kamiya, and K. Shiraishi, Appl. Phys. Lett., **100**, (2012) 212110.

[3] A. Chanthaphan et al. Appl. Phys. Lett. **102**, (2013) 093510.

Development of Measurement Technique of Local Optical Property and Analysis of Hydrogen Embrittlement Properties of Steel and Aluminum

Yuji KUNISADA

Center for Advanced Research of Energy and Materials, Faculty of Engineering, Hokkaido University, Sapporo, Hokkaido 060-8628

We studied the new measurement technique of local optical property and analysis of hydrogen embrittlement properties of steel and aluminum, with the aid of the first principles calculation based on the density functional theory (DFT).

At first, we investigated the optical properties of Al_2O_3 using scanning transmission electron microscopy (STEM). The dielectric function can be calculated from through Kramers-Kronig analysis of experimentally obtained electron energy-loss spectra (EELS). We have to take into account the effect of kinetic momentum transport from the incident electron beam to the electron in materials in the optical property analysis with STEM-EELS. Therefore, we calculated the electronic structure of Al_2O_3. We performed the band structure calculations using VASP code. [1] We installed parallelized VASP with Intel® MPI Library and Intel® Math Kernel Library. We found that the calculated band gap of Al_2O_3 with GGA-PBE and hybrid HSE06 functional are 6.0 and 7.4 eV, respectively. We also clarified that the effect of kinetic momentum transport is negligible because the corresponding valence band structures of Al_2O_3 near Fermi level are almost flat.

We also investigated the hydrogen atom behaviors in Fe(111) and Al(111) subsurfaces. [2] We obtained the most stable adsorption sites from the corresponding potential energy surfaces. We found that hydrogen atoms negatively charge and weakly adsorbe in both of Fe(111) and Al(111) subsurfaces through ionic bonding between hydrogen atoms and surface atoms.

References

[1] G. Kresse and J. Hafner: Phys. Rev. B **47** (1993) 558. G. Kresse and J. Hafner: Phys. Rev. B **49** (1994) 14251. G. Kresse and J. Furthmüller: Comput. Mater. Sci. **6** (1996) 15. P. E. Blöchl: Phys. Rev. B **50** (1994) 17953. G. Kresse and J. Furthmüller: Phys. Rev. B **54** (1996) 11169.

[2] Y. Kunisada and N. Sakaguchi: J. Japan Inst. Met. Mater. **79** (2015) 447.

First-Principles Calculation of Transition-Metals and Their Alloys and Compounds

Tamio OGUCHI, Masayuki TOYODA, Kunihiko YAMAUCHI,
Hiroyoshi MOMIDA, Masayuki FUKUICHI, Tetsuo TANAKA, Hiroshi KATSUMOTO
Institute of Scientific and Industrial Research, Osaka University, Ibaraki 567-0047

In this project, we study the electronic properties of several transition metals and their alloys and compounds and explore their chemical trends and effects associated with structure and symmetry. In addition, continuing developments of numerical methods related to the first-principles calculations are also pursued. In FY2015, we theoretically investigated the magnetism of the *A*-site ordered perovskite-type transition-metal oxides, the mechanical properties of hard materials such as WC, and the x-ray optical activity in noncentrosymmetric materials. Among them, results of first-principles electronic-structure calculations for the *A*-site ordered perovskites [1] are summarized below.

$YMn_3Al_4O_{12}$ (YMAO) is one of the A-site ordered perovskite oxides (Fig. 1) and its magnetic ordering is a G-type antiferromagnetic (G-AFM) arrangement of Mn^{3+} (spin S=2) determined by a neutron powder diffraction measurement. Magnetic coupling parameters between neighboring Mn ions are estimated by using total-energy calculations for several magnetic configurations. It is found that the G-AFM is stabilized by the nearest-neighboring exchange coupling J_1 mainly originating form a superexchange mechanism, not direct exchange, and exchange interactions between farther neighboring Mn ions J_2 and J_3 are also AFM but relatively small, being in consistent with the neutron experiment. Calculated mean-field Néel temperature 53.5 K is slightly higher than the experimental value (35K) and the overestimation may be partially due to the mean-field approximation. This dominant nature of J_1 over J_2 and J_3 is in striking contrast with the situation of competing J_1 and J_2 leading to the stability of the E-AFM in $LaMnO_3$, showing a difference of Mn^{3+} ions between the A' and B sites. This also sharply contrasts with the other G-AFM A-site ordered perovskite $CaCu_3Ti_4O_{12}$ (CCTO) previously studied [2]. In CCTO, J_1 between Cu ions is ferromagnetic and the stability of G-AFM originates from the third neighbor J_3 via long-range superexchange paths realized by strong Ti-3*d* and O-2*p* hybridization. In YMAO, on the other hand, the relevant Al states are far in energy from the O-2*p* preventing from sizable hopping integrals in the superexchange couplings.

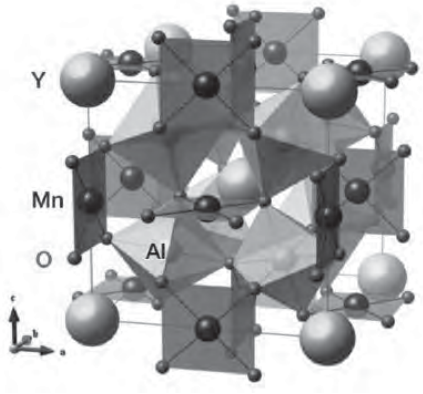

Figure 1: Crystal structure of $YMn_3Al_4O_{12}$.

References

[1] M. Toyoda, T. Saito, K. Yamauchi, Y. Shimakawa, and T. Oguchi, Phys. Rev. B **92**, 014420 (2015).

[2] M. Toyoda, K. Yamauchi, and T. Oguchi, Phys. Rev. B **87**, 224430 (2013).

DFT study of excess electrons introduced by Ti interstitials in rutile TiO_2 (110) surface

Kenji Yasuoka

Department of Mechanical Engineering,

Keio University, Kohoku, Yokohama, Kanagawa 223-8522

As a model surface of transition metal oxide, rutile TiO_2 (110) surface have been studied intensively by experiments and theories. Excess electrons are known to be important in considering the surface chemistry of TiO_2. Until recently, surface bridging-oxygen vacancy was considered to be the main source of these excess electrons, however an experimental result suggested that subsurface Ti interstitial is the main source of these excess electrons [1]. Following this result, theoretical works have revealed that Ti interstitial in bulk TiO_2 can introduce excess electrons to the surface [2, 3]. However, the behavior of these excess electrons on the surface is still unclear.

In this work, we have studied the stability of these excess electrons in rutile (110) surface theoretically using static density functional theory (DFT) and Born-Oppenheimer molecular dynamics (BOMD). It was difficult to explicitly calculate all the possible combination of Ti sites that excess electrons localize. So we performed BOMD to find Ti sites where the excess electrons are more likely to exist. We then performed over 40 DFT simulations targeting those sites. All

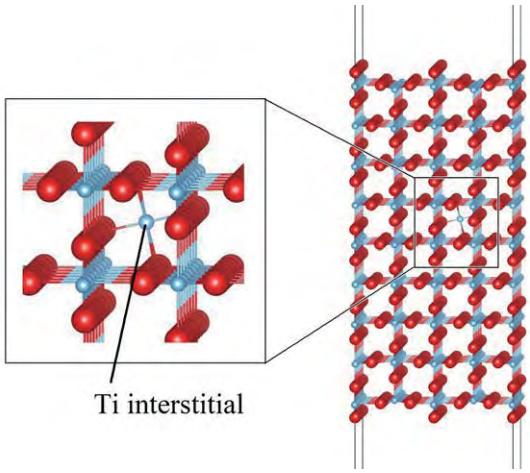

Figure 1: (right) Image of one calculation cell in a slab model, large (small) sphere is oxygen (Titanium) and (left) image enlarged near Ti interstitial

calculations were done using VASP on System B. VASP was chosen here, because it is implemented with plane wave DFT, and it is known to have high parallel efficiency. For exchange-correlation functional, PBE+U was used, which was confirmed by our previous work to sufficiently describe defect state in TiO_2 [4]. The surface was described using slab model with 649 atoms (Fig. 1). Different slab models were compared including larger slab models. Also, stability of slab models with different localization sites of excess electrons

was compared.

As a result, excess electrons introduced by Ti interstitial were more stable near the surface compared to sites near Ti interstitial. This indicates that, Ti interstitials can provide excess electrons to the surface. This result is in agreement with the experimental result by Wendt et al.

References

[1] S. Wendt, P. T. Sprunger, E. Lira, G. K. H. Madsen, Z. Li, J. Ø. Hansen, J. Matthiesen, A. Blekinge-Rassmussen, E. Lægsgaard, B. Hammer, and F. Besenbacher: Science **320** (2008) 1755.

[2] E. Finazzi, C. D. Valentin, and G. Pacchioni: J. Phys. Chem. C. **113** (2009) 3382.

[3] H. Y. Lee, S. J. Clark, and J. Robertson: Phys. Rev. Lett. **86** (2012) 075209.

[4] T. Shibuya, K. Yasuoka, S. Mirbt, and B. Sanyal: J. Phys. Condens. Matt. **24** (2012) 435504.

Theoretical Analyses on Ionic Transport Properties, Electrical Properties and Interfacial Electronic States of Nanostructures

Satoshi WATANABE
Department of Materials Engineering, the University of Tokyo
7-3-1 Hongo, Bunkyo-ku, Tokyo, 113-8656

1 Introduction

Although the properties of nanostructures have been extensively investigated in the last few decades, our understanding on them is still insufficient to design and control novel nanoscale information and energy devices. In particular, further studies on complicated situations and phenomena, such as the effects of interface between novel two-dimensional materials and substrates and ionic transport at nanoscale in metal-oxide heterostructures, are strongly desired.

Keeping the above in minds, we have been investigating these topics using theoretical analyses based on atomic/electronic level simulations, taking various nanostructures as target systems. In the followings, some of our results in the fiscal year 2015 are described.

2 Interfacial electronic properties of graphene on Si-terminated SiC

The epitaxial growth of graphene on a SiC substrate has attracted much attention because of its potential for wafer-size high mobility graphene on a high-quality insulating substrate. However, the interface electronic structure of graphene on SiC is complicated due to the strong bonding between them.

We have examined the atom-specific interfacial electronic properties of the epitaxial graphene on Si-terminated SiC substrate using density functional theory (DFT) calculation with van der Waals interaction correction [1]. In doing so, we focused on the dependence of the local electronic state on the chemical environment. The band structure projected on the respective atomic orbitals reveals that the dangling bonds of the carbon atoms in the buffer layer and uppermost Si atoms form electronic states around the Fermi level. The contribution of each atom to the dangling bond states strongly depends on the presence/absence of the interlayer Si–C covalent bond. This affects the atom-specific local density of states of the top-layer graphene through its interaction with the substrate/buffer layer, which implies that the bias voltage dependence of the scanning tunneling spectroscopy mapping image reflects the presence of the dangling bonds of the buffer layer carbon or uppermost Si atom in the substrate.

3 Electronic structure of quasi-free-standing germanene on monolayer group III monochalcogenides

Germanene has high potential as a novel electronic device material owing to high intrinsic carrier mobility, large spin-orbital interaction and small electron-phonon coupling compared with graphene and silicene. However, germanene synthesized on a substrate often loses the Dirac-cone, which involves the loss of the above fascinating properties.

We have examined the stability and electronic structures of germanene on monolayer GaS, GaSe, GaTe and InSe using the DFT [2]. We have found that the germanene keeps its buckled-honeycomb structure on all the above substrates similar to the free-standing case. In addition, germanene preserves its Dirac-cone-like band structure on monolayer GaTe and InSe. In these two cases, a small bandgap of 0.14-0.16 eV opens at the Dirac point, and the effective masses are as small as 0.05-0.06 times the free-electron mass. The estimated carrier mobility is up to 2.2×10^5 cm^2 V^{-1} s^{-1}. These results suggest that the monolayer GaTe and InSe would be promising substrates for germanene devices.

4 Cu Diffusion in Amorphous Ta_2O_5

In some of novel information and energy devices such as the atomic switch, atom diffusion plays crucial role. Atomistic simulations using reliable method such as the DFT are powerful for understanding the atom diffusion behavior at nanoscale, but performing such simulations for amorphous materials is computationally very heavy.

Considering the above, we have constructed a simplified neural network (NN) interatomic potential to predict the diffusion behavior of Cu atom in amorphous Ta_2O_5 efficiently [3]. First, the amorphous Ta_2O_5 was generated by melt quenching method with ab-initio molecular dynamics. Then one Cu atom was inserted into the amorphous Ta_2O_5 randomly, and the structure was optimized. The NN potential was constructed using the method proposed by Behler and Parrinello [4].

After training using 540 samples, the mean absolute error of energy prediction is less than 0.1 eV. Using the NN potential combined with the nudged elastic band (NEB) method, the pathways and activation energy barriers for the Cu hopping were estimated. The results agree well with those obtained from the DFT+NEB method.

References

[1] M. Kajihara, T. Suzuki, S. M. F. Shahed, T. Komeda, E. Minamitani and S. Watanabe: Surf. Sci. **647** (2016) 39.

[2] Z. Ni, E. Minamitani, Y. Ando and S. Watanabe: Phys. Chem. Chem. Phys. **17** (2015) 19039.

[3] W. Li, Y. Ando and S. Watanabe: in preparation.

[4] J. Behler and M. Parrinello: Phys. Rev. Lett. **98** (2007) 146401.

First-Principles Study of Excited Electronic States and Dynamics of Nanostructures under External Fields

Kazuyuki WATANABE, Yasumitsu SUZUKI, Elena SILAEVA, Satoshi HAGIWARA, Yoshihiro UEDA, Kazuki UCHIDA
Department of Physics, Tokyo University of Science
1-3 Kagurazaka, Shinjuku-ku, Tokyo 162-8601

In the project we investigated the following four topics this year. 1) Laser-assisted field evaporation of Si clusters by time-dependent density functional theory combined with molecular dynamics (TDDFT+MD), 2) dc-field enhanced photoexfoliation of bilayer benznene by TDDFT+MD, 3) development of first-principle non-adiabatic molecular dynamics simulation method based on the exact factorization of molecular wavefunction, and 4) spin-polarized annihilation lifetime of a positron in defective GaN by two-component DFT (TC-DFT).

1) *Laser-assisted field evaporation of Si clusters by TDDFT+MD*[**?**]: We studied laser-assisted field evaporation using the TDDFT+MD approach and including the laser as a time-dependent optical field. We have shown a drastic decrease of the HOMO-LOMO gap of a hydrogen molecule and a silicon cluster under high dc field, which is believed to be a common trend for different atomic systems and solids. The obtained photoabsorption spectra of the present systems also demonstrated strong changes with increasing the dc field. In particular, a pronounced redshift in the low-energy region was observed at high dc fields. The TDDFT+MD approach enabled monitoring the evaporation dynamics. The position and charge state of an atom evaporated from a hydrogen molecule and a silicon cluster as a function of time has been obtained under dc field without laser illumination and together with a laser field. The dc field and laser intensity conditions needed to generate the field evaporation have been analyzed and an agreement with experiments has been found. Evaporation was observed at lower dc fields when high-intensity laser is applied. The demonstrated field-induced changes in electronic and optical properties were shown to affect significantly laser-assisted field evaporation dynamics and are believed to play an important role also in other laser-assisted field emission techniques and nano-optoelectronics. The large scale TDDFT-MD calculations have been performed using System B.

2) *DC-field enhanced photoexfoliation of bilayer benznene by TDDFT+MD*[**?**]: We studied the exfoliation of bilayer benzene induced by intense laser pulse and external dc field by TDDFT+MD simulation. We showed that the dc field can accelerate the athermal photoexfoliation by dc-field induced force on one of benzene molecules in addition to the repulsive force between the benzene molecules caused by photoemission. Dc-field and photoemission lead to the increase in positive charge of benzene molecules that determines the dynamics of athermal exfoliation. The charge state of benzene is shown to be more important than absorbed laser energy during exfoliation process under given conditions of laser pulse and dc field parameters. Our theoretical study

thus demonstrated that a field-enhanced photoexfoliation can be an efficient technique for producing intact graphene sheets because dc field helps to avoid the laser-induced thermal melting and ablation of graphite. The present study also provides important insights on the field evaporation of graphite that can be an interesting and challenging problem for atom probe tomography experiments because evaporation not of individual atoms but entire monolayers of graphene is expected. The large scale TDDFT-MD calculations have been performed using System B.

3) *Development of first-principle non-adiabatic molecular dynamics simulation method based on the exact factorization of molecular wavefunction*: The exact factorization of the electron-nuclear wave function allows to define the time-dependent potential energy surfaces (TDPESs) responsible for the nuclear dynamics and electron dynamics. We are aiming to develop a novel first-principle non-adiabatic molecular dynamics simulation method based on this TDPES. To this end, we made a new algorithm that combines two methods; one is a coupled-trajectory mixed quantum-classical (CT-MQC) method, which is derived from the exact factorization and has been shown to reproduces quantum nuclear dynamics of small model systems very well, and the other is the linear response (LR) TDDFT, which is known as a very effective method to calculate the excitation energy, the nonadiabatic coupling (NAC) vectors, and the gradient of the excited state potential energy surfaces. We succeeded to formulate the algorithm, and then tested the efficiency and accuracy of LR-TDDFT calculation by our in-house code on System B. We also developed an algorithm that uses the wave-function theory instead of LR-TDDFT to calculate the excited-state properties, and made a code of it by implementing CT-MQC algorithm into SHARC code, which is a free program package of surface-hopping dynamics.

4) *Spin-polarized annihilation lifetime of a positron in defective GaN by TC-DFT*[**?**]: We determined the spin-polarized annihilation lifetime of a positron (SPALP) trapped by the Ga vacancies in GaN by TC-DFT with geometry optimization. SPALP clearly depends on the charged states of the Ga vacancies and the induced magnetization. The dependence is attributed to the overlap between the positron and electron densities at the defect. Thus, the present study proves the useful role of SPALP for probing and determining the mechanism of d^0 ferromagnetism. The calculations have been performed using System B.

References

[1] E. P. Silaeva, K. Uchida, Y. Suzuki, K. Watanabe, Phys. Rev. B**92**, 155401 (2015).

[2] K. Uchida, E. P. Silaeva, and K. Watanabe, to appear in Appl. Phys. Express.

[3] S. Hagiwara, Y. Suzuki, and K. Watanabe, Appl. Phys. Express **9**, 041001 (2015).

Structural and magnetic anisotropy analyses in Fe/Cu ultra-thin films by first-principles calculation

Yasutomi TATETSU

The University of Tokyo, Hongo, Bunkyo, Tokyo 113-0033

Magnetic thin films have been studied due to its peculiar magnetic behaviors compared to their bulk systems. These behaviors can come from structural transitions depending on the temperature and growth conditions. Fe/Cu(001) magnetic thin films have been studied for the past decades, because of their uncertain magnetic structures [1, 2]. As is well know, the ground state of Fe has the bcc structure, but the fcc-Fe, which is stable above 1184 K in general, can epitaxially grow on a Cu(001) substrate even below room temperature, since the lattice parameters of Cu (3.615Å) and fcc Fe (3.58Å) are quite close to each other. Many kinds of studies for the systems have been reported, but its ground state is controversial.

We applied first-principles calculations to the fcc-Fe/Cu(001) system using a computational code OpenMX [3] for understanding its electronic and magnetic structures. Mainly, the system B super computer was used for all calculation. Our structure model is a slab model consisting of seven Cu layers and several Fe layers capped by a 10-Å vacuum layer. According to our collinear spin calculations, an antiferromagnetic structure is stable in the 4 to 7-ML systems and a ferromagnetic coupling at the top two layers can be obtained, which is in good agreement with experimental results (see Fig. 1). We also calculated the non-collinear spin configuration, which considers the spin-orbit interaction. This calculation indicates that the spin-orbit coupling in Fe sites can be ignored due to the weakness of the orbital moments of Fe.

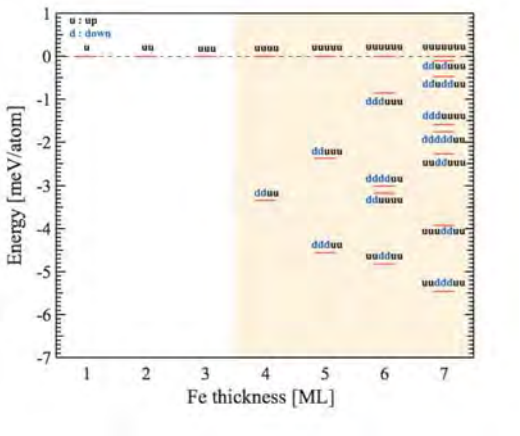

Figure 1: Energy differences of the collinear spin structures in each Fe/Cu system. Orange region indicates the antiferromagnetic states.

References

[1] H. Abe *et al.*: Phys. Rev. B **77** (2008) 054409.

[2] D. Pescia *et al.*: Phys. Rev. Lett. **58** (1987) 2126.

[3] http://www.openmx-square.org

[4] Z. Torbatian *et al.*: Appl. Phys. Lett. **104**, (2014) 242403.

Numerical studies on anharmonic phonon properties based on density functional theory

Terumasa TADANO
Department of Applied Physics, The University of Tokyo
Hongo, Bunkyo-ku, Tokyo 113-8656

Lattice anharmonicity has gained much attention in recent years because of its significant importance for characterizing various material properties. For example, SnSe is attracting strong interest because of its severe anharmonicity and ultralow thermal conductivity, which makes the thermoelectric figure-of-merit as high as ∼2.7 [1]. Strong anharmonic effect is also suggested for a superconducting sulfur hydride H_3S [2], which is associated with the large zero-point motion of hydrogen atoms. Since anharmonic effects in these materials are quite large, they cannot be treated by perturbative methods.

To model anharmonic effects of phonons nonperturbatively, we have been developing an efficient numerical approach based on density functional theory (DFT). In our method, we first extract harmonic and anharmonic force constants (FCs) from displacement-force data sets sampled with accurate DFT calculations. Using the calculated FCs, we then solve the self-consistent phonon (SCPH) equation to obtain anharmonic phonon frequencies [3].

The validity of our approach has been demonstrated for the high-temperature phase of $SrTiO_3$ [3, 4] and sulfur hydrides H_3S and H_2S under pressure [5]. We also examined anharmonic phonon properties of the high-temperature *Cmcm* phase of SnSe. Here, the DFT calculations were conducted using the Quantum-ESPRESSO package [6], and FCs were estimated using *least absolute shrinkage and selection operator* (LASSO) implemented in the ALAMODE package [7]. Figure 1 shows the anharmonic phonon dispersion of SnSe calculated using the SCPH method. As can be seen in the figure, the phonon dispersion is strongly temperature-dependent, especially for the soft mode at Y point associated with the structural phase transition. We also calculated the lattice thermal conductivity of SnSe and obtained good agreements with experimental values at high temperatures.

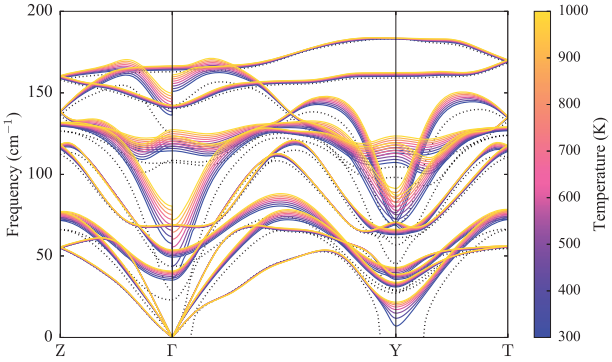

Figure 1: Calculated anharmonic phonon dispersion of SnSe (*Cmcm* structure)

References

[1] L.-D. Zhao *et al.*: Nature **508** (2014) 373.
[2] I. Errea *et al.*: Phys. Rev. Lett. **114** (2015) 157004.
[3] T. Tadano and S. Tsuneyuki: Phys. Rev. B **92** (2015) 054301.
[4] T. Tadano and S. Tsuneyuki: AIP Conf. Proc. **1702** (2015) 090063.
[5] W. Sano, T. Koretsune, T. Tadano, R. Akashi, and R. Arita: Phys. Rev. B **93** (2016) 094525.
[6] http://www.quantum-espresso.org
[7] https://github.com/ttadano/alamode

Ab initio GW calculation for low-dimensional metal $K_{0.3}MoO_3$

Kazuma NAKAMURA
Quantum Physics Section, Kyushu Institute of Technology
1-1 Sensui-cho, Tobata, Kitakyushu, Fukuoka, 804-8550

Using an *ab initio* GW calculation, we study quantitative accuracy of plasmon fluctuation in various materials. The quantum fluctuation is important in a metallic system, especially having isolated low-energy bands near the Fermi level. In the isolated-band materials, the plasma excitation can occur in this band, and then its energy scale is usually smaller than the bandwidth. In this case, the plasmon fluctuation can relevantly renormalize the bare band structure via the self-energy effect.

In this report, we present a study for the low-energy electronic structure of transition-metal oxide $K_{0.3}MoO_3$ which is a typical isolated low-energy band system. This is a typical low-dimensional metal and exhibits transition to the charge density wave state at the low temperature. In the metallic region, this material exhibits a large renormalization in the photoemission spectrum. From this observation and the quasi-one-dimensional nature, the origin of the renormalization has been discussed in view of the Tomonaga-Luttinger liquid. On the other hand, this material exhibits clear low-energy plasma edges around 0.1-1 eV in the reflectance spectra.

We study the low-energy electronic structure of $K_{0.3}MoO_3$ using our developed GW calculation code [1, 2]. We calculate density-functional band structure, maximally localized Wannier functions, reflectance spectra, and spectral functions. The crystal structure is centered monoclinic (a=9.880$\mathring{A}$, b=9.880$\mathring{A}$, c=9.894$\mathring{A}$, α=115.34°, β=115.34°, γ=45.01°) and contains 43 atoms in the unit cell. The developed code is massively parallelized, capable to treat large systems such as the present case. All calculations were done at Supercomputer center at Institute for Solid State Physics, University of Tokyo.

Figure 1(a) is our calculated density-functional band structure of $K_{0.3}MoO_3$. The isolated low-energy bands are drawn by blue dotted curves and its bandwidth is ∼1.5 eV. The panel (b) shows the maximally localized Wannier function for these isolated bands.

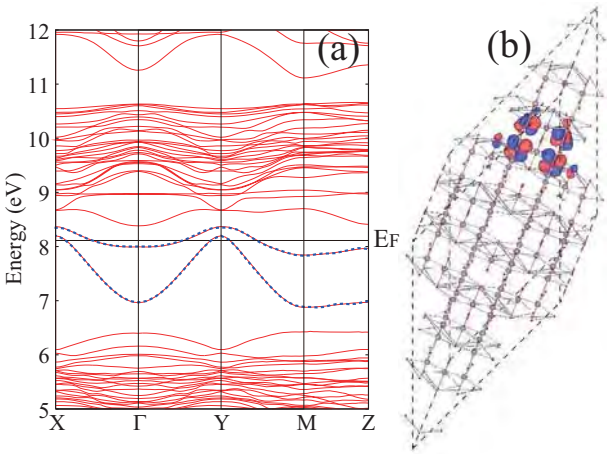

Figure 1: (a) Calculated band structure of $K_{0.3}MoO_3$, where the isolated low-energy bands are drawn by the blue dotted lines. (b) Calculated maximally localized Wannier function for the isolated bands.

Figure 2(a) compares the calculated reflectance spectra (solid curves) with the experimental data (open circles). The light-red and

dark-blue colors specify the results in the light polarization of $E\|a$ and $E\|b'$, respectively, and the a axis is the one-dimensional conducting axis. The plasma edge is found to be $\sim$1 eV.

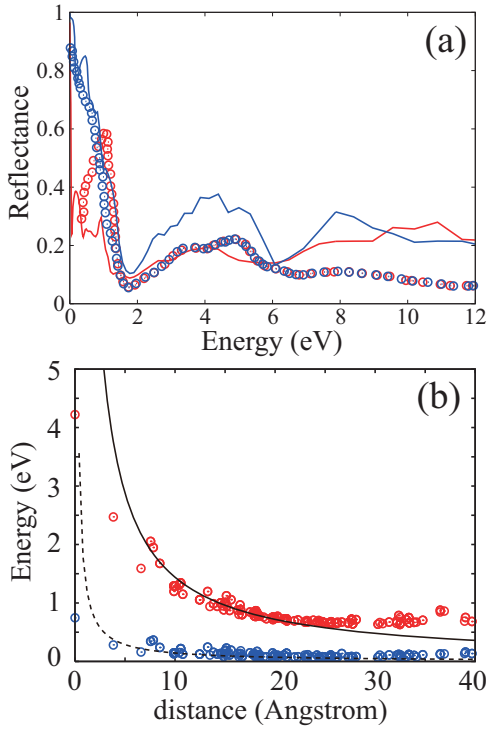

Figure 2: (a) Comparison between calculated reflectance spectra (solid curves) and experimental data (circles) of $K_{0.3}MoO_3$. (b) The calculated screened interaction with the constrained random phase approximation (dark-blue circles) compared with the bare interactions (light-red circles).

We show in Fig. 2(b) screened Coulomb interactions of $K_{0.3}MoO_3$, calculated with the constrained random phase approximation. The dark-blue and light-red circles describe effective and bare interactions, respectively. The effective onsite interaction $U - V$ is estimated as 0.59 eV which is smaller than the bandwidth and plasma excitation.

Figure 3(a) compare the calculated GW spectral function with the density-functional bands (blue solid curve). The GW spectra are basically similar to the density-functional one. We next in Fig. 3(b) the comparison among the GW (thick-red curve), density-functional theory (thin-black curve), and experiments (circles). The GW result is appreciably renormalized from the non-interacting one, thus resulting in a reasonable agreement with the experimental result.

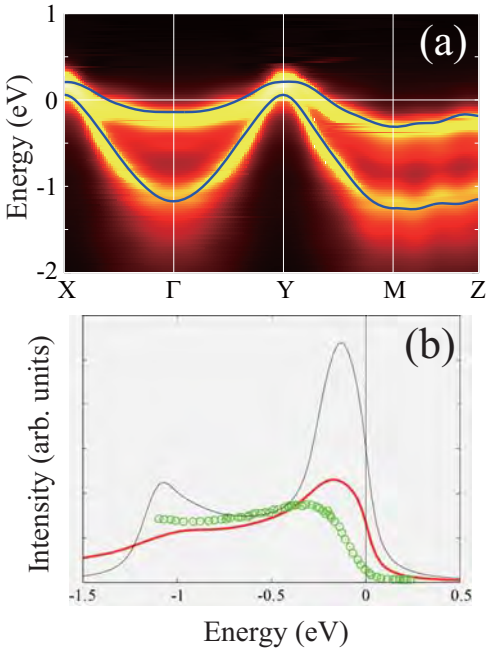

Figure 3: (a) Calculated GW spectral function of $K_{0.3}MoO_3$, where the isolated low-energy bands are superposed with blue solid curves. (b) Comparison of photoemission spectra among the GW, density-functional, and experimental ones.

In summary, we have studied low-energy plasmon fluctuation of low-dimensional metal $K_{0.3}MoO_3$. To investigate this effect on the electronic structure, we have calculated the GW spectral function, and compared it with the experimental data.

References

[1] K. Nakamura, S. Sakai, R. Arita, K. Kuroki, Phys. Rev. B 88, 125128 (2013)

[2] K. Nakamura, Y. Nohara, Y. Yoshimoto, Y. Nomura, Phys. Rev. B 93, 085124 (2016).

Parallelized ultra-large-scale electronic-structure theory based on first principle calculation and novel numerical method

Takeo Hoshi and Hiroto Imachi

Department of Applied Mathematics and Physics, Tottori University,

4-101 Koyama-Minami, Tottori 680-8550, Japan;

Large-scale electronic structure calculations were carried out by our original simulation code ELSES (http://www.elses.jp/) mainly for the structural and transport calculations of condensed organic polymers. Large-scale calculations are realized by novel massively parallel order-*N* algorithms. The transport calculations were carried out as a theoretical extension with the quantum wavepacket (QWP) dynamics simulation in which a dynamical equation ($i\,\partial_t\,\Psi = H_{\mathrm{eff}}\Psi$) is solved for a hole wavepacket based on *ab initio* based tight-binding formulations.

Figure 1 shows the preliminary result of the QWP dynamics [1][2]. The results of the organic polymer in Fig. 1(a) on calculated mobility are consistent to the experimental trend [3] in which the mobility of meta(zig-zag) type polymers is larger than that of para (linear) type polymers. Here single polymer simulations were carried out among different conditions and polymer lengths. The maximum length of polymer is 700nm or 1,000 monomer units. Figures 1(b), (c) (d) shows (b) pentacene thin film and (c)(d) a condensed organic polymer as a test calculation of condensed organic molecules. One can observe that the wavepacket progapagetes between molecules, as expected.

Related methodologies are also developed for *ab initio* transport calculation with non-equillibrium Green function theory [4] and optimal hybrid generalized eigenvalue solver for massively parallel computations [5][6].

References

[1] H. Imachi, S. Yokoyama, T. Kaji, Y. Abe, T. Tada, T. Hoshi, ‘One-hundred-nm-scale electronic structure and transport calculations of organic polymers on the K computer’, submitted, Preprint http://arxiv.org/abs/1603.09616

[2] (invited talk) T. Hoshi, ‘Massively parallel electronic structure calculations and transport property of organic materials’, Computational Chemistry Symposium of 12th International Conference of Computational Methods in Sciences and Engineering (ICCMSE 2016), 17-20, Mar., 2016, Athens, Greece.

[3] J. Terao, A. Wadahama, A. Matono, T. Tada, S. Watanabe, S. Seki, T. Fujihara and Y. Tsuji, ‘Design principle for increasing charge mobility of π-conjugated polymers using regularly localized molecular orbitals', Nat.

Commun. **4**, 1691 (2013).

[4] S. Iwase, T. Hoshi, T. Ono, 'Efficient numerical solver for first-principles transport calculation based on real-space finite-difference method', Phys. Rev. E 91, 063305, 9pp. (2015).

[5] H. Imachi and T. Hoshi, 'Hybrid numerical solvers for massively parallel eigenvalue computation and their benchmark with electronic structure calculations', J. Inf. Process. 24, pp. 164 -- 172 (2016).

[6] Eigenkernel: https://github.com/eigenkernel/eigenkernel

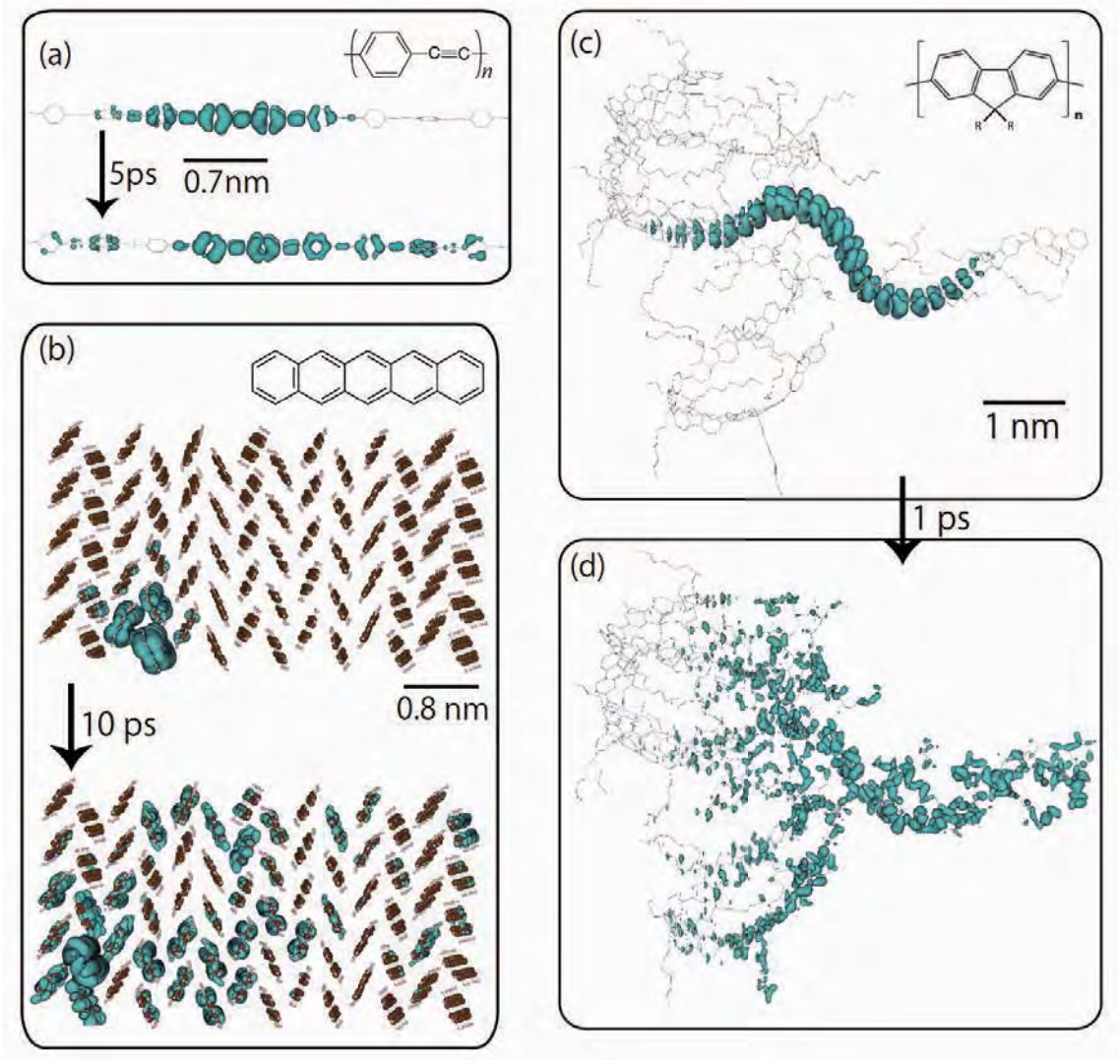

Fig. 1 Example of transport calculation of organic materials by the quantum wavepacket (QWP) dynamics[1][2]; (a) QWP dyanamics on a polymer of poly-(phenylene–ethynylene). The figre is a close-up. (b) QWP dyanamics on pentacene thin film with single layer. (c) QWP dyanamics on a condensed polymer of poly-((9,9)-dioctyl fluorene)(PFO). The three polymers in a periodic cell form an amourphous-like strcutures.

Ab-initio molecular dynamics study on organic molecules

Kazume NISHIDATE and Masayuki HASEGAWA
Faculty of Engineering, Iwate University
Ueda 4-3-5, Morioka, Iwate 020-8551

Graphene (GR) has attracted considerable attention due to its outstanding electronic, optical, thermal and mechanical properties. Recently, a particular attention has been paid to its transparency for a wide range of light frequencies since it can be used as a transparent electrode instead of the expensive tin-doped indium oxide (ITO) in the device applications. Organic semiconductors have also attracted considerable interest because of their favorable electrical properties in the development of flexible electronic devices such as the light emitting diode (LED) and the solar cells. Pentacene ($C_{22}H_{14}$, PEN) and perfluorinated pentacene ($C_{22}F_{14}$, PFP) molecules, in particular, are considered to be promising organic semiconductors due to their novel electronic properties. It has been suggested that the charge redistribution at the interfaces between the organic molecules and the substrate causes the changes in the electron energy levels and the carrier injection barrier. However, theoretical studies on the energetics of the organic molecules on GR have been a challenging subject due to the computational difficulties arising from a demand to use a large system. In this work, we investigate the energetics of the PEN and PFP molecules on GR using molecular dynamics simulation (MD) based on the density functional theory (DFT). We used the same methodology used in the DFT computation of collapsed armchair nanotube: the vdW interactions were supplemented either by the semi-empirical method (DFT-D2 and D3) or by the vdW DFT (optB86-DFT)[1].

Initially, three PEN or PFP molecules were placed on the GR in flat-laying orientation. Time step is 1 fs. We first evaluated the micro-canonical ensemble of the MD system and confirmed its energy convergence. And then the temperature was controlled at 500 K by way of the Nose method. In the Figure 1, we show the snapshot of the PFP on the GR at the 3000 time step. The coverage of the molecules on GR corresponded to roughly 1.5 ML. In all cases, a PEN or PFP molecule started to stand up with respect to the other molecule. We believe that the T-type stacking formation will lead to the herringbone structure which is typical to the molecular crystals.

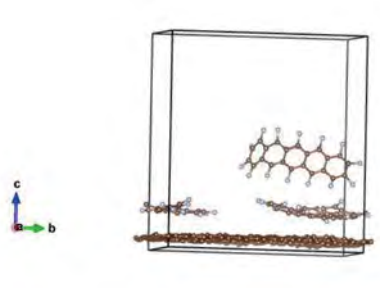

Figure 1: PFP molecules on GR.

References

[1] M. Hasegawa, K. Nishidate, and Y. Yoshimoto: Phys. Rev. B, **92** pp. 245429-1-13, 2015

Exploration of structure motifs characterizing “function” of metal oxides

Kazuto AKAGI

Advanced Institute for Materials Research,

Tohoku University, Katahira, Aoba-ku, Sendai, Miyagi 980-8577

We have explored the key motifs in metal oxides characterizing their “function” in this project. The brief summaries are as follows:

Li_2O_2 in a Li-Air battery

Li-Air battery is expected as one of the next generation batteries. In order to make it rechargeable, discharge product Li_2O_2 should be decomposed into Li^+ and O_2 during the charging process. It is known that TTF (Tetra thiafulvalene) promotes such decomposition of Li_2O_2 with the combination of DMSO solvent and nano-porous gold electrode, but its critical role was still unrevealed.

First, we performed a series of classical molecular dynamics (MD) simulations to see the formation and decomposition process of LiO_2 cluster in DMSO solvent. The parameters of force field were optimized using the information on total energies and atomic forces derived from a set of one-point first-principles calculations with rev-vdW-DF2 functional [1]. The obtained results showed a LiO_2 cluster is spontaneously decomposed under charging condition, *i.e.* at low [O_2^-] condition [2].

Thus, we focused on the decomposition of Li_2O_2 into LiO_2. Since an excess electron given to a Li_2O_2 cluster was localized, it is considered this oxidation proceeds locally. We also checked O_2^- and TTF can be oxidized to O_2 and TTF^+ on a Au(111) surface, respectively, and prepared model systems containing a cluster of Li_2O_2 or $Li_3O_2^+$ (more stable form of Li_2O_2: Li_2O_2+Li^+) with O_2 or TTF^+ in DMSO solvent. The amount of charge transfer and free-energy profile were evaluated by the first-principles MD calculations performed at 400K using a 1.7 nm cubic cell with 20-23 DMSO molecules. Thermodynamic average was done over 100 ps time evolution.

The obtained results showed the special role of TTF as a redox mediator. While O_2 oxidized only the Li_2O_2 cluster, TTF^+ was able to oxidize both the Li_2O_2 or $Li_3O_2^+$ clusters. Since “$Li_3O_2^+$” is not only stable in DMSO but also exists as a key motif in a larger Li_2O_2, we cannot avoid the release of $Li_3O_2^+$ clusters with the decomposition of Li_2O_2. TTF^+ was suppressing their accumulation and formation of byproducts, which lead to improvement of the cycle lifetime as a rechargeable battery.

Electron trapping sites in a-HfO_2

Degradation phenomena in metal-insulator-semiconductor devices are often associated with unwanted charging of the insulating layers. This stimulated efforts to understand the nature of the charge traps in polycrystalline and amorphous oxide films of HfO_2 and Al_2O_3 grown on semiconducting and metal substrates. In order to identify the character of electron trapping sites, amorphous hafnium oxide (a-HfO_2) models were generated by classical MD simulation and structure optimization by first-principles calculation using hybrid functional HSE06 were performed with extra electrons. We choose 35 structures with density in the range of 9.2-9.9 g/cm^3 in order to investigate a possible trend of property changes as a function of density.

An extra electron can be spontaneously trapped on pre-existing structural precursors like longer Hf-O bonds or under-coordinated Hf atoms. About 90% of the electron spin density was localized predominantly on two or three Hf ions sharing a three coordinated oxygen atom. Electrons were trapped in deep states in the gap at ~2.0 eV ranging from 1.0 to 2.7 eV below the bottom of the conduction band in good agreement with experimental data. These results show that the behavior of electrons in crystalline and amorphous HfO_2 is radically different as no polaron trapping has been observed in crystalline HfO_2 so far. In the next step, extraction of structural characteristics of such trapping sites is planned.

Topological data analysis

Another important aspect of this project is application of the topological data analysis based on “persistent homology”, which helps us find hidden orders in a complex system [3]. The output is obtained as a two-dimensional “persistent diagram (PD)” in which birth and death of rings or cavities are plotted. Identification of local structures around the doped Co in rutile TiO_2 and precursor structures of electron trapping site in a-HfO_2 was tried as case studies, and some potential structural motifs were obtained by classification of the PDs. Finding correlation between such motifs and “function” is now in progress.

References

[1] I. Hamada: Phys. Rev. B **89** (2014) 121103.

[2] S. Jung, F. F. Canova and K. Akagi: J. Phys. Chem. A **120** (2016) 364.

[3] T. Nakamura, Y. Hiraoka, A. Hirata, E. G. Escolar and Y. Nishiura: Nanotechnology **26** (2015) 304001.

First-Principles Study of Coercivity in Hard Magnetic Materials

Daisuke HIRAI
The University of Tokyo
7-3-1 Hongo, Bunkyo, Tokyo 113-0033

Hard magnetic materials are widely used in applications such as permanent magnets, high-density magnetic recording media, and high-frequency electromagnetic wave absorbers. Until now, the high coercivity has been realized by using rare metals with large spin-orbit interactions. Recently, however, their shortage and price increase require us to design hard magnetic materials with no use of rare metals.

Keeping the above in minds, we investigated the magnetocrystalline anisotropy (MCA) of the rare-metal-free magnetic materials from first principles. In the following, some of our results in the fiscal year 2015 are described.

Understanding the MCA at each atom is crucial to identify weak parts for possible nucleation cores of magnetization reversal, which leads to the designing of hard magnetic materials. In general, however, the MCA is given for an entire phase of a material. To examine the local MCA, we developed the method to locally analyze the MCA on the basis of the second-order perturbation theory on spin-orbit interaction [1, 2].

Using this method, we calculated the MCA of ε-Fe_2O_3 in terms of the effect of a single oxygen vacancy as an example [2]. As a result, we obtained an increase in the magnetocrytalline anisotropy energy (MAE) due to a single oxygen vacancy. Our local MAE analysis also showed that two Fe sites near the oxygen vacancy dominantly contribute to the change. In addtition, by decomposing the MAE contributions from respective orbital components for Fe atom nearest to the vacancy, we clarified that the spin-orbit coupling between occupied $3d^{\downarrow}_{x^2-y^2}$ orbital and unoccupied $3d^{\downarrow}_{xy}$ one gives the largest contribution to the MAE enhancement. This enhancement can be understood as follows. First, among the matrix elements related to the selection rule in the perturbation, $\langle d^{\downarrow}_{x^2-y^2}|V_{\rm SO}|d^{\downarrow}_{xy}\rangle = i\xi$, is largest, where ξ is the spin-orbit coupling constant. Second, a sharp peak as the dangling-bond state in occupied $3d^{\downarrow}_{x^2-y^2}$ states appears due to the vacancy, the appearance of which near the Fermi level is also significant to the MAE enhancement. Indeed, our Mulliken charge analysis confirmed the large increases in the number of states for $3d^{\rm occ.}_{x^2-y^2,\downarrow}$ and $3d^{\rm unocc.}_{xy,\downarrow}$ from 0.20 and 0.79 to 0.62 and 0.89, respectively. We also examined the effect of an interstitial hydrogen on the MAE, and showed that the contribution of Fe site nearest to the oxygen bonding with the hydrogen is dominant for the MAE enhancement. Moreover, our analysis has been applied to the relatively large-scale complicated system such as a $Nd_2Fe_{14}B/Nd_4O$ interface model and we clarified the importance of the MCA of Fe atoms as well as that of Nd atoms [3].

References

[1] Z. Torbatian, T. Ozaki, S. Tsuneyuki, and Y. Gohda, Appl. Phys. Lett. **104**, 242403 (2014).

[2] D. Hirai, S. Tsuneyuki, and Y. Gohda, in preparation.

[3] Y. Tatetsu, private communication.

Theoretical analysis of electrochemical interfaces by first-principles calculation and statistical approach

Yasunobu ANDO
Department of Materials Engineering,
The University of Tokyo, 7-3-1 Hongo, Bunkyo-ku, Tokyo, 113-8656

A new, large family of atomic-layered materials found in 2011; called MXenes ($M_{n+1}X_n$) synthesized from MAX phases ($M_{n+1}A_nX_n$) have attracted increasing attention as promising candidates for new types of electrode materials in secondary batteries.

First of all, we studied basic properties of functinalized Ti_2C that is the simplest MXene compound by using first-principles simulations [1]. Our results reveals that oxygen terminated Ti_2C: Ti_2CO_2 is insulating with an indirect band gap of 0.44 eV. Upon atomic adsorption of H, Li, or Na, Ti_2CO_2 becomes metallic. This metal–insulator change may be used to produce switching devices with a high on/off ratio and low energy consumption by controlling ionic movement, as in ion batteries.

We also investigated the feature of the electric double-layer potential at the electrochemical interface

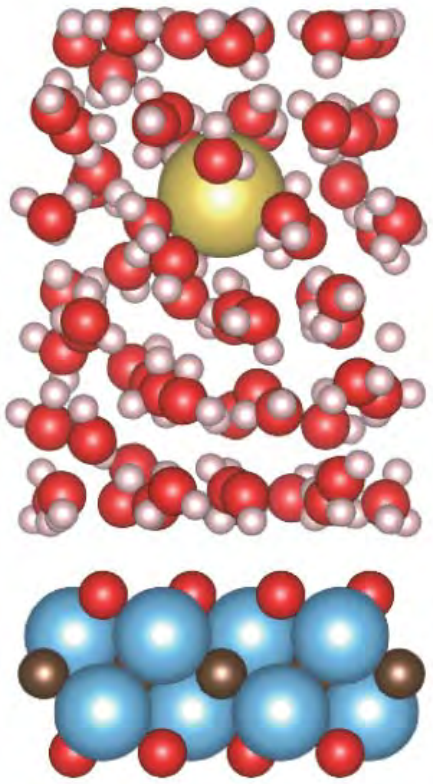

Fig. 1 Structure model of Ti2CO2-sodium solution interfaces

models of functinalized Ti_2C shown in Fig. 1. We found that the depedence of the potential drop on the surface functionalizations.

References

[1] 1. Y. Ando, and S. Watanabe, Appl. Phys. Express **9**, 015001 (2016).

Defect generation at metal/semiconductor interfaces: stability and ionization diffusion

Takashi NAKAYAMA
Department of Physics, Chiba University
1-33 Yayoi, Inage, Chiba 263-8522

Germanium (Ge) is expected as a promising material for post-Si high-speed devices because of its high carrier mobility. It was found very recently that metal/Ge interfaces have many defects; defect density around interface is 2-3 order larger than in bulk Ge, which promotes serious degradation of semiconducting properties. However, it has not been clarified why so many defects exist at metal/Ge interfaces. One purpose of the present project is to answer this question by the first-principles calculations. On the other hand, metal/semiconductor interface is not stable for a long time and changes its structure by metal-atom diffusion. The most serious case occurs at metal/SiO_2 interface; the application of voltage promotes meta-atom diffusion and induces large leakage currents. The other purpose is to clarify the effects of applied voltage on interface structure changes. In this report, we show some of the results.

We first consider the defect generation around metal/Ge interfaces, which is simulated by using repeated slab geometry as shown in Fig.1(a). Figure 1(b) shows calculated formation energies of Ge vacancy defect at Al/Ge interface as a function of distance from interface. The formation energy far from the interface, about 2.3eV, corresponds to values in bulk Ge. It is noted that the formation energy gradually increases with increasing the distance from interface to inner layers around 10Å, thus existing some transition region. Using these energies and assuming Boltzmann distribution, we can estimate the vacancy density as shown in the inset. The density increases and is 10^2-10^5 times larger around interface than in inner layers, which is in good agreement with recent experiments.

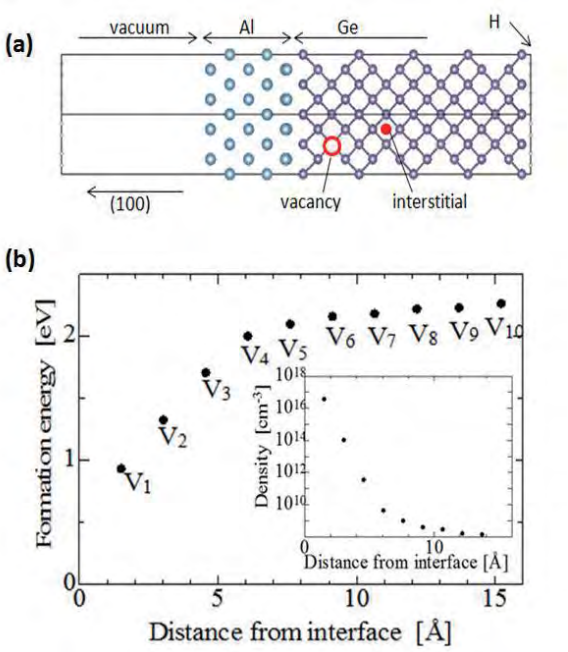

Fig.1. (a) Repeated slab model used in this study. (b) Calculated formation energies of Ge vacancy defect around Al/Ge interface as a function of distance from interface. Inset shows estimated vacancy density.

Then, we explain why defect density increases around interface. By analyzing electronic states, we found that the vacancy-related defect state is localized only around vacancy when the vacancy is located far from interface. On the other hand, when the vacancy is located near interface, we can see the hybridization between vacancy-related state and metal-induced gap states (MIGS), which correspond to evanescent states of metal Al. Owing to this hybridization, the formation energy of vacancy becomes smaller near the interface. We have also analyzed formation energies of various defects such as interstitials together with varying metal kinds and interface orientation and found that the same scenario is applicable; the defect density is large around the

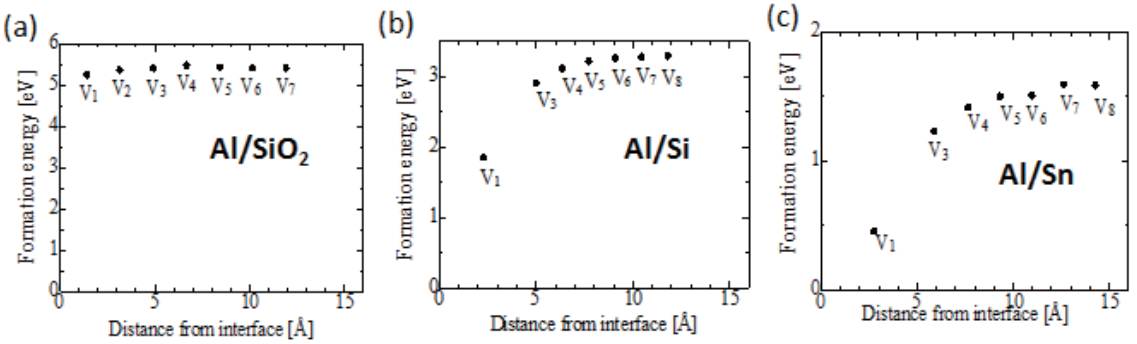

Fig.2. Calculated formation energies of vacancy defect as a function of distance from interface for (a) Al/SiO_2, (b) Al/Si, and Al/Sn (100) interfaces.

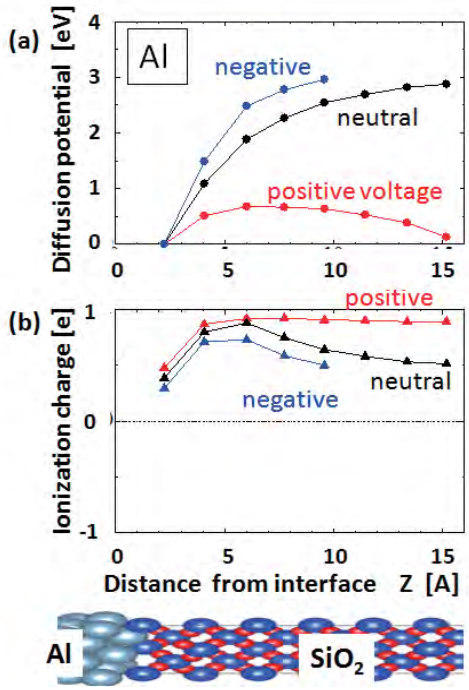

Fig.3. (a) Calculated potential of Al-atom diffusion from Al/SiO_2 interface into SiO2 layers and (b) ionic charge during the diffusion, for cases of neutral and positive/ negative voltage applications. Bottom panel shows atom positions at Al/SiO_2 interface.

interface due to the hybridization of defect states with MIGS.

To demonstrate the important roles of MIGS, we calculated formation energies of vacancy for various Al/semiconductor (insulator) interfaces. The results are shown in Figs.2(a)-2(c). It is clearly seen that the width of transition region increases with going from SiO_2 having 9.0eV band gap to Sn with about 0eV gap. This is because the penetration length of MIGS into semiconductor layers is roughly proportional to the inverse of band-gap energy of semiconductor.

Finally, we consider the metal atom diffusion into SiO_2 under the electric field. Figure 3(a) and 3(b) show adiabatic potential and ionic charge of Al during the diffusion around Al/SiO_2 interface when neutral and positive/negative voltages are applied to Al layers. It is clearly seen that Al atom is positively ionized and the potential barrier into SiO_2 layers remarkably decreases in case of positive voltage application, which well explains observations. Even when negative voltage is applied, on the other hand, because Al atom is still positively ionized in SiO_2, the potential barrier increases and the diffusion into SiO_2 is remarkably suppressed.

All these calculations were performed using the xTAPP and VASP codes. In order to realize calculations for the present interface systems, because the system is made of a large number of atoms (200-500 atoms) and one has to consider a variety of atom configurations during metal-atom diffusion, the advanced computing facility having higher-speed CPU (more than 100G Flops), larger-size memory (around 100GB), larger-size strange (more than 1.0TB), and a multi-task operation is indispensable. These conditions are never prepared in personal research laboratory. Only the present super-computing system of the ISSP can realize these calculations.

First-principles analysis on the strain effect on the thermoelectric properties of nanomaterials

Junichiro SHIOMI

Department of Mechanical Engineering,

The University of Tokyo, 7-3-1, Hongo, Bunkyo-ku, Tokyo, 113-8656

Since interfacial thermal transport determines device performance, its analysis is of importance in the thermal management technology. While extremely high/low thermal boundary conductance is demanded for heat dissipation/thermal insulating device, thermal switching material, whose thermal conductivity can be tuned by an external force, is also required. Here an approach that has been recently paid attention is applied elastic strain in namomaterial. Different with bulk, it is known that one can apply large elastic strain to the nanomaterials without large lattice defect and dislocation. The impact of uniform elastic strain to heat conduction has been evaluated by molecular dynamics method, and it has been confirmed that an elastic strain as high as 20% can be applied [1]. In addition to this, recent theoretical study on local elastic strain in MoS_2 suggests that local elastic strain changes band structure of charge carrier locally, and it is possible to manipulate electric property of entire material [2].

In this work, in analogy to manipulation of electrical property of nanomaterial by local elastic strain, we have analyzed phonon transport in graphene under the presence of local and large elastic strain by means of the atomistic Green's function (AGF) method [3].

In order to locally apply elastic strain, we have considered the tapered graphene structures as shown in the inset figure in Fig. 1. For the structure, we have performed AGF method to calculate phonon transmission functions, $\zeta(\omega)$. Figure 1 shows frequency-dependent $\zeta(\omega)$ of tapered graphenes with different conditions. When comparing pristine (black line) and tapered structure (blue line), phonon transport is strongly suppressed by chocking structure, which results in the 50% reduction of thermal boundary conductance (G_{TBC}) at room temperature (G_{TBC}=3.5 and 1.8 W/m^{2}K for pristine and tapered structures, respectively). Next, we have calculated $\zeta(\omega)$ of tapered graphene with local strain (brown line). Here the local strain was introduced by pulling both ends of tapered graphene. After this process, it was found that 0.5% uniform strain leads to the 10% local elastic strain.

As seen in Fig. 1, high-frequency $\zeta(\omega)$ is suppressed, nevertheless, obtained G_{TBC} is as small as 1.2 W/m^{2}K because high-frequency phonons are not well excited at room temperature. In addition to this, by performing AGF calculation for the pristine with artificial strain (green line), it was found that low-frequency $\zeta(\omega)$ is not affected by large local strain. To summarize, we have investigated large local elastic strain to heat conduction in material for thermal switching device. Despite the local strain is as high as 10%, its impact to heat conduction is relatively small since the chocking structure is dominant in the reduction of thermal boundary conductance.

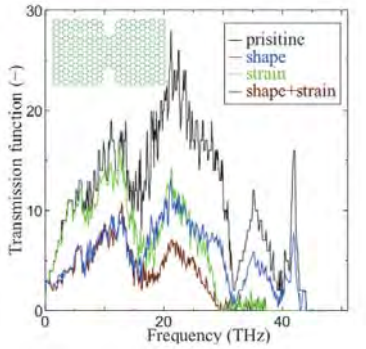

Fig. 1 Frequency-dependent phonon transmission functions, $\zeta(\omega)$, of graphenes with different conditions. Inset shows the tapered graphene structure.

References

[1] Z. Guo, *et al.*, *Appl. Phys. Lett.* **95** (2009).
[2] J. Feng, *et al.*, *Naature Photonics*, **6** (2012).
[3] W. Zhang, *et al*., Numeriacal Heat Transfer, **51**, (2007).

First-Principles Study on Device Properties of Emerging Phase-Change Memory Devices

Masaaki Araidai

Institute of Materials and Systems for Sustainability, Nagoya University
Furo-cho, Chikusa-ku, Nagoya, 464-8603

Toward a realization of high-speed and low power non-volatile memory, a new type of phase change RAM (TRAM) has been examined intensively [1]. The high-resistive state (HRS) and low-resistive state (LRS) of TRAMs are switched by the movement of Ge atoms (Fig.1(a)). We showed that the movement of Ge atoms in TRAMs was enhanced by carrier injections [2]. Recently, it has been found that TRAMs consisting of Ge_xTe/Sb_2Te_3 superlattice with Ge deficiency have higher speed operation and lower switching power than stoichiometric $Ge_{1.0}Te/Sb_2Te_3$ superlattice TRAMs [3]. However, the conventional theoretical models for TRAMs [4] cannot rationalize the improvement in switching properties of Ge-deficient TRAMs.

In this study, we investigated on-off switching properties of Ge_xTe/Sb_2Te_3 superlattice TRAMs by first-principles molecular dynamics simulation. We prepared a stoichiometric $Ge_{1.0}Te/Sb_2Te_3$ superlattice and a Ge-deficient $Ge_{0.44}Te/Sb_2Te_3$ superlattice. The atomic and electronic structures were calculated by VASP code [5], which is based on the density-functional theory. The set operation was simulated by heating and hole injection. On the other hand, the reset operation was simulated by heating only (Fig. 2).

Our simulations showed that high-speed and low power switching operations can be realized in Ge-deficient TRAMs. Ge atoms at the interfaces between the GeTe and Sb_2Te_3 become the conduction channel (Fig.1(b)). Thus, the presence of Ge atoms at these interfaces determines the resistance of TRAMs. Moreover, we confirmed that Ge vacancies in the GeTe layer enhance the Ge mobility, leading to low power and high-speed memory operations of Ge-deficient TRAMs. We also found that the resistance of the LRS can be controlled by changing the number of injected holes during the set operation.

This work was performed in collaboration with LEAP. It was funded by the “Ultra-Low Voltage Device Project" and supported by METI and NEDO.

References

[1] M. Tai, et al., VLSI Technology (VLSIT), 2015 Symposium on, T96-T97 (2015).
[2] S. Kato, et al., Solid State Devices and Materials, A-3-1 (2013).
[3] N. Takaura, et al., 2014 IEEE International Electron Devices Meeting, 29.2.1-29.2.4 (2014).
[4] J. Tominaga, et al., Jpn. J. Appl. Phys. **48**, 03A053 (2009).
[5] G. Kresse and J. Hafner, Phys. Rev. B **47**, 558 (1993).

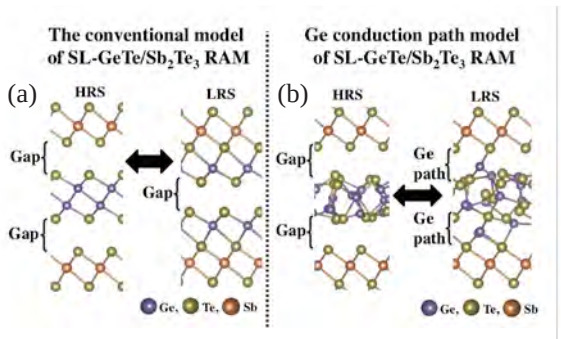

Figure 1: (a) Conventional HRS and LRS models of TRAM and (b) Ge-conduction channel models.

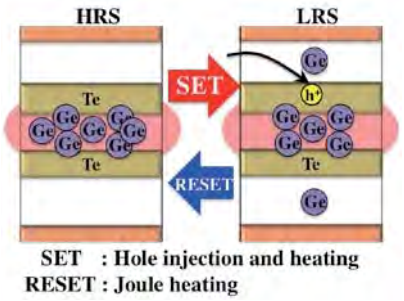

Figure 2: On-off switching is simulated by carrier injection and heating in first-principles molecular dynamics.

Magnetization in Twisted Bilayer Ribbons of Graphene

Kazuyuki Uchida
Department of Physics, Kyoto-Sangyo University

Magnetic structures in twisted bilayer ribbons of graphene have been explored by our first-principles calculations based on the density-functional theory (DFT) within the local-spin-density approximation (LSDA).

It has been known that peculiar electron states appear at zigzag edges of graphene ribbons [1]. The energy levels of the zigzag-edge states are located near the Fermi level. They are shown to be magnetized by LSDA calculations [2].

When two graphene ribbons are stacked, interactions between them lead to splitting of the energy levels of the zigzag-edge states, and the energy scale of the splitting depends on the stacking pattern of the ribbons [3]. This infers that magnetization of the edge states in twisted bilayer ribbons of graphene also reflects the stacking pattern of the bilayer.

To make this point clear, in this work, we have calculated magnetic structures in twisted bilayers ribbon of graphene with changing the twist angle between them. Thousands of atoms must be calculated for this purpose. We have used the real-space DFT (RSDFT [4]) code to perform such ultra-large-scale spin-density calculations.

A result of our calculations is shown in Fig.1, showing that the stacking pattern of the bilayer influences the magnetization: The magnetization is localized at the AB-stacking edge; The AA-stacking edge is not magnetized. Our results show that magnetic structures of systems can reflect Moiré patterns in the systems.

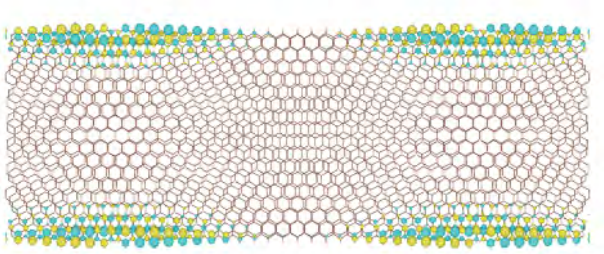

Figure 1: Magnetization in a twisted bilayer ribbon of graphene, reflecting the Moiré pattern in the system.

References

[1] M. Fujita, K. Wakabayashi, K. Nakada, and K. Kusakabe, J. Phys. Soc. Jpn. bf 65, 1920 (1996).Y. Miyamoto, K. Nakada, and M. Fujita, Phys. Rev. B 59, 9858 (1999). 10.1103/PhysRevB.59.9858.Y. Niimi, T. Matsui, H. Kambara, K. Tagami, M. Tsukada, and H. Fukuyama, Phys. Rev. B 73, 085421 (2006).

[2] S. Okada and A. Oshiyama, Phys. Rev. Lett. 87, 146803 (2001).

[3] E. S. Morell, R. Vergara, M. Pacheco, L. Brey, and L. Chico, Phys. Rev. B **89**, 205405 (2014).

[4] J.-I. Iwata, D. Takahashi, A. Oshiyama, B. Boku, K. Shiraishi, S. Okada, and K. Yabana, J. Comput. Phys. **229**, 2339 (2010).

Doping effects on Light Absorption of Light-harvesting Molecules: ab initio Molecular-Dynamics Study

Satoshi Ohmura

Research Center for Condensed Matter Physics,

Department of Civil Engineering and Urban Design,

Hiroshima Institute of Technology, 2-1-1 Miyake, Saeki-ku, Hiroshima 731-5193

Doping effect on optical response of a molecular graphene with covalently linked fullerene [the hexabenzocoronene (HBC)-triethylene glycol (TEG)–C_{60} molecule], a building block in a self-assembled supramolecular solar cell, has been explored by using *ab-initio* theoretical simulations. In HBC-TEG-C_{60} system, C_{60} attracts electron as electron transport layer whereas the HBC attracts hole as hole transport layer after irradiation of the light to the HBC.

We have evaluated HOMO/LUMO energy gaps and light absorption spectra of the HBC-TEG–C_{60} doped with B, N, O and F in the HBC. The substitutional doping affects the relative energies of the HBC significantly leading to broader spectrum of light absorption. Especially in O-doped case, maintaining the staggered structure of the HOMO/LUMO relationship between the HBC and C_{60} and narrow HBC gaps are identified. In order to investigate effects of the HOMO/LUMO levels modified by the O-doping on carrier dynamics, we have performed a nonadiabatic quantum-mechanical molecular-dynamics simulation that incorporates electronic transitions through a surface-hopping approach.

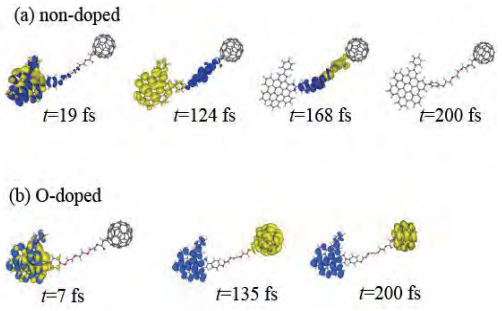

Fig. 1: Time evolution of the spatial distributions of the charge densities for quasi-excited electron and hole for non-doped (a) and O-doped (b) systems.

Figure 1 shows the time evolution of the spatial distributions of the charge densities for quasi-excited electron and hole for non-doped (a) and O-doped (b) systems obtained from the simulation. The simulation demonstrates that doping oxygen into HBC enhances the charge mobility after charge separation in HBC-TEG-C_{60} super molecule.

References

[1] S. Ohmura, K. Tsuruta, F. Shimojo, and A. Nakano: AIP advances **6** (2016) 015305

Large scale calculations on the fundamental processes of solar cells and their optimization in conversion efficiency

Koichi YAMASHITA

Department of Chemical System Engineering,

The University of Tokyo, Hongo, Bunkyo-ku, Tokyo 113-8656

Hydrogen production by splitting water with photo(electro)chemical system has been attracting many interest as it is sustainable way of solar energy. The oxygen evolution reaction (OER) is the key in water-splitting system because large part of overpotential is caused by OER. We studied electrocatalyst/water interfaces for OER by focusing on (i) pH and electrode potential dependent RuO_2/water interfacial structure, and (ii) electrode potential dependent Schottky-type barriers at n-type Ta_3N_5/water for efficient hole transfer.

First, interfacial structures of RuO_2/water under given electrode potential and pH are examined. As models for interfacial structures, RuO_2(110) is selected, and the formal valence of surface Ru atoms and orientations of water molecules are varied. In this manner a total of almost 100 configurations were modeled. All the calculations were performed using GPAW with the ASE simulation package. The GGA/RPBE functional and PAW method were employed with F4cpu and F36cpu queues. Based on the calculations of interfacial Gibbs energy as functions of both pH and electrode potential, surface Pourbaix diagram is generated. As a result, a significant structural difference is found between pH values of 0 and 14[1]. Next, interfacial band diagram on Ta3N5/water as a photoanode for photoelectrochemical water-splitting is discussed. For the examination of the interfacial Schottky barrier height under given electrode potential, Ta_3N_5 (6.5×1×1) supercell with explicitly introduced ice-like water molecules is employed with F36cpu, F18acc and F72acc queues. From the calculations of the position of valence band in bulk, position of valence band at the surface, and semiconductor barrier height at given electrode potentials, it is clearly shown that the interface of n-type Ta_3N_5/water shows the intermediate behavior between band edge pinning and Fermi level pinning. Consequently, the importance of surface modification is addressed from a viewpoint of utilizing the Schottky barrier height to get a driving force for charge separation.

References

[1] E. Watanabe, J. Rossmeisl, M. E. Björketun, H. Ushiyama, and K. Yamashita: *J. Phys. Chem. C*, **120** (2016) 8096-8103.

First principles calculation of point defects in electrodes of solid oxide fuel cells

Akihide Kuwabara

Nanostructures Research Laboratory,

Japan Fine Ceramics Center, Atsuta-ku, Nagoya, Aichi 456-8587

In complex oxides, considering the Gibbs' phase rule, more than one degree of freedom remain, even when the material is in a single phase at constant temperature and oxygen partial pressure. This means a variation of the cation composition leads to a variation of the oxygen nonstoichiometry, consequently material properties. In this study, we investigated how the cation nonstoichiometry influences the oxygen nonstoichiometry from theoretical points of view. For this purpose, perovskite-type oxide $SrFeO_{3-x}$ was chosen as a model oxide, and first principle calculations were performed on this oxide. Based on our preliminary calculations, $Sr_2Fe_2O_5$ (x = 0.167) was chosen as a target material.

Total energy calculations were carried out using VASP code. Plane wave cut-off energy was set to be 400 eV. We used the GGA-PBE type of an exchange-correlation potential. GGA+U approach was applied to 3d orbital of Fe and Hubbard U potential was set to be 5.4 eV. For calculations of point defects, supercell models of 2×1×2 unit cells of $Sr_2Fe_2O_5$ composed of 144 atoms were constructed. An oxide ion vacancy, an excess oxide ion, a cation vacancy were separately introduced into the supercell and defect formation energies were calculated according to the formalism reported by Zhang and Northrup [1]. In two-phase co-existing states, the chemical potentials of cations can be defined. Thus the chemical potentials of the components in Sr and Fe excess conditions can be determined, and consequently formation energies of defects can be calculated. From the calculated formation energies of defects together with the electrical neutrality conditions, the concentrations of defects in Sr and Fe excess conditions can be evaluated.

The calculated concentrations of oxygen vacancy [Vo], interstitial oxygen [O_{int}] and electron hole [h] as a function of oxygen partial pressure at 900 K are given in Fig. 1. Interstitial oxygens are estimated as dominant defects. However there were no significant differences in the defect concentrations between Sr and Fe excess conditions, especially in relatively higher pO_2. This is inconsistent with the results observed in the measurements of the oxygen nonstoichiometry, that is, the oxygen content was relatively larger in Sr excess than Fe excess conditions [2]. The assumption used for the calculation must be reconsidered and improved to reveal the influence of the cation nonstoichiometry on the defect structure.

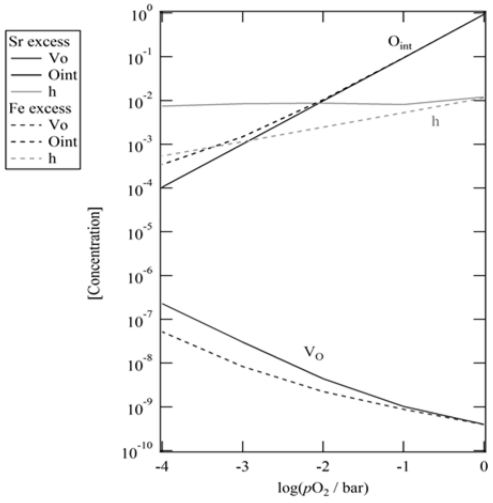

Fig. 1: Concentration of interstitial oxygen "O_{int}", oxygen vacancy "Vo", and electron hole "h" in $Sr_2Fe_2O_5$ at 900 K.

References

[1] S. B. Zhang and J. E. Northrup, *Phys. Rev. Lett.*, **67** (1991) 2339.

[2] Y. Okamoto, *et al.*: *20th Int. Conf. Solid State Ionics (SSI-20)*, Keystone, USA, (2015)

First-Principles Molecular Dynamics Simulations of Water Dissociative Adsorption at Stepped Pt Surface and at SiC–Pt Interfaces

PHO VAN BUI, TAKUYA NISHITANI, HIDETOSHI KIZAKI, KOUJI INAGAKI, and YOSHITADA MORIKAWA

Graduate School of Engineering,

Osaka University, 2-1, Yamada-oka, Suita, Osaka 565-0871

Water interaction with Pt surface plays important roles in many catalytic surface reactions, corrosion processes, and electrochemistry. Recently, intact adsorption and dissociation of water on flat Pt have been extensively studied by both experiments and simulations [1, 2]. A recent study on adsorption and dissociation of water at the edge of Pt(211) surface showed that the dissociation energy is about 0.5 eV for a monomer, 0.2 eV for a dimer, and nearly zero in the case of a trimer [3]. Moreover, water adsorption on a stepped Pt(111) surface, which is observed after deposition of Pt by X-ray diffraction [4] and commonly occurring in realistic situations, is not well understood.

Recently, Isohashi and co-workers [5] reported experimentally that silicon carbide (SiC) surface can be etched by just water with the presence of Platinum (Pt) as a catalyst. The results suggested that Pt plays an essential role in the catalytic reaction of water and SiC. To clarify the mechanism of the reaction and role of Pt as a catalyst, in this study, we use first-principles simulation tool for atom technology program package (STATE) to elucidate the adsorption and dissociation of water on a stepped Pt(111) surface and at Pt/SiC interface. The calculations are based on the density functional theory within a generalized gradient approximation of Perdew et al. Barrier height is evaluated by means of climbing image nudged elastic band method [6].

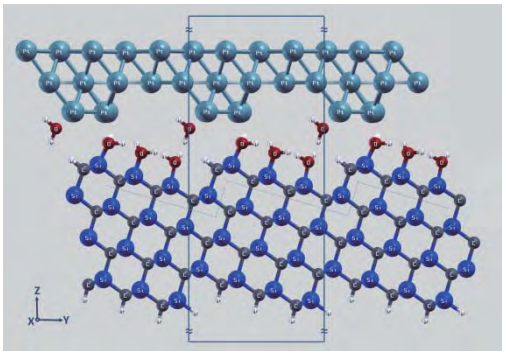

Fig. 1: 3C-SiC(111) and Pt(111) surfaces in the simulation model. The box showed a unit cell.

A stepped Pt(111) surface composed of 3-layer slab, in which the two topmost layers are kept fixed to mimic the bulk. A step-and-terrace 3C–SiC (111) surface was used as a model for the simulation as shown in Fig. 1. The model is periodically repeated unit cells of four bi-layers. During the simulations, the two topmost atomic layers

with terminated surface atoms were allowed to fully relax, while the remaining atoms were kept fixed to maintain the substrate structure.

In this study, we focus on the reaction pathways and reaction barriers of the interaction between water molecules and OH-terminated step edge Si with the present of platinum (Pt) catalyst in the calculation model. The adsorption of water on a stepped Pt surface is preferentially at the step edge of Pt, stabilized by the effect of chemical bonds with Pt and hydrogen bonds. The atomic geometries at initial state (IS), metastable state (MS) & final state (FS), and energy profile of the water dissociative adsorption on the edge of the Pt (111) surface are shown in Figs. 2 and 3, respectively.

Fig. 2: Atomic geometries of the water dissociative adsorption on the edge of the Pt (111) surface at IS, MS, and FS.

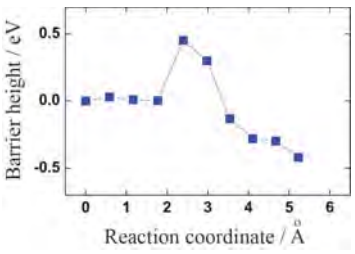

Fig. 3: Energy profile of the water dissociative adsorption on the edge of the Pt (111) surface

The results show that the barrier height of the water dissociation on the edge of Pt(111) surface is about 0.5 eV, which is about 0.3 eV lower than that on a terrace site [2].

With the presence of the SiC, the results show that the activation barrier of the water dissociation at the SiC–Pt interface affected by the distance of the Pt and SiC surfaces. The shorter distance between Pt and SiC surfaces, the smaller the barrier height. The adsorption and dissociation of water at Pt/SiC interface play important roles in etching of SiC in water.

After the water dissociative adsorption, the OH group may transfer to the topmost Si atom and break the Si–C bond. The activation energy and reaction pathway are now under investigation.

References

[1] A. Hodgson et al., Sur. Sci. Reports **64**, (2009) 381-451.

[2] J. L. Fajín, et al., J. Phys. Chem. A **118**, (2014) 5832-5840.

[3] D. Donadio et al., J. Am. Chem. Soc. **134**, (2012) 19217-19222.

[4] T. Aoltonen et al., Chem. Matter. **15**, (2003) 1924.

[5] Isohashi et al., Mater. Sci. Forum **778–780** (2014) 722.

[6] Henkelman et al., J. Chem. Phys. **113** (2000) 9901.

First-principles calculations of iron solid solution effects on the lattice thermal conductivity of lower mantle minerals

Haruhiko DEKURA

Geodynamics Research Center

Ehime University, 2-5 Bunkyo-cho, Matsuyama 790-8577, Japan

Iron-bearing Bridgmanite (Mg,Fe)SiO_3 is believed to be the most constituent mineral in the earth's lower mantle. Determination of the phonon transport property, *i.e.*, lattice thermal conductivity (κ), of the material should be therefore a key to understanding the dynamics and evolution of the earth's deep interior. Lattice anharmonicity owing to the phonon-phonon interaction strongly relates the phonon transport. The primary purpose of this project in this period is to determine the anharmonic properties of the iron-bearing system at deep mantle pressure conditions.

We have performed density-functional theoretic calculations combined with the LDA+*U* method [1] and have extracted the large number of anharmonic force constants (AFC) by higher order derivatives of the adiabatic potential surface [2]. All of the calculations were performed using the QUANTUM-ESPRESSO package [3]. The simulation cell of $(Mg_{0.9375},Fe^{2+}_{0.0625})SiO_3$ that includes totally 160 atoms was adopted in this study. The ferrous iron was treated in the high spin state ($S = 2$).

During this period, by the use of supercomputer (system B), we have almost finished the determination of the 3rd order AFC at 100 and 150 GPa relevant to the Earth's lowermost mantle conditions. Those obtained AFC will be analyzed and used for evaluation of the phonon lifetimes, combining with harmonic phonon properties determined also by the real-space method. The phonon lifetimes and thus κ are known to very sensitive to the choice of a mesh for the Brillouin zone integration, and we normally need a dense mesh for acceptable numerical accuracy. We will continue to promote this kind of analysis and perform anharmonic lattice dynamics simulation in other systems.

References

[1] T. Tsuchiya and X. Wang: J. Geophys. Res. **118** (2013) 83.

[2] K. Esfarjani and H. T. Stokes: Phys. Rev. B **77** (2008) 144112.

[3] http://www.quantum-espresso.org/

Ab initio calculation of superconducting pairing interactions in materials with complex Fermi surface

Ryosuke AKASHI
Department of Physics, University of Tokyo
Hongo, Bunkyo-ku, Tokyo 133-0033

In this project, we calculated the electron-phonon coupling strength in systems having complicated shapes of the Fermi surfaces. The recent development in the density functional theory has enabled us to calculate the superconducting transition temperature (T_c) in the conventional phonon-mediated superconductors [1, 2]. The accuracy of the present T_c-calculation method relies on that of the first-principles phonon calculation [3]. Although the Hermite-Gaussian broadening approximation [4] for describing the metallic occupation has been used as a standard treatment, this treatment in principle results in serious error in the systems with complicated Fermi surfaces. On the other hand, a recently developed tetrahedron-based method has been shown to yield quantitatively more reliable results [5].

We calculated the dynamical matrix and electron-phonon coupling strength in yttrium halogen-carbides and hydrogen sulfide using the tetrahedron-based method. These materials have been shown to exhibit the Fermi surfaces with complicated structures formed by multiple bands [6, 7]. QUANTUM ESPRESSO code package (5.0.3)(Ref. [8]) has been used for the calculations. The PBE-sol [9] and GGA-PBE [10] exchange-correlation potentials were used for the respective materials. Parallelization scheme with respect to **k** points (*-npool* option) as implemented in *ph.x* code was employed. The calculations were mainly done in System B (sekirei). In particular, the calculation for hydrogen sulfide with composition of $H_{31}S_{11}$ required $\lesssim$24 hour per **q** point with 32 nodes and *-npool 32*.

Table 1: Calculated factors representing the electron-phonon coupling strength and superconducting transition temperatures. The latter values were estimated using the strong-coupling-corrected McMillan-Allen-Dynes equation [12] with the empirical Coulomb-repulsion parameter $\mu^* = 0.13$

	YClC	YBrC	YIC	$H_{13}S_5$	$H_{31}S_{11}$
λ	0.527	0.650	0.831	1.301	1.481
$\omega_{\ln}$ (K)	283	248	218	1285	1351
ω_2 (K)	502	470	434	1569	1606
T_c (K)	2.7	5.4	9.5	124	153

The resulting Eliashberg function $\alpha^2F(\omega)$ (Ref.[11]) representing the electron-phonon coupling strength is shown in Fig. 1. The coupling strength λ and characteristic phonon moments $\omega_{\ln}$ and ω_2 (for their definitions, see Ref. [12]) are summarized in Table 1. The T_cs estimated from these values agree well with the experimental trends [13, 14, 15]. These results will be published in later papers.

References

[1] M. Lüders, M. A. L. Marques, N. N. Lathiotakis, A. Floris, G. Profeta, L. Fast, A. Continenza, S. Massidda, and E. K. U. Gross, Phys. Rev. B **72**, 024545 (2005).

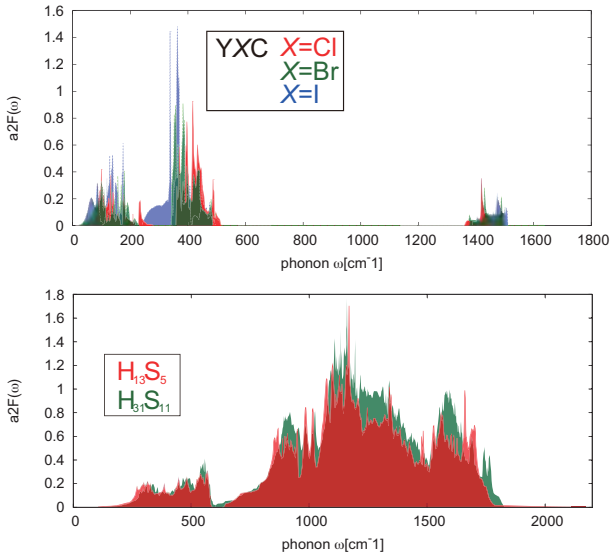

Figure 1: Calculated Eliashberg functions $\alpha^2F(\omega)$ for yttrium halogen carbides YXC (X =Cl, Br, I) and hydrogen sulfide H_xS. The pressures for the latter systems were set to be 190 ($H_{13}S_5$) and 200GPa ($H_{31}S_{11}$), respectively

[2] M. A. L. Marques, M. Lüders, N. N. Lathiotakis, G. Profeta, A. Floris, L. Fast, A. Continenza, E. K. U. Gross, and S. Massidda, Phys. Rev. B **72**, 024546 (2005).

[3] S. Baroni, S. de Gironcoli, A. Dal Corso, and P. Giannozzi, Rev. Mod. Phys. **73**, 515 (2001).

[4] M. Methfessel and A. T. Paxton, Phys. Rev. B **40**, 3616 (1989).

[5] M. Kawamura, Y. Gohda, and S. Tsuneyuki, Phys. Rev. B **89**, 094515 (2014).

[6] P. Puschnig, C. Ambrosch-Draxl, P. W. Henn, and A. Simon, Phys. Rev. B **64**, 024519 (2001).

[7] N. Bernstein, C. S. Hellberg, M. D. Johannes, I. I. Mazin, and M. J. Mehl, Phys. Rev. B **91**, 060511(R) (2015).

[8] P. Giannozzi *et al*, J. Phys.: Condens. Matter **21**, 395502 (2009); http://www.quantum-espresso.org/.

[9] J. P. Perdew, A. Ruzsinszky, G. I. Csonka, O. A. Vydrov, G. E. Scuseria, L. A. Constantin, X. Zhou, and K. Burke, Phys. Rev. Lett. **100**, 136406 (2008).

[10] J. P. Perdew, K. Burke, and M. Ernzerhof, Phys. Rev. Lett. **77**, 3865 (1996).

[11] D. J. Scalapino, in *Superconductivity* edited by R. D. Parks, (Marcel Dekker, New York, 1969) VOLUME 1.

[12] P. B. Allen and R. C. Dynes, Phys. Rev. B **12**, 905 (1975).

[13] A. Simon, A. Yoshiasa, M. Backer, R. W. Henn, C. Felser, R. K. Kremer and H. Mattausch, Z. anorg. allg. Chem. **622**, 123 (1996).

[14] R. W. Henn, W. Schnelle, R. K. Kremer, and A. Simon, Phys. Rev. Lett.**77**, 374 (1996).

[15] A. P. Drozdov, M. I. Eremets, and I. A. Troyan, V. Ksenofontov, and S. I. Shylin, Nature (London) **525**, 73 (2015).

Study on catalyst synthesis and surface reaction analysis for novel energy storage systems

Fumihiko KOSAKA and Junichiro OTOMO

Department of Environment Systems, Graduate School of Frontier Sciences,

The University of Tokyo, 5-1-5, Kashiwa-no-ha, Kashiwa, Chiba 277-8581, Japan

Redox reaction of metal oxides (MO) such as nickel oxide and iron oxide can be utilized for energy conversion and storage systems by using the energy gap between metals and metal oxides [1,2]. For example, a new energy storage system has been proposed utilizing the redox reaction of iron oxide with a solid oxide fuel cell (SOFC) using H_2–H_2O as a mediator [2]. In this system, electrical energy is converted to chemical energy of Fe during charging process. Reduction and oxidation of iron oxide by hydrogen and water proceed in charging and discharging processes, respectively. Therefore, investigation of the mechanisms that promote the redox reactions of metal oxides is of great importance and lead to highly efficient energy storage systems.

In this study, to discuss in a simple case, we focus on reduction process of NiO(111) by hydrogen. Hydrogen adsorbs on the surface of NiO, and then water desorbs and oxygen vacancy forms. The energy profile was investigated using the density functional theory (DFT). SIESTA code [3] was used for the DFT calculations. The generalized gradient approximation (GGA) using the RPBE functional [4] was used as the exchange correlation function. p(2×2) unit cell and vacuum layers of 10 Å was sampled with 2×2×1 k-point grid automatically generated using the Monkhorst-Pack method [5]. During relaxation, positions of atoms in bottom two layers were fixed. Crystal structures were visualized using VESTA software [6].

Fig. 1 shows the calculated energy profile and positions of Ni, H and O during the initial NiO reduction step by hydrogen. Hydrogen approached the surface of NiO and was stabilized by adsorption on the surface. Oxygen vacancy formed by desorption of water and

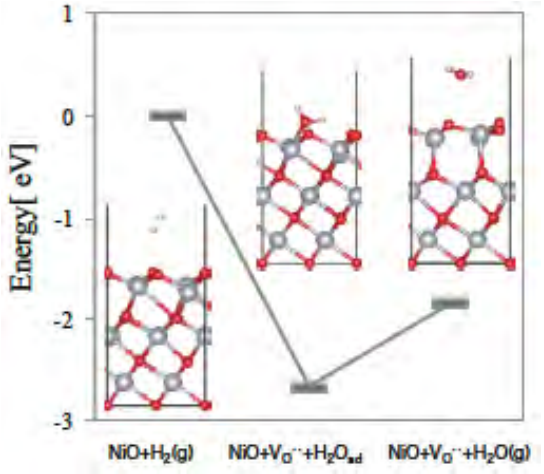

Fig. 1: Calculated energy profile of initial NiO reduction step by hydrogen. Red: O, white: H, grey: Ni.

surface relaxation occurred. Because of the oxygen vacancy formation, the total energy increased. In the future plan, we will calculate the reaction barrier using the nudged elastic band (NEB) method. Then, the investigation will be expanded to other materials such as iron oxide and ilmenite which will be used for the novel energy storage systems using redox cycles of the oxides.

References

[1] J. Adanez et al., *Prog. Energy Combust. Sci.*, **38** (2012) 215.

[2] N. Xu et al., *Energy Env. Sci.*, **4** (2011) 4942.

[3] J. M. Soler et al., *J. Phys.: Condens. Matter.*, **14** (2002) 2745.

[4] Y. Zhang et al., *Phys. Rev. Lett.*, **80** (1998) 890.

[5] H.J. Monkhorst et al., *Phys. Rev. B*, **13** (1976) 5188.

[6] K. Momma et al., *J. Appl. Crystallogor.*, **44** (2011) 1272.

Interface structure of β-$FeSi_2$(100) and Si(001)

Ken HATTORI
Graduate School of Materials Science, Nara Institute of Science and Technology
Takayama, Ikoma, Nara 630-0192

The authors' group found the formation of β-$FeSi_2$(100) on Si(001) prepared in ultra-high vacuum, using scanning tunneling microscopy (STM) and low-energy electron diffraction (LEED) [1]. Using Simulation Tool for Atom TEchnology (STATE)-Senri [2] in SCC-ISSP system A, the author calculated STM simulation images for β-$FeSi_2$(100)1×1 surface based on the LEED results, where the model consists of 1st-layer Si (8 atoms per β(100)1×1 unit-cell, corresponding to Si(001)2×2)/2nd-Fe (2 atoms)/3rd-Fe (2)/4th-Si (8)/5th-Fe (4)/6th-Si (8)/7th-Fe (2)/8th-Fe (2)/9th-Si (8)/10th-Fe (4)/11th-Si (8)/12th-H (8) (64 atoms in total)[1].

Recently the authors' group has confirmed such a slab structure using high-angle annular dark-field scanning transmission electron microscopy (HAADF-STEM) in atomic resolution. Furthermore, the STEM has revealed atomic interface structure of β-$FeSi_2$(100) and Si(001). Based on the experimental interface structure, the author calculated interface structures using STATE-Senri, from a small model ((Si (8)/Fe (2)/Fe (2)/Si (8)/Fe (4))/Si (8)/1st-Si-sub (4)/.../6th-Si-sub (4)/7th-H (8) (64 atoms)) to a certain large-scale moedel ((Si/Fe/Fe/Si/Fe)×3/Si/Si-sub×24/H (184 atoms), Fig. 1), step by step, under fixing the last three layers (Si/Si/H), within 0.3 eV/Å in residual force. The k-mesh gird was 4×4×1, and the spin polarization was not treated.

As shown in Fig. 1, the bottom Si atoms of β-$FeSi_2$ did not fully bond to the substrate Si atoms, suggesting loosely bonding at the interface. Indeed, the main residual force located at interface Si layers in calculated five models, implying interface stress. One of the interesting features of this system is nano-carpet formation; different β-$FeSi_2$(100) nano-film domains on different-height Si(001) terraces smoothly connected over the substrate steps, implying that the interface bonding is weaker than the lateral bonding inside the nano-film. The calculated interface stress might be a key point to reveal the nano-carpet growth.

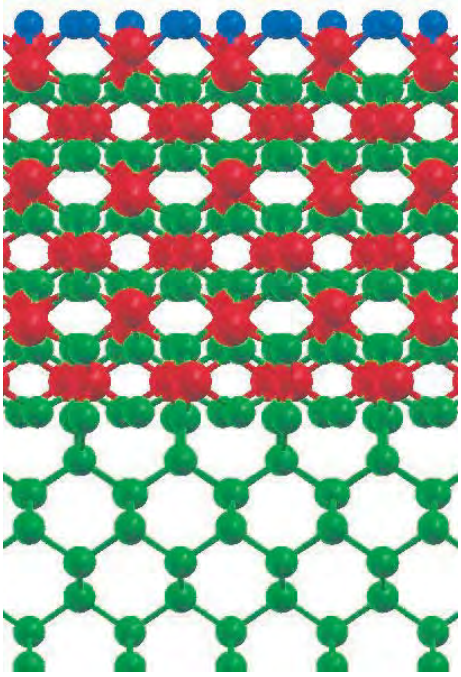

Figure 1: Calculated interface structure of β-$FeSi_2$(100) on Si(001). Red (blue and green) balls represent Fe (Si) atoms.

The author thank Prof. Morikawa in Osaka University, Dr. Yanagisawa in Ryukyu University, and Dr. Hamada in NIMS for their great support in STATE-Senri calculations.

References

[1] O. Romanyuk, K. Hattori, M. Someta, and H. Daimon: Phys. Rev. B **90** (2014) 155305.

[2] Y. Morikawa: Phys. Rev. B **63** (2001) 033405, and references therein.

Development of first-principles electronic structure calculation package xTAPP

Yoshihide YOSHIMOTO
Graduate School of Information Science and Technology, University of Tokyo
7-3-1 Hongo, Bunkyo-ku, Tokyo 113-0033

xTAPP is a first-principles electronic structure calculation package based on plane wave basis sets, pseudo potentials, and density functional theory. It has been opened for public under GNU General public license since April 2013 and it is acquiring users afterward.

One of the major request to xTAPP after its release was the calculation for spin-orbit interaction and relating non-collinear magnetism. The major aim of this project was to extend xTAPP to support these functions.

The developed version of xTAPP which supports these functions has been publicly available after 20th April 2016[1]. This release also contains a translated version of a pseudo potential library which takes the spin-orbit interaction into account by solving the Dirac equation instead of the Schrödinger equation in its generation processes. The library covers from H to Bi if they are not radioactive. In addition, stress calculations by the analytic expression is also available for the calculations with spin-orbit interaction and non-collinear magnetism in this new version. The developed code including the one for stress calculation supports up to f orbital.

Fig. 1 shows the simulated band structure of Au. The solid and the dotted lines correspond to the calculations with and without the spin-orbit interaction, respectively. The d-band splitting by the spin-orbit interaction at the Γ point is reproduced. Fig. 2 shows the stress of GaAs as a function of the lattice constant by using the analytic expression and by using numerical derivative of the total energy. We can not distinguish these two calculations.

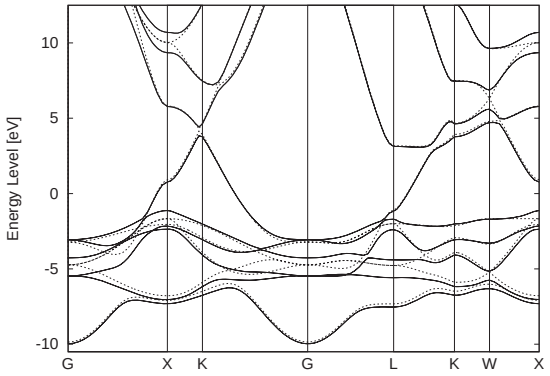

Fig. 1: calculated band structure of Au.

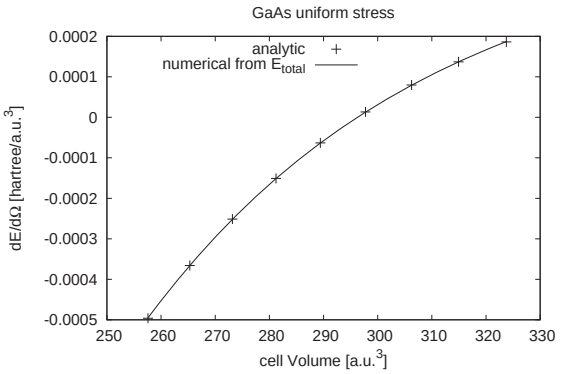

Fig. 2: calculated stress of GaAs.

References

[1] xTAPP web site: http://xtapp.cp.is.s.u-tokyo.ac.jp.

First-principles study of magnet materials and spin-orbit systems

Takashi MIYAKE
CD-FMat, National Institute of Advanced Industrial Science and Technology
Umezono, Tsukuba 305-8568

Synthesis of a $NdFe_{12}N$ film [1], followed by a theoretical calculation [2], has attracted renewed interest in exploration of new magnet compounds having large saturation magnetization and strong magnetocrystalline anisotropy. Interstitial nitrogen enhances the magnetization and induces strong uniaxial magnetic anisotropy in $NdFe_{12}N$, and both the magnetization and anisotropy field are superior to those of $Nd_2Fe_{14}B$ over wide temperature range between the room temperature and Curie temperature [1].

One problem in $NdFe_{12}N$ is that the compound is thermodynamically unstable. A third element, such as Ti, is necessary to stabilize the bulk phase. Another question is whether or not the magnetic properties can be improved further by changing the interstitial dopant. To address this problem, we have performed first-principles calculations of $NdFe_{11}TiX$, where X=B, C, N, O, F, using the QMAS code. The calculations are based on the density functional theory in the generalized gradient approximation. The Nd-4f electrons are treated as open-core states.

The magnetic moment is enhanced by doping X compared to $NdFe_{11}Ti$ in all the five elements we have studied. The amount of the enhancement significantly depends on X, and is larger in X= N, O, F than in X = B, C. Analysis of the density of states clarified that the X dependence is associated with the anti-bonding states between Fe-3d and X-2p. The anti-bonding states appear above the Fermi level in the X=B system. As the atomic number increases, the X-2p energy level is shifted down. In the X=N system, the anti-binding states are partially filled in the majority spin channel, whereas the minority-spin anti-bonding states are not filled. This results in enhancement of the magnetization.

The magnetocrystalline anisotropy is evaluated based on the crystal field theory as

$$K_1 = -3J(J-1/2)\alpha_J \langle r^2 \rangle A_2^0 n_R \ , \qquad (1)$$

where $J = 9/2$ is the total angular moment of the Nd ion, $\alpha_J = -7/1089$ is the Stevens factor, and n_R is the concentration of Nd atoms. The crystal-electric-field parameter $\langle r^2 \rangle A_2^0$ is calculated as

$$\langle r^l \rangle A_l^m = F_l^m \int W_l^m(r) \phi^2(r) dr \ , \qquad (2)$$

where F_l^m is a prefactor of the real spherical harmonics Z_l^m, W_l^m is the Kohn-Sham effective potential expanded by Z_l^m, and ϕ is the radial function of the Nd-4f orbital. We have found that the $\langle r^2 \rangle A_2^0$ is sensitive to X, and has the maximum for X=N. These results indicate that nitrogen is the best dopant among X=B, C, N, O and F in terms of magnetization and magnetocrystalline anisotropy.

References

[1] Y. Hirayama et al., Scr. Mater. **95** (2015) 70.

[2] T. Miyake et al., J. Phys. Soc. Jpn. **83** (2014) 043702.

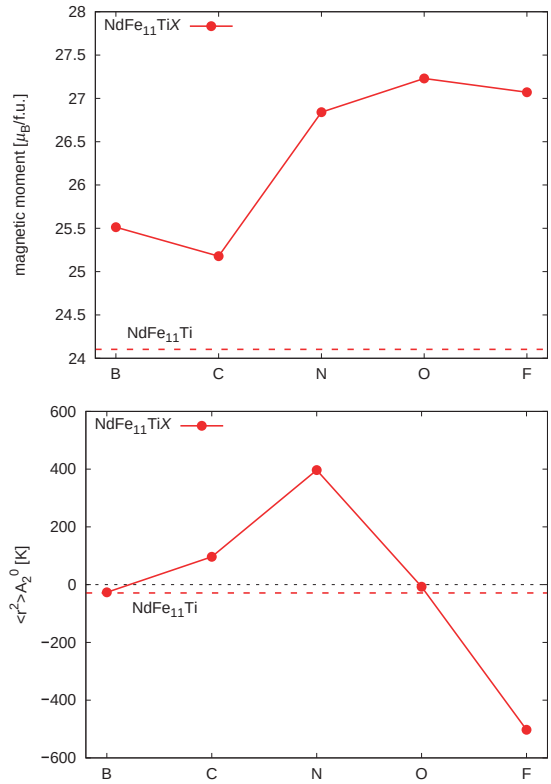

Figure 1: Magnetic moment and crystal electric field parameter of $NdFe_{11}TiX$ (X= B, C, N, O, F).

[3] Y. Harashima et al., Phys. Rev. B **92** (2015) 184426.

Computational Simulation of the Hydrostatic Pressure Effect on the Néel Temperature in Corundum-type Cr_2O_3

Yohei KOTA
National Institute of Technology, Fukushima College
Nagao 30, Taira-Kamiarakawa, Iwaki, Fukushima 970-8034

Corundum-type Cr_2O_3 is an antiferromagnet with a Néel temperature of $T_N = 308$ [K]. The effect of lattice compression on the Néel temperature of Cr_2O_3 has been experimentally observed using hydrostatic pressure; and the variation of T_N was reported in the range from -16 to $+15$ K/GPa [1, 2, 3, 4]. However, these previous experimental studies could not reach a consensus, even with respect to the sign of the pressure dependence of T_N. To provide a theoretical perspective, the effect of hydrostatic pressure on the T_N of Cr_2O_3 is examined by first-principles calculations and Monte-Carlo simulations.

First-principles calculations of the electronic structure of corundum-type Cr_2O_3 [Fig. 1(a)] were performed using the Vienna *ab-initio* Simulation Package (VASP) [5, 6]. The exchange-correlation functional was described within the local spin-density functional approximation by considering the on-site Coulomb interaction correction. Note that the $U-J$ parameter [7] in the Cr 3d orbital was set to 3.2 eV [8], which was non-empirically determined by the unrestricted Hartree-Fock method. The cutoff energy of the plane wave basis was set to 520 eV and a Γ-point cenered 4×4×1 k-point grid was used. Structural optimization for ionic positions and cell shape was carried out with a fixed cell volume. the exchange coupling constants between Cr spins up to the fifth-nearest neighbors, J_1–J_5 [Fig. 1(b)], were evaluated by fitting the energy variation of the ground state and excited states with a noncollinear spin configuration. [9] Parallel computations were performed using 1 CPU (12×2 cores) of the System B.

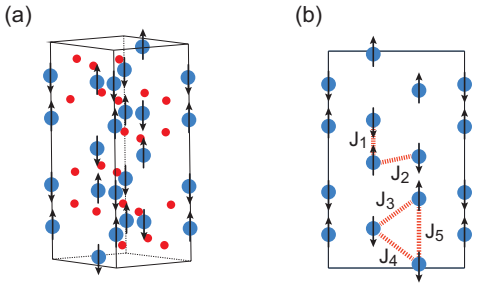

Figure 1: (a) Schematics of the hexagonal unit cell and spin configuration of corundum-type Cr_2O_3 (blue and red spheres are Cr and O, respectively). (b) The exchange coupling constants up to the fifth-nearest neightbors, J_1–J_5.

Figure 2 shows the pressure dependence of J_1–J_5. Note that the positive (negative) value indicates the antiferromagnetic (ferromagnetic) interaction. The first-nearest neighbor constant J_1, and the second-nearest neighbor constant J_2, linearly increase with increasing pressure, whereas the other constants, J_3, J_4, and J_5, are basically constant (although the J_3 and J_4 points seem to overlap, they are not equal; the $|J_3|$ values are approximately 0.2 meV smaller than the $|J_4|$ values over the entire region).

By substituting the J_1–J_5 values shown in Fig. 2(a) into the classical Heisenberg model,

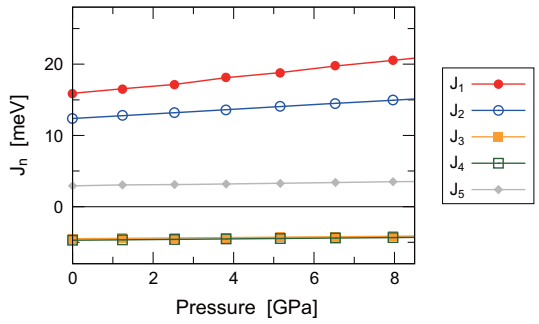

Figure 2: Pressure dependence of the exchange coupling constants up to the fifth-nearest neighbors, J_1–J_5.

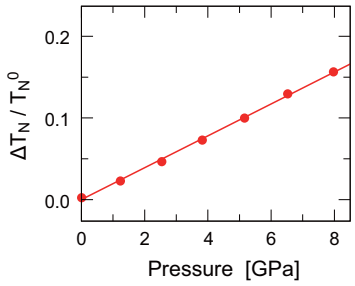

Figure 3: Néel temperature variation of Cr_2O_3 as a function of pressure, where T_N^0 denotes T_N at $P = 0$, and $\Delta T_N = T_N - T_N^0$.

the Néel temperature T_N for Cr_2O_3 is evaluated by Monte-Carlo simulation. The result is shown in Fig. 3, where T_N increases monotonically with pressure due to the increase in J_1 and J_2. Estimation of the slope of T_N with respect to P from Fig. 3 gives:

$$\frac{1}{T_N} \cdot \frac{dT_N}{dP} = +1.9 \times 10^{-2} \ [\mathrm{GPa}^{-1}].$$

In previous experiments on the effect of hydrostatic pressure, the obtained $(1/T_N)(dT_N/dP)$ values were -5.2×10^{-2} GPa^{-1} by Worlton *et al.* [1], $+4.9 \times 10^{-2}$ GPa^{-1} by Gorodetsky *et al.* [2], $+1.6 \times 10^{-2}$ GPa^{-1} by Alberts [3], and -0.3×10^{-2} GPa^{-1} by Bayarjargal and Winkler. [4]. Comparison of the results of the present calculation and previous experiments indicates that the absolute values of the slope are around the same. The sign of the slope for the calculated result is in agreement with the experimental results of Gorodetsky *et al.* and Alberts. In particular, the calculated result $+1.9 \times 10^{-2}$ GPa^{-1} is similar to an experimental value of $+1.6 \times 10^{-2}$ GPa^{-1}.

In summary, the effect of hydrostatic pressure on the Néel temperature T_N for Cr_2O_3 is studied by employing first-principles calculations and Monte-Carlo simulations. The obtained results indicate an increase in T_N with increasing pressure P, because the exchange coupling constants between Cr spins in the first and second nearest neighbors are enhanced. The calculated $(1/T_N)(dT_N/dP)$ is quantitatively comparable with an experimental value by Alberts [3].

This work was supported by ImPACT Program of Council for Science, Technology and Innovation (Cabinet Office, Government of Japan).

References

[1] T. Worlton, R. Brugger, and R. Bennion, J. Phys. Chem. Solids **29**, 435 (1968).

[2] G. Gorodetsky, R. M. Hornreich, and S. Shtrikman, Phys. Rev. Lett. **31**, 938 (1973).

[3] H. L. Alberts, J. Phys. Soc. Jpn. **38**, 1541 (1975).

[4] L. Bayarjargal and B. Winkler, Appl. Phys. Lett. **102**, 182403 (2013).

[5] G. Kresse and J. Hafner, Phys. Rev. B **47**, 558 (1993).

[6] G. Kresse and J. Furthmüller, Phys. Rev. B **54**, 11169 (1996).

[7] S. L. Dudarev, G. A. Botton, S. Y. Savrasov, C. J. Humphreys, and A. P. Sutton, Phys. Rev. B **57**, 1505 (1998).

[8] N. J. Mosey, P. Liao, and E. A. Carter, J. Chem. Phys. **129**, 014103 (2008).

[9] Y. Kota, H. Imamura, and M. Sasaki, J. Appl. Phys. **115**, 17D719 (2014).

Study on structure, formation, and physical properties of multiatomic vacancies and clusters of 2D semiconductors

Hiroyuki KAGESHIMA
Interdisciplinary Graduate School of Science and Engineering, Shimane University
Nishi-Kawatsucho, Matsue, Shimane 690-8504

Two dimensional (2D) semiconductors such as graphene, h-BN, and transition metal dichalcogenide (TMD) show very unique physical properties. In our project, we focus on the physical and structural properties of defects, surfaces and interfaces of them [1].

TMD recently attracts many researchers because of its two-dimensional feature as graphene. The field effect transistor based on TMD shows very high on/off ratio, which cannot be realized in that based on graphene [2]. TMD is also expected as a unique two-dimensional light emitting material because of its direct band gap nature [3]. Therefore, the crystal growth of TMD is studied widely. To obtain TMD crystal with high quality, it is important to know its growth mechanism. We focus on the very initial stage of the crystal growth of MoS_2, which is the most commonly studied material between the TMDs.

We have calculated Mo_xS_y clusters for the purpose. We put Mo and S atoms in different ways at the initial, optimize the atomic structures, and select the most stable one from each set of Mo and S complexes. The calculations were performed based on the first-principles calculation with the GGA density functional, plane wave bases, and pseudopotentials. Program package PHASE [4] was employed.

The results indicate that Mo atoms prefer direct bonding with each other (Fig. 1). We can obtain clusters with only Mo-S bonds and without any Mo-Mo bonds when the cluster contains more than 8 S atoms. This indicates that the ratio of Mo and S exceeds 1 and 2 of bulk MoS_2 crystal to obtain a good seed cluster. We can conclude that S rich condition is important in the crystal growth process to obtain crystal with high quality.

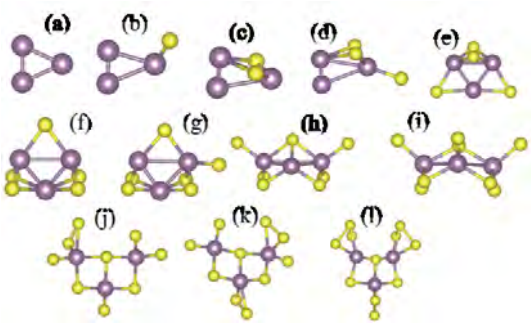

Figure 1: Optimized atomic structures for Mo_3S_y clusters.

References

[1] S. Urasaki and H. Kageshima, Extended Abstract of 2015 International Conference on Solid State Devices and Materials, PS-13-17 (2015).

[2] B. Radisavljevic, et al, Nature Nanotechnol. 6, 147 (2011).

[3] R. S. Sundaram, et al, Nano Lett. 13, 1416 (2013).

[4] https://azuma.nims.go.jp/cms1

First-principles simulation of electrolyte diffusion processes on constant-potential electrodes

Chunping HU[1,2]
[1]*Elements Strategy Initiative for Catalysts and Batteries (ESICB), Kyoto University, 1-30 Goryo-Ohara, Nishikyo-ku, Kyoto 615-8245, Japan*
[2]*Research Center for Computational Design of Advanced Functional Materials (CD-FMat), National Institute of Advanced Industrial Science and Technology (AIST), Tsukuba, Ibaraki, 305-8565, Japan*

In recent years, there have been much progress on the study of sodium-ion battery (SIB), which is a promising alternative to widely-used lithium-ion battery. To improve the efficiency of such second-battery systems, it is necessary to clarify the diffusion mechanism of electrolytes on electrodes. In the experimental condition, bias voltages are applied during charging or discharging, and thus electrode reactions (including diffusion) proceed at constant electrode potentials, as in the case of scanning tunneling microscope (STM). However, in theoretical research, especially in the study of reaction paths and energy barriers, it is traditionally assumed that the charge injected to the electrode is constant, without control on the potential.

In the present work, we aim to perform realistic first-principles simulation of electrolyte diffusion processes on constant-potential electrodes, using nudged elastic band (NEB) calculations at constant chemical potentials of electrons (constant μ_e). This method is realized by using the static version of the constant-μ_e scheme of Bonnet *et al.*, originally developed for molecular dynamics simulations [1]. In connection to a potentiostat, the system is automatically supplied with charges driven by the force arising from the difference of the instantaneous and the target μ_e. The constant-μ_e condition can be efficiently achieved by minimizing this force.

As a benchmark calculation, we have carried out simulations of bias-dependent diffusion of water on an Al(111) surface, using the above scheme. All calculations are carried out on System B and C, using the program package Quantum ESPRESSO [2]. Our results show that there are significant changes in diffusion barriers and paths under bias voltages. This serves to clarify the origin of experimental observations. Comparative studies also show that the conventional scheme with a constant charge cannot give a good description of bias-dependent molecular diffusion because of strong interaction between the molecular dipole and the electric field: To maintain a constant potential, the charge supplied by the potentiostat varies significantly along the pathway [3].

References

[1] N. Bonnet, T. Morishita, O. Sugino, and M. Otani, Phys. Rev. Lett. **109**, 266101 (2012).

[2] P. Giannozzi *et al.*, J. Phys.: Condens. Matter **21**, 395502 (2009).

[3] C. Hu and M. Otani, to be submitted to Phys. Rev. Lett.

Stabilities, structures, and electronic properties of atomic-layered materials

Yoshitaka FUJIMOTO
Depertment of Physics, Tokyo Institute of Technology
Oh-okayama, Meguro, Tokyo 152-8551

Since the discovery of graphene, hexagonal boron nitride (h-BN) atomic layers have received much attention because of the structural and mechanical properties similar to graphene. On the other hand, the electronic structure of the h-BN layers is quite different from that of graphene; h-BN layer is a gapped material and graphene is a gapless material. Hence, the h-BN layered materials are promising candidates for future semiconducting device materials in nano-electronics and opto-electronics applications.

We here report atomic structures and electronic properties of carbon defects in h-BN monolayer using a first-principles total-energy calculation within the density-functional theory. We show that the donor and acceptor states can be induced when carbon atoms are replaced with boron and nitrogen atoms, respectively. We also show that the ionization energies of the donor and acceptor states are controllable by applying tensile as well as compressive strains [1].

The pristine h-BN monolayer has a two-dimensional unit cell with the optimized lattice constant of 2.48 Å, and it is in good agreement with experimental result, 2.49 Å. Calculated band gap of pristine h-BN sheet is 4.64 eV, which is also in good agreement with other results. The calculated B-C bond and C-N bond lengths in the h-BN monolayers replaced with the C atom at the N site and the B site are 1.48 Å and 1.38 Å, respectively, and those are longer and shorter than the B-N bond length of 1.43 Å in the pristine h-BN monolayer. These structural behaviors are in agreement with other results.

The ionization energy of the acceptor state monotonically decreases as the tensile strain increases, and it increases as the compressive strain increases. For the donor state, on the other hand, the ionization energy shows the unique behavior: The ionization energy decreases as the tensile strain increases, and the ionization energy also decreases rapidly when h-BN monolayer is under the compressive strain of less than 1 %, being different from the case of the acceptor state. Interestingly, the ionization energies for the acceptor and the donor states show different behaviors, especially in the compressive region. The ionization energy increases for the acceptor state, while it rapidly diminishes for the donor state with increasing the compressive strain.

In order to study the behavior of ionization energies for the donor state under the strains, we exmaine the energy differences between the donor-state level and the conduction-band minima at the K and the Γ points. The value of the energy gap at the K point decreases as tensile strains increase. On the other hand, the energy-gap value at the Γ point diminishes when the h-BN monolayer is compressed, and it remains almost unchanged in the region of the tensile strains. It is thus found that conduction-band minimum changes from the K point to the Γ point at the compressive strain of around 1 %.

In summary, we have examined the relationship between the strains and the electronic properties of carbon defects in h-BN monolayers on the basis of the first-principles density-functional calculations. The donor and acceptor states can be induced when boron and nitrogen atoms are replaced with the carbon atom, respectively. The ionization energies

are controllable for donor and acceptor states by applying tensile and compressive strains. For the donor state, the conduction-band minimum changes from the K point to the Γ point at the compressive strain of around 1 %.

References

[1] Y. Fujimoto and S. Saito, Phys. Rev. B **93**, 045402 (2016).

Electronic Structure of Rare Earth Magnets

Hisazumi AKAI
Institute for Solid State Physics, University of Tokyo
Kashiwa-no-ha, Kashiwa, Chiba 277-8581

We have pointed out in our previous study that the chemical bonding between N and Sm plays an important role in the magnetic anisotropy change of Sm_2Fe_{17} from in-plane to uniaxial ones caused by the introducing of N [1]. This effect of N insertion was discussed in terms of change in the electronic structure calculated in the framework of LDA+SIC. Now, the main issue is whether the 4f states are dealt with properly in SIC. In the present study, we examine the applicability of SIC for the evaluation of the magnetic anisotropy of rare-earth (RE) magnets by comparing the results with various methods, in particular, the optimized effective potential (OEP) method. In this study, OEP is applied only on the RE sites. Admittedly, this is a drawback from the viewpoint of performing a consistent treatment of uncertainly inherent in the so-called KLI (Krieger-Li-Iafrate) constants. Putting this aside for the moment, we have calculated the electronic structure of RE magnets $R_2Fe_{17}N_x$ and RCo_5 (R=light RE), by OEP with exact-exchange (EXX) energy combined with Colle-Salvetti correlation energy.

Figure 1 shows the total energy changes as functiona of the tile angle of the crystal calculated using SIC, 0° corresponding to the magnetization along the z direction, 90° to the xy direction. Three different curves are the result of self-consistent calculations, the band energy, and the total energy obtained using the potential for the zero tilt angle, respectively. The three curves are more or less the same, indicating that these results are reliable.

Unexpectedly, our preliminary results using

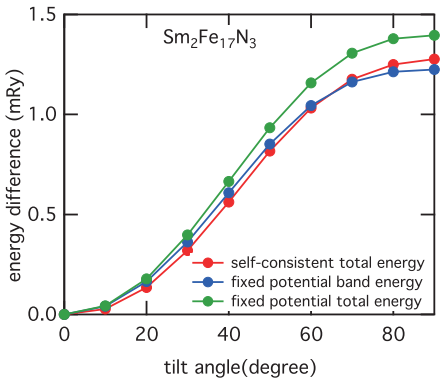

Figure 1: Total energy changes as functions of the tile angle of the crystal calculated using SIC

OEP have shown considerable differences from the SIC results. There, the fixed potential total energy, which is supposed to be virtually the same as the self-consistent potential result, shows a considerably larger anisotropy energy than the result of the SIC calculations. Moreover the fixed potential band energy energy largely deviates from the behavior of total energy. These facts indicate that the OEP results are not reliable anymore for the calculation of the magnetic anisotropy. We are now analysing the origin of this inconsistency.

The calculations are performed using system B of the ISSP supercomputer systems and KKR-Green's function code (AkaiKKR).

References

[1] M. Ogura and H. Akai, J. Phys. Soc. Jpn 84, (2015) 084702.

First-principles study on the defects in semiconductors

Jun YAMAUCHI
Faculty of Science and Technology, Keio University
3-14-1 Hiyoshi, Kohoku-ku, Yokohama-shi, Kanagawa 223-8522

As the size of devices on integrated circuits decreases, the behavior of dopant atoms make relatively larger effect on the device performance. Especially, it is very important to understand the unfavorable defects including the dopant atoms. The experimental observations on each defect is extremely difficult. One of the major difficulties for detecting dopant configurations is the very weak signals from the defects of very low concentration comparing to those from the matrix semiconductors. However, recently, as a solution for the above problem, it is suggested to use powerful synchrotron radiation facilities to measure the X-ray photoelectron spectroscopy (XPS) signals of defects. On the other hand, there have been few reliable first-principles core-level XPS calculations for impurity defects in semiconductors, because the local potential boundary condition of defect model systems has not yet been sufficiently evaluated. To obtain reliable shifts in the XPS binding energy, it is necessary to take a sufficiently large supercell for a defect.

To investigate the dependence of the substrate semiconductors on the XPS binding energies, we carried out a comprehensive study on the B 1s core-level XPS binding energies for B defects in crystalline Si using a first-principles calculation with careful evaluation of the local potential boundary condition for the model system. We adopted cubic supercell corresponding to 1000 Si atoms and also considered the charged state and spin effect. The code used in this study is xTAPP, which is a hybrid paralleled density functional theory calculation program with plane-wave basis[1].

It is found that, while the spin polarization does not make large effect on the formation and XPS binding energy of defects, the charge state change those energies up to several tenth of eV in some cases. The electrically active clusters without any postannealing of ion-implanted Si were identified as icosahedral B_{12} clusters. The experimentally proposed threefold coordinated B was also identified as ⟨001⟩B-Si defects. For as-doped samples prepared by plasma doping, it is proposed that assuming that the XPS peak at 187.1 eV is due to substitutional B, the experimental XPS peaks at 187.9 and 186.7 eV in as-doped samples correspond to interstitial B at the H-site and ⟨001⟩B-Si defects, respectively.

References

[1] xTAPP (eXtended Tokyo Ab initio Program Package)
(http://xtapp.cp.is.s.u-tokyo.ac.jp)

[2] J. Yamauchi, Y. Yoshimoto, and Y. Suwa: J. Appl. Phys. (in press).

Ab-initio DFT Calculations of Photocatalyst Material for Water Splitting

Kaoruho SAKATA, Takashi HISATOMI, Yosuke GOTO,
Taro YAMADA, Kazunari DOMEN
Artificial Photosynthetic Chemical Process Project,
The University of Tokyo, Kashiwa-no-ha, Kashiwa, Chiba 277-8581

Water splitting by photocatalyst under visible light irradiation is investigated keenly to reveal H_2 generation in practical use. Among the photocatalyst material, $La_5Ti_2CuS_5O_7$, and $La_5Ti_2Cu_{1-x}Ag_xS_5O_7$, which is partially substituted constituent elements from Cu to Ag, is one of candidate for photocatalyst of H_2 generation [1]. $La_5Ti_2CuS_5O_7$ has superior property having higher onset-potential compared with other materials when we used them as cathodic material, and also it is indicate to have one-dimensional conductive from experimental results [1]. However, it has not been clarified most of the material property yet, such as electric structures. This year, we focused on the assessment of band structure, especially its crystal orientation dependence of $La_5Ti_2CuS_5O_7$. Our group already studied Density of States of $La_5Ti_2CuS_5O_7$ and $La_5Ti_2AgS_5O_7$ using DFT calculation [2], therefore, we calculated the band structures of $La_5Ti_2Cu_{1-x}Ag_xS_5O_7$ (x= 0.08, 0.25, 0.5, 0.75), and assessed the correlation between its composition and calculated band gaps.

In this study, PW-DFT is used for all the calculation, which is implemented in VASP program. Structure of $La_5Ti_2CuS_5O_7$ is referred from Inorganic Crystal Structure Database (ICSD) [3], and $[La5Ti_2Cu_{1-x}Ag_xS_5O_7]_8$ or $[La_5Ti_2Cu_{1-x}Ag_xS_5O_7]_{12}$ was used as unit cell. DFT calculation is performed using PBE functional, and under GGA-level. Kinetic-energy cutoff was set to 300 eV, Monkhorst-pack set 4×12×4.

Fig. 1 shows the band structures including VBM and CBM of $La_5Ti_2CuS_5O_7$ in [100],

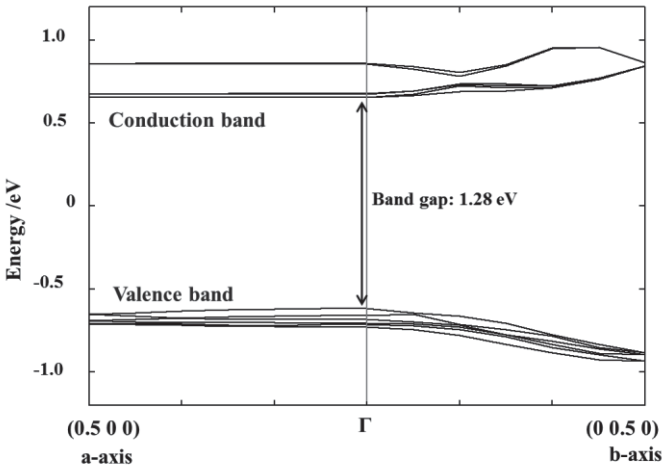

Fig. 1: Band structure of $La_5Ti_2CuS_5O_7$

obtained when $[La_5Ti_2Cu_{1-x}Ag_xS_5O_7]_8$ was used as an unit-cell. It is suggested that gradient of the band in [100] direction is flat compared with that in [010] direction. Previous experimental results [1] indicated that $La_5Ti_2CuS_5O_7$ has one-dimensional conductive, and our calculation results may have comparable to experimental tendency. In addition, band gap of $La_5Ti_2Cu_{1-x}Ag_xS_5O_7$ was calculated and it is indicated that band gap of $La_5Ti_2Cu_{0.5}Ag_{0.5}S_5O_7$ was smaller than that of $La_5Ti_2CuS_5O7$ and $La_5Ti_2AgS_5O_7$. This results is corresponds to the experimental results which is studied using ultraviolet-visible diffuse reflectance spectroscopy (DRS).

.

References

[1] T. Hisatomi, *et al.*, Energy Environ. Sci., **8** (2015) 3354.

[2] T. Suzuki, *et al.*, Phys. Chem. Chem. Phys., **14** (2012) 15475.

[3] V. Meignen, *et al.*, J. Solid State Chem., **177**, (2004) 2810.

Ab Initio Simulations of SiC Surface Reactions for Water Splitting and High-temperature Oxidation.

Kenji TSURUTA, Kazuhiro SHINIKE, Keiichi MITANI, and Atsushi ISHIKAWA

Graduate School of Natural Science and Technology, Okayama University, Okayama 700-8530

SiC surface provides versatile fields for catalytic reactions keeping the high chemical stability as well as its controllability of carrier injection as a wide-gap semiconductor. Using first-principles simulations, we have studied two types of reaction processes on SiC; H_2 production in the water splitting reaction and C-ring formation through high-temperature oxidation. All simulations are performed by using VASP, Vienna Ab-initio Simulation Package.

We have performed *ab-initio* molecular-dynamics (MD) simulations of H_2 production processes on 3C-SiC [001] surfaces. We first found that a Si-terminated (001) surface was more reactive than an O-terminated one against water adsorptions, and the reaction on the Si terminated surface was proceeded through the water dissociation as $2Si+H_2O \rightarrow Si\text{-}OH + Si\text{-}H$ or $Si+2H_2O \rightarrow Si\text{-}OH + H_3O^+$. For H_2 generation, we estimated reaction barriers of two reaction paths using Nudged Elastic Band (NEB) algorithm; (i) reaction between neighboring H atoms bonded to the Si's on the surface; (ii) reaction of H atoms between H_3O^+ molecule generated in the H_2O dissociation and Si-H. We find the process (ii), so called "Heyrovský process", has a lower barrier being approximately 0.55eV, while it's 2.4eV for the process (i). The process (ii) was also observed in the MD simulation at 900K (Fig. 1).

We have also investigated C-ring formation on [0001] surface of 4H-SiC via high-temperature oxidation. The C-ring formation is an incipient process of the graphene formation observed by high-resolution TEM measurement [2] and is proceeded through the desorption of Si atoms by oxidation on the SiC surface. We thus estimated the desorption energy from the energies required to remove Si atoms and create SiO_2 in bulk. Figure 2 depicts the Si desorption energy as a function of sequence of the removal from the terrace (atomically flat surface) and a $[11\bar{2}0]$ step[3]. We find that after the reaction reaches 7th removal, the process becomes unstable expediting the desorption and, in turn, the C-ring formation.

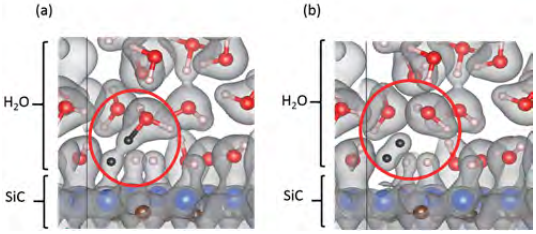

Fig. 1: Snapshots of surface reaction for (a) before and (b) after H_2 production.

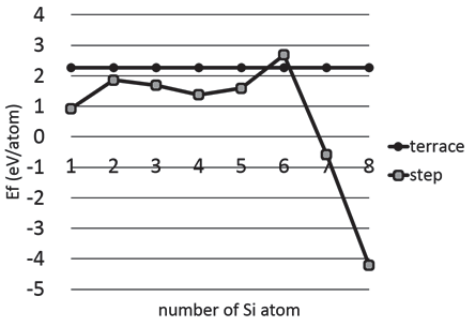

Fig. 2: Si desorption energy

References

[1] M. Kato *et al.*, Int. J. Hydrogen Energy **39**,4845(2014).

[2] W. Norimatsu *et al.*, Chem. Phys. Lett.**468**, 52(2009).

[3] T. Ohta *et al.*, Phys. Rev B **81**, 121411(R) (2010).

Calculation of Fe compounds Magnetism

Shuji OBATA
School of Science & Engineering, Tokyo Denki University
Ishizaka, Hatoyama, Hiki, Saitama 350-0394, Japan

The electronic binding energies J_{ij} of 3d electrons in Ni-Fe are induced from the tight binding interactions of the directed magnetic moments $\boldsymbol{\mu}_i$ bounded by the Hunts rule. These 3d and 4s electrons construct the eigenstates in external field environments. The magnetization processes are calculated by the Hamiltonian

$$\hat{H} = \sum_{i \le j} J_{ij} \hat{\boldsymbol{\mu}}_i \cdot \hat{\boldsymbol{\mu}}_j + \sum_{i \le j} W_{ij} + \sum_j \boldsymbol{\mu}_j \cdot \boldsymbol{H} \qquad (1)$$

including magnetic dipole moment interactions composed of spin magnetic fields

$$W_{ij} = \frac{1}{4\pi\mu_0 d_{ij}^3}\{(\boldsymbol{\mu}_i \cdot \boldsymbol{\mu}_j) - 3(\boldsymbol{\mu}_i \cdot \boldsymbol{e}_{ij})(\boldsymbol{\mu}_j \cdot \boldsymbol{e}_{ij})\}. \qquad (2)$$

The third term is magnetization energy in the external field $\boldsymbol{H}$. Distance vector is set as $\boldsymbol{d}_{ij}=\boldsymbol{e}_{ij}d_{ij}$ between the dipole moments at i and j.

Most of recent studies of the magnetizations are calculated with the quantum coulomb spin-spin interactions (Heisenberg model etc.) without the magnetic spin-spin interactions. However, one electron has the two fields as the static Coulomb field and the dynamic Ampere field. These fields are quantized with a Planck constant h. This Ampere field is called the Bohr magneton with the moment μ_B caused by the rotational motion of the spin. Thus, we must consider these two electron fields for the magnetization processes.

The well-known Hamiltonian excluding the second term cannot represent the Hysteresis magnetization curves in magnetic materials. The hysteresis loss in the magnetization processes are induced from the magnetic field energy, which do not include the coulomb energy J_{ij}. In this study, only the Hamiltonian composed of the second and the third terms are calculated for only clearing the hysteresis characteristics. The domain structures, the magnetization curves and the Barkhausen effects are investigated in these calculations.

Calculation processes of the energy in Eq. (2) require very much calculation resources, because the precise results are not obtained in restricted arias. The Barkhausen effects caused by the magnetic dipole moment interactions in FCC Ni_3Fe metal are cleared in this work. Using the ISSP system, the Fortran programs of the nano-Ni_3Fe magnetizations are executed by about 500 line programing. The used times are about 18 hours using PC cluster systems for drawing the Fig.1.

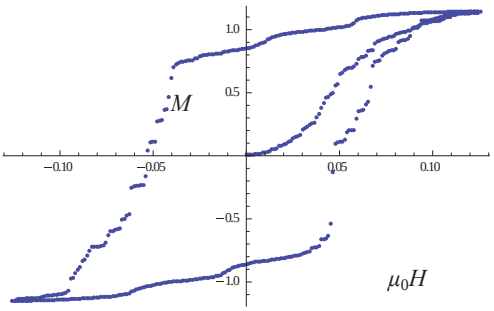

Fig.1. Ni_3Fe hysteresis curve of a 20×2×20 lattice point thin film.

The dipole moment freedom is tentatively selected to 26 directions as not the energy minimum.[1][2] This limited condition may not fit with the real system. However now, it is not clear the existence of the quantized dipole moment directions instead of electromagnetic energy minimum states. The precise structures at the jump points of a circle in Fig. 2 are drawn in Fig. 3. Crystal Fe takes the BCC structure with the lattice constant a=2.86×10^{-10} [m] up to 911 ℃ and have the dipole moments of $2n_b\mu_0\mu_B$ per a lattice. The constants are n_b=2.22, permeability μ_0 and the Bohr magneton μ_B respectively. Through these results, the processes of the Barkhausen effects are clarified as the transitions of the dipole-moment arrangements in the magnetic domains.

1) S. Obata: Mater. Trans. **55** No 10 (2014) 1591-8.
2) S. Obata: IEEJ Trans. FM, **133** No 9 (2013) 489.

A First-principles study on magneto-crystalline anisotropy of ferromagnetic metal interfaces with spinel barrier

Yoshio MIURA

Kyoto Institute of Technology, Matsugasaki, Sakyo-ku, Kyoto 606-8585

In spintronics devices, required performance in magnetic tunnel junctions (MTJs) are a high tunneling magnetoresistance (TMR) ratio over 300% at 300K, low writing energy less than 1fJ/bit, and large thermal stability factor at room temperature. To this end, required properties for spintronic materials are the high spin polarization with low resistance, large perpendicular magnetic anisotropy with small magnetic damping constant α and a small saturation magnetization with large Curie temperature. Electric filed dependence of magneto-crystalline anisotropy of ferromagnetic materials is one of the crucial issue in the spintronics application, because of the suppression of energy consumption in the magnetization reversal. Control of magnetization reversal by voltage has been demonstrated in MgO-based magnetic tunnel junctions (MTJs), where the perpendicular magnetic anisotropies (PMA) of bcc-Fe interface had been changed, corresponding to the rate of 144fJ/Vm for the PMA enhancement [1]. Furthermore, the voltage control of the magnetic damping constant α of FM layer is also important in order to control the magnetization reversal with small energy consumption. Recent experiments show that the magnetic damping constant α of thin CoFeB layer in CoFeB/MgO/CoFeB MTJs strongly depends on the applied electric field when the CoFeB layer is less than 1.4nm[2].

In this study, we theoretically investigate the electric field (EF) modulation of magnetic damping constant of thin Fe-layer using the first-principles calculations. We calculated the magnetic damping constant of free-standing thin Fe-layer on the basis of the torque correlation model proposed by Kambersky[3] using the wave-function obtained by the first-principles calculations. We found that the magnetic damping constant α of free-standing thin Fe-layer increases with increasing the applied positive EF (Increase of electron accumulation at surface), which is opposite electric filed dependence as compared with the magneto-crystalline anisotropy, corresponding to 7% of damping constant α can be changed by EF=1[V/nm]. Furthermore, we found that EF dependence of magnetic damping of Fe surface can be attributed to the spin-conservation term of torque operator.

References

[1] D. Yoshikawa, *et al*., APEX **7**, 113005 (2014).

[2] A. Okada, et al., APL **105**, 052415 (2014).

[3] V. Kambersky, CJPB **26**, 1366 (1976).

Search for new electronic properties of new nanoscale interfaces

Katsuyoshi KOBAYASHI
Department of Physics, Ochanomizu University
2-1-1 Otsuka, Bunkyo-ku, Tokyo 112-8610

In 2015 we studied IV-VI monolayers on alkaline-earth chalcogenide surfaces.

It is theoretically proposed that IV-VI monolayers are topological crystalline insulators (TCIs) in two dimensions (2D). Electronic states of insulators are classified according to topological numbers defined by point group symmetries of crystals. The first realistic materials of TCI are SnTe and its alloy with Pb. They are three-dimensional materials. Recently 2D materials of TCI are theoretically predicted, and their new applications were proposed [1]. However, they have not been materialized experimentally. We theoretically studied electronic states of 2D TCI thin films.

In 2014 we studied SnTe and PbTe monolayers as candidates of 2D TCIs [2]. Theoretical calculations show that isolated SnTe and PbTe monolayers are TCIs. However, planar structures of the monolayers are unstable, and TCI states are lost in buckled structures. For maintaining the planar structures of the monolayers we consider systems of the monolayers sandwiched between two alkali halide surfaces. We optimized atomic structures of the systems, and found that the planar structure of the monolayer maintains in SnTe monolayers sandwiched between NaBr surfaces. The electronic states of this system is TCI.

A problem is that the distorted-NaCl structure is energetically favorable than the single-layer structure for isolated IV-VI monolayers. The distorted-NaCl structure is formed by two single-layer structures. Total-energy calculations show that the interaction between a SnTe monolayer and a NaBr surface is weaker than that between SnTe monolayers. As a candidate of forming single-layer IV-VI monolayers on surfaces we consider alkaline-earth chalcogenide surfaces. The reason is that alkaline-earth chalcogenides are divalent ionic compounds, and the interaction with IV-VI monolayers is expected stronger.

Table 1: Calculated results.

	a (Å)	Δa (%)	ΔE (eV)
SnTe-NaBr	5.97324	−1.6	−0.463
SnTe-CaS	5.6903	−6.3	−0.380
SnTe-CaSe	5.91	−2.6	−0.152
SnTe-SrS	6.0198	−0.8	0.031
SnTe-SrSe	6.23	2.6	0.182
SnTe-CaTe	6.345	4.5	0.212
SnTe-BaS	6.3875	5.2	0.187

We computed total energy of IV-VI monolayers on various alkaline-earth chalcogenide surfaces. Some results for SnTe monolayers are listed in Table 1 as an example. a is the lattice constant of substrates. Δa is the difference of lattice constants between substrates and SnTe monolayers where the lattice constant of SnTe monolayers is 6.070 Å. ΔE is the difference of total energy per 1×1 2D unit cell between single-layer and double-layer structures of SnTe monolayers on substrates. Positive ΔE means that single-layer monolayers are favorable. This result suggests that single-layer monolayers may stably exist on some alkaline-earth chalcogenide substrates. Similar results are obtained for other IV-VI monolayers.

References

[1] J. Liu *et al.*: Nature Mat. **13** (2014) 178.

[2] K. Kobayashi: Surf. Sci. **639** (2015) 54.

Ab initio calculations for the silicon cluster superlattice

Nozomi ORITA, Yasushi IWATA
National Institute of Advanced Industrial Science and Technology
Tsukuba Central 2, Tsukuba, Ibaraki 305-8568

Recently, Iwata *et al.* found out the crystallographic coalescence of silicon (Si) clusters into a bcc superlattice structure with a lattice constant of 2.134 nm by direct deposition of a Si cluster beam on a graphene substrate[1]. The Si cluster superlattice have sp^3 structures in both the inside and the boundary of Si clusters. The size of the Si clusters composing the Si cluster superlattice and the electronic structure are unknown yet. Therefore, we have studied the crystal structure and the electronic structure of the silicon cluster superlattice using OpenMX[2] and obtained two suitable model structures constructed by Si_{211} and Si_{235} clusters as shown in Fig.1[3]. The lattice constants of the Si_{211} and Si_{235} cluster superlattices are 2.167 and 2.133 nm, respectively, and are in good agreement with the experimental value, 2.134nm.

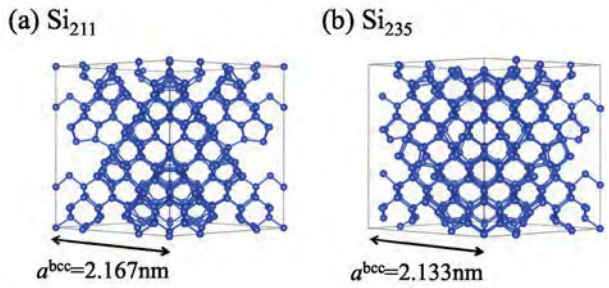

Figure 1: (a) Si_{211} and (b) Si_{235} cluster superlattices in the conventional bcc unit cells.

This year, we have performed *ab initio* calculation of the electron energy-loss spectra (EELS) of those Si cluster superlattices using QMAS code[4] on the ISSP supercomputer system B and the results are shown in Fig.2. The EELS of the Si_{211} cluster superlattice is more similar spectrum to that of the actual superlattice than that of the Si_{235} cluster superlattice.

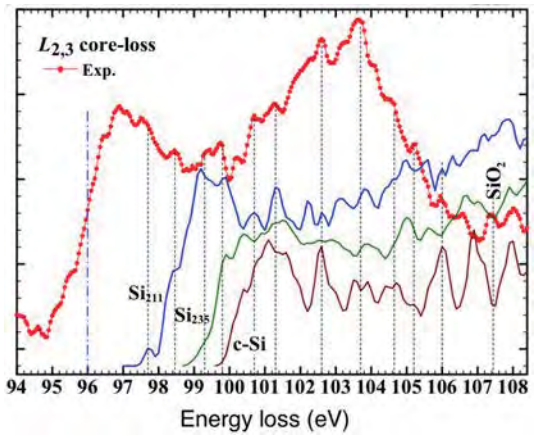

Figure 2: Si $L_{2,3}$ electron energy-loss spectra.

References

[1] Y. Iwata, K. Tomita, T. Uchida, and H. Matsuhata, Cryst. Growth Des. **15** (2015) 2119.

[2] T. Ozaki *et al.*, http://www.openmx-square.org/

[3] Y. Iwata, N. Orita, T. Uchida, and H. Matsuhata, Proc. Advanced Materials World Congress 2015, Chapter 10, p. 5.

[4] S. Ishibashi *et al.*, http://qmas.org/

Trapping of hydrogen isotopes in tungsten vacancy

Kazuhito Ohsawa

Institute for applied mechanics, Kyushu University

Kasuga-koen 6-1, Kasuga-shi, Fukuoka 816-85802

Tungsten (W) and its alloys are plausible candidates for plasma facing materials (PFMs) in fusion reactors due to their excellent properties, e.g. high melting point and low hydrogen solubility etc. However, a large amount of hydrogen isotopes (H, D, T) is retained in W specimens at lattice defects nucleated in irradiation circumstance. In particular, T inventory in W materials is an important issue for the safety of fusion reactors because T is a radioisotope whose half-life is about 12 years.

In the present study, the amounts of H isotopes trapped at monovacancies in the W materials are calculated in a thermodynamic model. Binding energies are estimated in terms of first-principle calculations on the basis of density functional theory. The isotope effect is derived from the difference of the zero-point energy of each H isotope.

The binding energies of H isotopes to a W monovacancy are shown in Fig. 1 as a function of the number of H isotopes. A maximum of 12 H atoms are accommodated in a vacancy. An important result is that the lighter H isotopes have the larger binding energies. H isotope retentions are shown in Fig. 2. In the present study, we assume that coexistence of two types of H isotopes, H and D or D and T, because the W materials will be exposed to the high fluxes of D and T particles in actual fusion reactors. The initial H isotope concentrations, (C_H, C_D, C_T) are assumed to be 5×10^{-5} and vacancy concentration is 10^{-5}. The lighter H isotopes are more trapped in the W vacancy than the heavier ones by reflecting the binding energies.

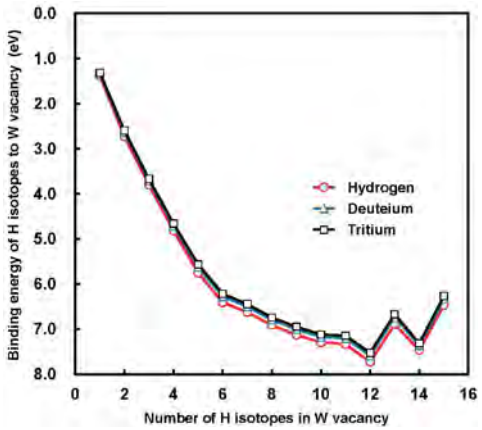

Fig. 1: Binding energy of each H isotope.

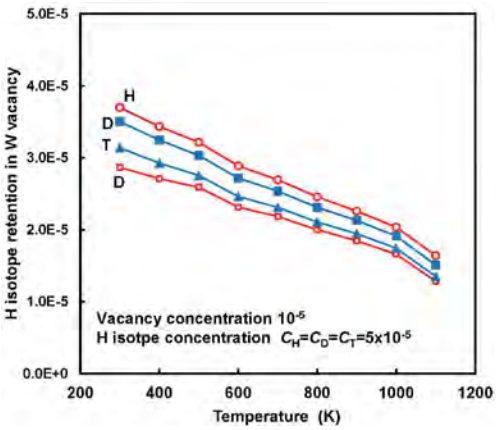

Fig. 2: H isotope retentions in W vacancy.

First principles calculations on electronic structures, magnetism, and electric field effects in transition-metal films and organometallic complexes

Kohji NAKAMURA
Department of Physics Engineering, Mie University
Tsu, Mie 514-8507

Symmetric and asymmetric exchange stiffnesses in transition-metal thin films — Controlling and designing spin-texture, which may be characterized by symmetric and asymmetric exchange stiffness, in transition-metal thin films have received much attention in fundamental and applied physics. Here, from first-principles calculations by using the full-potential linearized augmented plane wave (FLAPW) method, the exchange stiffnesses in a prototypical transition-metal thin films with perpendicular magnetic easy axis, a Co monolayer on Pt(111), were calculated. The formation energy as a function of the wave vector of the spin spirals, relative to that of the ferromagnetic state, were calculated. When the spin-orbit coupling is introduced, an asymmetry in the formation energy with respect to the spiral wave vector, so-called Dzyaloshinskii-Moriya interaction, appears. By fitting a liner curve in q^2 and q, the symmetric and asymmetric exchange stiffnesses were estimated to be 169.9 meVnm^2 and 6.5 meVnm, respectively.

Electron configurations in organic-metal complexes — In organometallic molecules, effective on-site Coulomb inter-actions (U_{eff}) and electron configurations of d electrons are essential aspects in magnetic properties but it is often difficult to analyze it. Here, by using FLAPW method based on the constraint density functional theory, we systematically investigated for prototypical molecules of metallocenes, $TMCp_2$ (TM=Cr, Mn, Fe, Co, Ni).[1] Moreover, using non-empirical values of U_{eff} determined from the linear response theory, the predicted electron configurations are in agreement with the experiments; the $^3E_{2g}$, $^6A_{1g}$, $^1A_{1g}$, $^2E_{1g}$, and $^3A_{2g}$ states for the $CrCp_2$, $MnCp_2$, $FeCp_2$, $CoCp_2$, and $NiCp_2$, respectively.

Carrier tuning in transition-metal dichalcogenides by external fields — Two-dimensional thin films with no inversion symmetry have considerable attention due to their unique electronic, magnetic and optical properties. Here, spin-valley band structure and hole carriers in a prototypical transition-metal dichalcogenide monolayer of MoS_2 in external electric and magnetic (Zeeman) fields were systematically investigated by using FLAPW method. The calculated results predict that a negative electric field excites linearly the hole carriers while the spin-valleys are attainable even in the high field of more than -10 V/nm. With a magnetic field, further, an imbalance in the number of the hole carriers in the opposite spin states can be introduced so as to tailor the hole carriers with a spin-polarization.

References

[1] Nawa,Y. Kitaoka, K. Nakamura, T. Akiyama, T. Ito, JAP**117**, (2015) 17E131.

Exploring of low-dimensional honeycomb materials consisting of heavy elements

Noriaki TAKAGI[1], Ryuichi ARAFUNE[2], Naoya KAWAKAMI[1], and Emi MINAMITANI[3]

[1]*Department of Advanced Materials Science, University of Tokyo Kashiwa-no-ha, Kashiwa, Chiba 277-8561,*

[2]*International Center for Materials Nanoarchitectonics, National Institute for Materials, Science, 1-1 Namiki, Ibaraki 304-0044,*

[3]*Department of Materials Engineering, The University of Tokyo, 7-3-1 Hongo, Bunkyo-ku, Tokyo 113-8656, Japan..*

The discovery of one-atom thick carbon honeycomb sheet, graphene, has triggered the competition to form exotic honeycomb materials and to uncover their hidden properties. Two-dimensional (2D) honeycomb sheets consisting of Bi, Si, Ge and Sn atoms have gathered lots of attention. Theoretically, these 2D materials are promising candidates of 2D topological insulator because these materials have an energy gap at the Dirac point due to the spin-orbit interaction [1, 2].

Recently, we have investigated the geometric and electronic structures of Bi thin films grown on Si(111) and Au(111) substrates mainly by using scanning tunneling microscopy and spectroscopy (STM/STS). We found that the Bi thin films have two types of step edges; One shows a regular step edge and the other exhibits a reconstruction. Interestingly, the latter edge hosts a localized 1D electronic state [3]. In order to reveal the origin of the electronic state, we carried out density functional theory (DFT) calculations.

The DFT calculations were carried out by the plane-wave-based Vienna Ab initio Simulation Package (VASP) [4, 5] with the projected augmented wave method [6]. We calculated the total energy and the electronic band structure for various structure models. Each model consists of 8 layers of Bi and a vacuum of 18 Å thick along the surface normal. The Bi layer consists of 2x10 lattices. Both surface layers possess the edges. The structure models we calculated did not reproduce the experimental results, but we will continue the DFT analysis.

Reference

[1] S. Murakami: Phys. Rev. Lett. **97**, 236805 (2006).

[2] M. Ezawa, Phys. Rev. Lett. **109**, 055502 (2012).

[3] N. Kawakami, C.-L. Lin, M. Kawai, R. Arafune and N. Takagi, Appl. Phys. Lett. **107**, 031602 (2015).

[4] G. Kresse and J. Furthmüller: Phys. Rev. B **56**, 11169 (1996).
[5] G. Kresse and J. Furthmüller: Comput. Mater. Sci. **6**, 15 (1996).
[6] P. E. Blöchl: Phys. Rev. B **24**, 17953 (1994) 17953.

Geometric and electronic structures of magnetic molecules at solid surfaces

Noriaki TAKAGI[1] and Emi MINAMITANI[2]

[1]*Department of Advanced Materials Science, University of Tokyo*

Kashiwa-no-ha, Kashiwa, Chiba 277-8561

[2]*Department of Materials Engineering, The University of Tokyo, 7-3-1 Hongo,*

Bunkyo-ku, Tokyo 113-8656, Japan.

Metal phthalocyanines (MPcs) and their derivatives have gathered considerable attention because they exhibit unique properties [1-3]. Among them, MnPc, FePc and CoPc are typical magnetic molecules and the adsorption of these molecules on solid surfaces have been intensively studied. Recently, we have investigated the magnetism of FePc on noble metal surfaces by using scanning tunneling microscopy/spectroscopy (STM/STS) and magnetic circular dichroism. The in-plane magnetic anisotropy (MA) of the bulk FePc changes to out-of-plane MA upon the adsorption on Cu(110) covered with a one-atom thick oxide layer [4] while the in-plane MA survives on Au(111) [5] and for FePc in the second layer on Ag(110).

In order to understand systematically the magnetic anisotropy of FePc and how the molecule-surface coupling impacts to the MA, we developed a theoretical approach. In this approach, we describe the electronic ground state as a linear combination of ^3E_g and $^3B_{2g}$ states. We calculated the eigenstates and eigenvalues by diagonalizing the molecular Hamiltonian with the linear combination. The molecular Hamiltonian includes the crystal field potential and the spin-orbit interaction at the Fe^{2+} ion. We used the deformations of molecular orbitals from the 3d atomic orbitals and the energy difference between the ^3E_g and $^3B_{2g}$ states. The deformations were evaluated by density functional theory (DFT) calculations. The DFT calculations were carried out by the plane-wave-based Vienna Ab initio Simulation Package (VASP) [6, 7] with the projected augmented wave method [8]. We found that the magnetism and MA of bulk FePc and the influence of the adsorption on solid surfaces can be understood reasonably with this approach.

Reference

[1] R. Bonnett: Chem. Soc. Rev. **24**, 19 (1995).

[2] C. C. Lanznoff and A. B. P. Lever: *Phthalocyanines, Properties and Applications* (Wiley, New York, 1996).

[3] K. Kadish, and R. Guillard: *Applications of Phthalocianines, The Porphrin Handbook* (Academic Press, San Diego, 2003).

[4] N. Tsukahara *et al.*: Phys. Rev. Lett.

102, 167203 (2009).
[5] E. Minamitani *et al*.: Phys. Rev. Lett. **109**, 086602 (2012).
[6] G. Kresse and J. Furthmüller: Phys. Rev. B **56**, 11169 (1996).
[7] G. Kresse and J. Furthmüller: Comput. Mater. Sci. **6**, 15 (1996) 15.
[8] P. E. Blöchl: Phys. Rev. B **24**, 17953 (1994).

Formation of C12A7 Surfaces and Work Function of C12A7:e$^-$

Yoichi KAMIHARA

Department of Applied Physics and Physico-Informatics, Keio University

3-14-1 Hiyoshi, Yokohama, Kanagawa 223-8522

1. Background

NH_3 is synthesized from N_2 and H_2 with an Fe-based double promoted catalyst for over 100 years[1]. In 21st century, it has been reported that Ru-loaded $[Ca_{24}Al_{28}O_{64}]^{4+}(e^-)^4$ (Ru/C12A7:e$^-$) works as an efficient catalyst for NH_3 synthesis[2] and characters of C12A7 surfaces are interested in. In this report, the forms of C12A7 surfaces are predicted and a work function of a C12A7:e- surface is derived by computation.

2. Method

All calculations were taken by Vienna *Ab-initio* Simulation Package (VASP)[3] with Projector Augmented Wave (PAW) method[4]. Perdew-Burke-Ernzerhof (PBE) functional[5] was adopted for exchange-correlation energy.

2.1 C12A7 surfaces identification

The forms of stoichiometric C12A7 surfaces should show several morphologies. Surfaces were formed by rupturing C12A7 crystal following to Sushko's work [6] in computation. A process of increasing lattice constant *c* and a process of structural optimization were repeated by turns.

2.2 Work function

A work function of C12A7:e$^-$ surface was derived from local potential distribution of a slab model optimized after self consistent calculations. The size of model is $1 \times 1 \times 3$ crystal with a vacuum region of 7.193 nm.

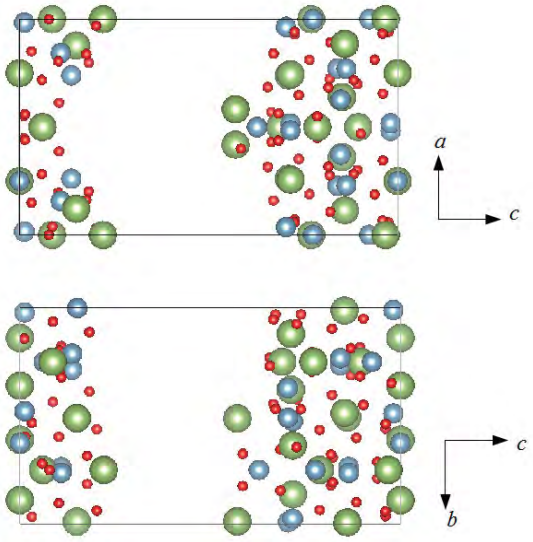

Fig. 1: Stoichiometric C12A7 model after rupturing process. Green, blue and red symbols represent Ca, Al and O ions, respectively.

3. Results

Figure 1 shows the ruptured C12A7 model. Obtained two surfaces have different forms. In the lower part, a nearly flat surface exists in the left and a rough surface exists in the right as

literature [6]. On the other hand, both surfaces are rough in the upper view. Al-centered tetrahedrons also remain in ruptured surfaces.

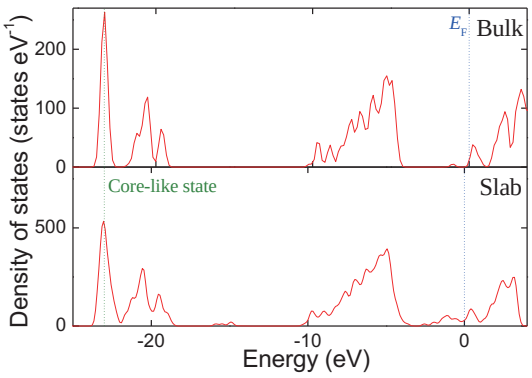

Fig. 2: Density of states of C12A7:e$^-$ bulk (upper) and slab (lower) models. A peak of core-like state lies at -23.0 eV and is defined as the standard.

Figure 2 shows density of states of C12A7:e$^-$ bulk and slab models. Since the Fermi level (E_F) of slab model does not correspond to that of bulk model, a core-like state of each is needed to be commonized to regard the E_F of bulk as real E_F. In Fig. 2, the E_F of bulk is 0.3 eV higher than that of slab. Considering E_F correction, the electronic potential distribution is plotted in Fig. 3. The periodic region in the left is the crystal and the constant region in the right is the vacuum. The work function of C12A7:e$^-$(001) surface was derived as 3.201(2) eV from the constant value of the vacuum region.

4. Conclusions

The form of C12A7 surfaces are predicted as two patterns. Besides, a work function of conducting C12A7:e$^-$ was derived as 3.201(2) eV by computation.

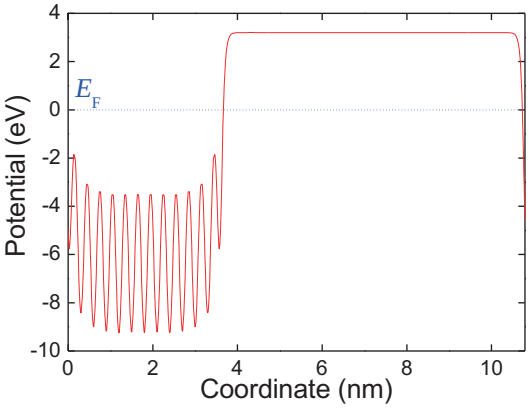

Fig. 3: Electronic potential distribution of C12A7:e$^-$(001) slab model. The horizontal axis is a coordinate perpendicular to the surface. The constant region in the right corresponds to the vacuum region.

References

[1] F. Haber: Z. Elktrochem. Angew. P. **16** (1910) 244.

[2] M. Kitano, *et al.*: Nature Chemistry **4** (2012) 934 .

[3] G. Kresse and J. Hafner: Phys. Rev. B **47** (1993) 558.

[4] P. E. Blöchl: Phys. Rev. B **50** (1994) 17953.

[5] J. P. Perdew, K. Burke and M. Ernzerhof: Phys. Rev. Lett. **77** (1996) 3865.

[6] P. V. Sushko, *et al.*: Proc. R. Soc. A **467** (2011) 2066.

First-principles calculation of electronic structure of thermoelectric material

Yukio SATO

Department of Materials Science and Engineering,

Kyushu University, 744 Motooka, Fukuoka, Fukuoka, 819-0395

Calcium cobalt oxide ($Ca_3Co_4O_9$: CCO) is known to exhibit excellent thermolelectric property mostly owing to its high Seebeck coefficient [1]. CCO has incommensurate layered misfit structure alternative stacking of CoO_2 and Ca_2CoO_3 layers (Fig.1) [2]. In particular, electronic state modulation of Co in the CoO2 layer is believed to be a key factor to obtain the high Seebeck coefficient. Thus, in order to understand the electronic structure of CCO, first-principles calculations were carried out in this study.

LSDA (local spin density approximation) calculations were carried out using the VASP code [4], where the effect of on-site Coulomb potential (U) was taken into account.

Figures 2 shows partial density of states (PDOS) of two particular Co sites in the CoO_2 layer for example. It is found that eighth and tenth Co sites from the left exhibit the magnetic moment of ~ 1.8 μ_B and slightly higher formal valence state from the others. Correspondingly, up-spin and down-spin PDOS is asymmetric with higher population in the energy range of 0 ~ 3 eV (Fig. 2(a)). Asymmetric PDOS but with smaller μ_B and is observed for the fourth, seventh, eleventh, and fourteenth Co from the left. On the other hand, in the case of other Co sites, symmetric PDOS and no magnetic moment is observed (Fig. 2(b)). It is thus considered that electronic structure of Co modulates in the CoO_2 layer.

References

[1] M. Shikano and R. Funahashi, Appl. Phys. Lett. **82** (2003) 1851.

[2] Y. Miyazaki, M. Onoda, T. Oku, M. Kikuchi, Y. Ishii, Y. Ono, Y. Morii, and T. Kajitani, J. Phys. Soc. Jpn. **71** (2002) 491.

[3] K. Momma and F. Izumi, J. Appl. Cryst. **44** (2011) 1272.

[4] G. Kresse and J. Hafner, Phys. Rev. B 47 , 558 (1993); ibid. 49 , 14 251 (1994).

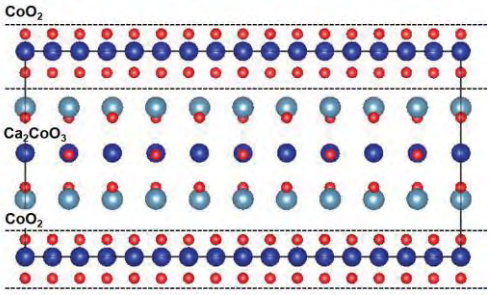

Fig. 1: Crystal structure of CCO. The figure is illustrated using VESTA [3]. The crystal structure is viewed along *a*-axis. Dark blue, light blue, and red circles represent Co, Ca, and O, respectively.

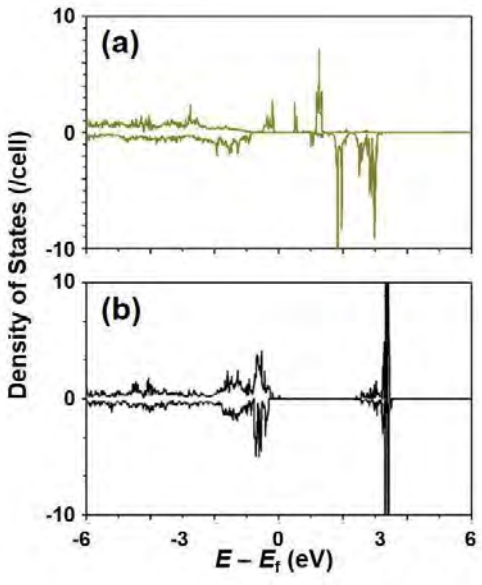

Fig. 2 PDOS of Co in the CoO_2 layer. Those of (a) eighth, (b) first Co site from the left.

Thermo-Chemical Wear Mechanism of Diamond Cutting Tool

Yutaka Uda, Shoichi Shimada

Osaka Electro-Communication University, Hatsu-cho, Neyagawa, Osaka 572-8530

Sakuro Honda

Technology Research Institute of Osaka Prefecture, Ayumino, Izumi, Osaka 594-1157

Demand has been increasing for highly durable molds of heat-resistant materials for the fabrication of complex and precise optical components with high aspect ratio. Diamond is the only ideal cutting tool material for high efficient ultraprecision metal cutting of complex three-dimensional metal works. However, it is well known that diamond cutting tool shows severe wear in cutting of heat-resistant materials such as steel. Preliminary ab-initio molecular orbital calculation by the authors showed that the essential mechanism of severe wear in cutting of steel is the dissociation of carbon atoms on diamond surface due to the chemical interaction with iron atoms in workpiece [1]. Therefore, to avoid chemical reactions between the carbon atoms of diamond and iron, modifying some chemical composition into steel for establishing a chemical bond between the iron atom and some other additional elements into iron is an effective method to suppress the tool wear. Nitrogen and carbon are the possible elements convenient for the purpose because they can easily diffuse into iron.

In this study, to understand the mechanisms of the initial stages of wear process of diamond cutting tool in machining of steel and effect of chemical modification of carbon and nitrogen, ab initio molecular dynamics calculations of chemical reaction on diamond surface in contact with Fe, Fe-C and Fe-N surfaces were carried out using double-grid method for real-space electronic-structure calculations developed by Professor T. Ono of University of Tsukuba [2].

At first step, the optimized atomic configuration of a $C_{10}H_{14}$ cluster was analyzed as the model of diamond (100) surface. And the thin Fe plate was analyzed as the models of Fe (100) surface. The dimensions of the plate, x × y × z, was 2a × 2a × a, where a is lattice constant of Fe. The model has periodic boundaries in *x* and *y* directions and aperiodic boundary in *z* direction. Both models were successfully calculated.

References

[1] S. Shimada, H. Tanaka, M. Higuchi, T. Yamaguchi, S. Honda, K. Obata: 2004, Annals of the CIRP, **53**, 1 (2004) 57-60.

[2] T. Ono, K. Hirose: Physical Review Letters, **82** (1999) 5016.

First-Principles Momentum Dependent Local Ansatz Theory and Its Application to Fe Compounds

Yoshiro KAKEHASHI and Sumal CHANDRA
Department of Physics and Earth Sciences, Faculty of Science, University of the Ryukyus, 1 Senbaru, Nishihara, Okinawa, 903-0213, Japan

Although the band theory based on the density functional theory (DFT) is well-known to describe the properties of many metals and insulators, quantitative aspects of the theory become worse with increasing Coulomb interaction strength as found in ϵ-Fe, Fe-pnictides, cuprates, as well as heavyfermion system. We need alternative approaches to quantitative description of correlated electrons. We have developed the first-principles momentum dependent local ansatz (MLA) wavefunction theory on the basis of the tight-binding LDA+U Hamiltonian in order to describe the ground-state properties of correlated electrons quantitatively [1].

Introducing the three kinds of momentum dependent operators (,*i.e.*, the intra-orbital correlator $\tilde{O}^{(0)}_{imm}$, the inter-orbital charge-charge correlator $\tilde{O}^{(1)}_{imm'}$, and the inter-orbital spin-spin correlator $\tilde{O}^{(2)}_{imm'}$), we construct the first-principles MLA wavefunction $|\Psi_{\rm MLA}\rangle$ as

$$|\Psi_{\rm MLA}\rangle = \Big[\prod_i \Big(1 - \sum_m \tilde{O}^{(0)}_{imm} - \sum_{m>m'} \tilde{O}^{(1)}_{imm'} - \sum_{m>m'} \tilde{O}^{(2)}_{imm'}\Big)\Big] |\phi\rangle. \quad (1)$$

The MLA takes into account all the two-particle excited states with the momentum-dependent amplitudes, so that it describes exactly the weak interaction limit, and describe well correlated electrons from the weak to strong Coulomb interaction regime.

In the implementation of the first-principles MLA, we first perform the Hartree-Fock band calculations for the LDA+U Hamiltonian. Using the energy eigenvalues and eigenvectors, we solve the self-consistent equations for the momentum-dependent variational parameters, correlation energy, and the Fermi level.

We performed the numerical calculations for the paramagnetic bcc Fe. Calculated Hund's rule correlation energy is found to be $\Delta\epsilon_{\rm H} \sim$ 3000 K, which explains the difference in magnetic energy between the LDA (5000K) and the DMFT, *i.e.*, DCPA (2000K). Calculated amplitude of local moment $\langle \boldsymbol{S}^2 \rangle = 2.58$ is in good agreement with the experimental value 2.56. We also found that the momentum distribution function bands along high-symmetry lines show a large deviation from the Fermi-Dirac function as shown in Fig. 1. Calculated mass enhancement factor 1.65 shows a good agreement with recent DMFT result 1.58 at finite temperatures as well as the experimental result 1.7 obtained by the ARPES.

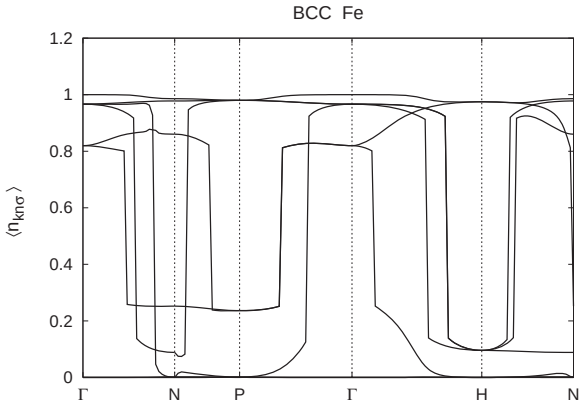

Figure 1: Momentum distribution functions along high-symmetry lines for bcc Fe

References

[1] Y. Kakehashi and S. Chandra, J. Phys. Soc. Jpn. **85**, 043707 1-5.

Electronic State and Proximity Effects around Interface in Layered Superlattices

Kunitomo HIRAI
Department of Physics, Nara Medical University
Kashihara, Nara 634–8521

The purpose of the present research is to elucidate characteristics of electronic state in superlattices with layered structures, in particular, to illustrate proximity effects of each layer on adjacent layers in the superlattices. This research of a first-principles electronic structure calculation is performed by means of the Korringa-Kohn-Rostoker (KKR) Green function method within the framework of the local spin density (LSD) functional formalism.

The calculation by means of the KKR method was so far carried out for superlattices of ferromagnetic layers with nonmagnetic spacer layers such as Fe/Cr, Fe/V, Fe/Cu, ... ones, with magnetizations of two successive Fe layers being aligned parallel or antiparallel. Oscillatory interlayer exchange coupling between ferromagnetic layers with respect to spacer thickness was investigated, and relation between bulk effects inherent in the spacer layer and the proximity effects due to the ferromagnetic layers was analyzed. In the calculation, every atom in a monolayer stacked in the superlattices is assumed to be equivalent, and there is one site in each monolayer. This assumption can be justified for the superlattices with ideal interfaces without structure, but not for those with realistic interfaces with structures like steps, islands, or such, and hence there are two or more sites in each monolayer for the superlattices with realistic interfaces.

A need of the calculation for superlattices with more sites in each monolayer arises also for layered superlattices of ordered alloys or compounds, which now attract broad interests particularly in viewpoint of spintronics. We then start preparation of the calculation for superlattices with more sites in each monolayer, which results in increase of the number of atoms in a unit cell and involves vast increase of computation times. In the preparation of the calculation, installation of parallelization with use of the OpenMP into program codes of the KKR methods is intended, together with parallelization with use of the MPI which was already achieved, that is, installation of hybrid parallelization is intended.

The installation of the OpenMP is in progress and will be achieved, and then the proximity effects in the superlattices with realistic interfaces will be investigated to elucidate the roles of the interfaces in the superlattices. The calculation will be carried out for Fe superlattices with steps, and magnetic frustration caused by the steps is investigated, in particular reference to possible mechanism of increase of total magnetization of the Fe layers, where fcc(001) or fcc(111) superlattices are considered together with usual bcc(001) ones and difference between those superlattices is to be analyzed. In addition, the calculation will be carried out for layered superlattices of ordered alloys, such as fcc(001) superlattices consisting of Fe and FePt layers, in particular reference to ferromagnetic or antiferromagnetic coupling between layers and within a monolayer.

Theory of magnetic alloys with octahedral frustration

Takashi UCHIDA
Hokkaido University of Science
4-1, 7-15, Maeda, Teine-ku, Sapporo 006-8585

Magnetic alloys with octahedral frustration such as Mn_3X (X=Pt, Rh, Ir) and Mn_3AN (A=Ga, Zn) have attracted attention because the competing and frustrated interactions in these systems give rise to temperature-driven magnetic phase transitions that accompany a peculiar magnetic structure (Mn_3Pt) or a large magnetovolume effects (Mn_3AN). Recently, we have applied the first-principles molecular spin dynamics (MSD) method to Mn_3X (X=Pt, Rh, Ir) and explained the magnetic phase transitions in terms of the temperature dependence of the electronic structure [1]. Although the obtained results are reasonable and consistent with experiment, they did not reproduce the details of the electronic structure because of using a small number of recursion levels in the local electronic structure calculations by the recursion method. In the present research, we have revised the calculation scheme of the MSD allowing for a large number of recursion levels in the recursion calculations. To test this scheme, we have calculated the electronic and magnetic structures of Mn_3X (X=Pt, Rh, Ir).

The MSD theory is formulated by incorporating the first-principles TB-LMTO Hamiltonian into the MSD approach for itinerant magnets on the basis of the functional integral method and the isothermal MSD technique [1]. The MSD approach allows us to determine automatically the magnetic structure of a large system with several hundred atoms in a unit cell at finite temperatures. In the present MSD analysis, we solved the isothermal MSD equations of motion by using site-dependent effective medium in order to treat the magnetic phase transition correctly. We used the recursion method to calculate the local electronic structure in determining the site-dependent effective medium and in calculating magnetic forces at each time step of the MSD equations of motion. Because the time-consuming recursion process consists of parallelizable loop calculations, we utilized the MPI parallel calculation scheme in the recursion calculation. In the calculations of the site-dependent effective medium, we embed the supercell with $4 \times 4 \times 4$ fcc lattice in a large cluster consisting of $5 \times 5 \times 5$ supercells, each of which are connected by the periodic boundary condition. By virtue of using the large cluster, we were able to calculate the local electronic structure up to recursion levels (7,9,19) for s, p, and d orbitals.

The calculated the d-electron densities of states (DOS) of Mn_3X (X=Pt, Rh, Ir) have a double-peak structure similar to those [1] obtained by the ground-state TB-LMTO calculations. With increasing temperature from 25 K, the Mn-Eg DOS of Mn_3Pt at the Fermi energy, which is located between the double peak, increases around 350 K, while those of Mn_3Rh and Mn_3Ir do not show appreciable increase. The results are consistent with the phase transitions of Mn_3X (X=Pt, Rh, Ir) [2].

References

[1] T. Uchida, N. Kimura, and Y. Kakehashi: J. Korean Phys. Soc. **62** (2013) 1748; Y. Kakehashi, S. Akbar, and N. Kimura, Phys. Rev. B**57** (1998) 8354.

[2] T. Uchida, Y. Kakehashi, and N. Kimura: J. Magn. Magn. Mater. **400** (2016) 103.